Title	DNA
Author(s)	,
Citation	
Issue Date	2015-03
Type	Thesis or Dissertation
Text version	ETD
URL	http://hdl.handle.net/10119/12775
Rights	
Description	Supervisor: , ,

JAIST
JAPAN
ADVANCED INSTITUTE OF
SCIENCE AND TECHNOLOGY

Japan Advanced Institute of Science and Technology

Doctoral Dissertation

Development of DNA nanoengineering based on ultrafast

DNA photocrosslinking

Shigetaka Nakamura

Supervisor : Prof. Kenzo Fujimoto

School of Materials Science
Japan Advanced Institute of Science and Technology

March 2015

Contents

Chapter 6. Template directed reversible photochemical ligation

of Oligodeoxynucleotides

General Introduction

The structure of DNA and its biological function

In 1869, DNA was isolated by Friedrich Miescher who discovered a microscopic substance in the pus of discarded surgical bandages [1]. He called it "nuclein" because it resided in the nuclei of cells, this was the first discovery of DNA. In 1878, Albrecht Kossei succeeded in isolating five nucleobases and named its five constituent organic compounds: Adenine(A), Cytosine(C), Gunanine(G), Thymine(T) and Uracil(U) [2]. These compounds are now known collectively as nucleobases, and they provide the molecular structure necessary for the formation of stable DNA and RNA molecules. In 1927, Nikolai Koltsov proposed that inherited traits were inherited via giant hereditary molecules made up of two mirror strands that would replicate in a semi-conservative fashion using each strand as template [3]. These ideas were confirmed in 1953 when Crick and Watson described the structure of the DNA helix. In 1929, Phoebus Levene identified the components of DNA and RNA, which consist of base, sugar, and phosphate nucleic units [4]. He suggested that DNA consists of a string of nucleotide unit linked together through the phosphate group. However, he thought the chain was short and bases repeated in a fixed order. In 1937, William Astbury succeeded in taking X-ray diffraction patterns that show the DNA duplex structure [5]. In 1953, Crick and Watson suggested the DNA double helix model which now accepted as the definitive model by the Journal of *Nature* [6]. The molecular model of DNA was based on a single X-ray diffraction image taken by Rosalind Franklin and Raymond Gosling in 1952. Later, in 1958, Crick was reported the concept of central dogma which foretold the relationship between DNA, RNA, and proteins [7]. In 1977, two sequencing methods of DNA were reported in "DNA sequencing by chemical degradation" by Maxam and Gilbert, and "DNA sequencing by enzymatic synthesis" by Sanger, the latter being known as the Sanger method [8]. In the 2000s, the human genome sequence was analyzed by the Human Genome Project and Celera corpolation, and was reported in the Journal of *Nature* and *Science* [9,10]. This project not only clarified the human genome but also advanced various technologies related to DNA such as reading the

5

sequence and synthesis of the DNA strand. The progress of these technologies had a massive influence on DNA nanotechnology very much.

In 1953, Crick and Watson reported that DNA a formed double strand helix and the characteristic structure captured the spotlight. The two strands of DNA are positioned in opposition to each other and are therefore anti-parallel, one backbone being 5' (five prime) and the other 3' (three prime), referring to 3rd and 5rd carbon on deoxyribose. The double stranded helix of the DNA molecule composed of nucleobase such as guanine(G), adenine(A), thymine(T), and cytosine(C), deoxyribose, and phosphate group was reported by Levene in 1929 (Fig. 1.1A). The human genome is made up of approximately 3 billion base pairs retained in 23 chromosomes. This genetic information was translated to a protein after the transcription to RNA according to the central dogma, with the protein responsible for various functions (Fig. 1.1B). Various biomolecules and bio-functions have been analyzed by many researchers in molecular biology and chemical biology. The fields of synthetic biology and DNA nanotechnology involve the creation of various entities such as artificial cells, structures, and devices using biomolecules and bio-functions.
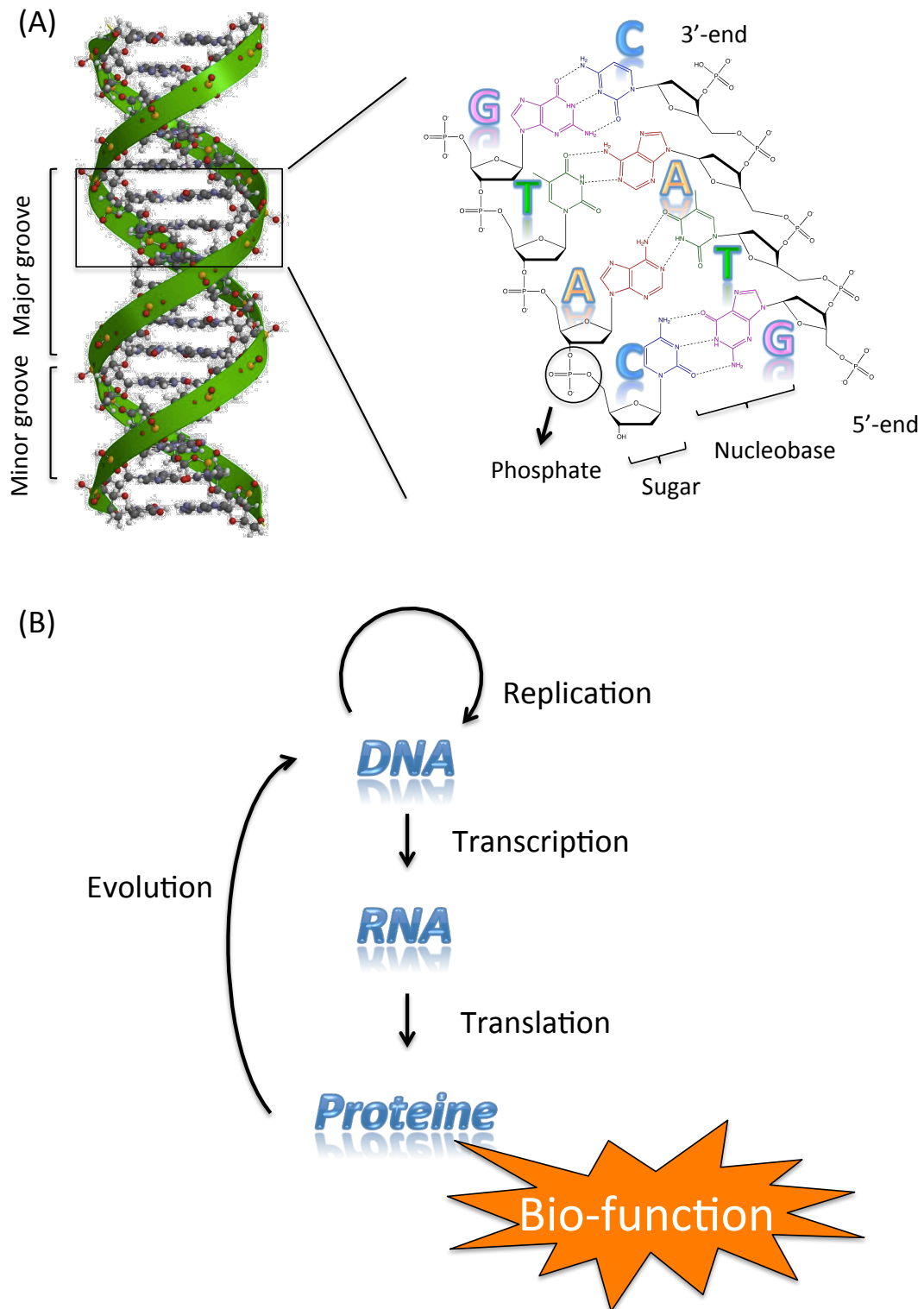
Figure. 1. 1 (A) Molecular model of DNA helical duplex; The conformation of DNA is double helical structure formed Watson Crick interaction. (B)The scheme of central dogma.

Chemical Synthesis of Oligonucleotides

One reason for developing DNA nanotechnology is to establish a synthetic method of producing the short DNA strands. Oligonucleotide synthesis is performed according to the phosphoramidite method [11-14]. The reaction scheme is shown in Scheme 1.1 and glow the oligonucleotide chain is developed as follows.

・Step 1. Detritylation

In DNA synthesis, first, the dimethoxytrityl (DMT) protection group at the 5' end is removed with 2% trichloroacetic acid (TCA) in dichloromethane. The orange-colored DMT cation formed is washed out and the step results in the solid support-bound oligonucleotide precursor bearing a free 5'-terminal hydroxyl group. Conducting detritylation for an extended time or support-bound oligonucleotide thus reduces the yield of the desired full-length product.

・Step 2. Coupling

The support-bound nucleoside is ready to react with the next base, which is added in the form of a nucleoside phosphoramidite monomer. A large excess of the appropriate nucleoside phosphoramidite is mixed with an activator, both of which are dissolved in acetonitrile. The diisopropylamino group of the nucleoside phosphoramidite is protonated by the activator, and is thereby converted to a good leaving group. It is rapidly displaced by attacking of the 5'-oxygen bound that is formed, creating a support bound phosphite teriester.

・Step 3. Capping

To block the unreacted 5'-hydroxy groups, deletion mutations are avoided by introducing a "capping" step after the coupling reaction. Two capping solutions are used on the synthesizer: acetic anhydride and N-methymidazole. These two reagents are mixed on the DNA synthesizer prior to delivery to the synthesis column. The electrophilic mixture rapidly acetylates alcohols, and the pyridine ensures that the pH remains basic to prevent detritylation of nucleoside phosphoramidite by the acetic acid

formed by the reaction of acetic anhydride with N-methylimidazole. Acetylation of the 5'-hydroxyl groups blocked the subsequent reactions.

・Step 4. Oxidation

The phosphite-triester formed in the coupling step is unstable in acid and must be converted to a stable species prior to the next TCA detritylation step. This is achieved by iodine oxidation in the presence of water and pyridine. The resultant phosphotriester is effectively a DNA backbone protected by a 2-cyanoethyl group. The cyanoethyl group prevents undesirable reactions at phosphorus during subsequent synthesis cycles.
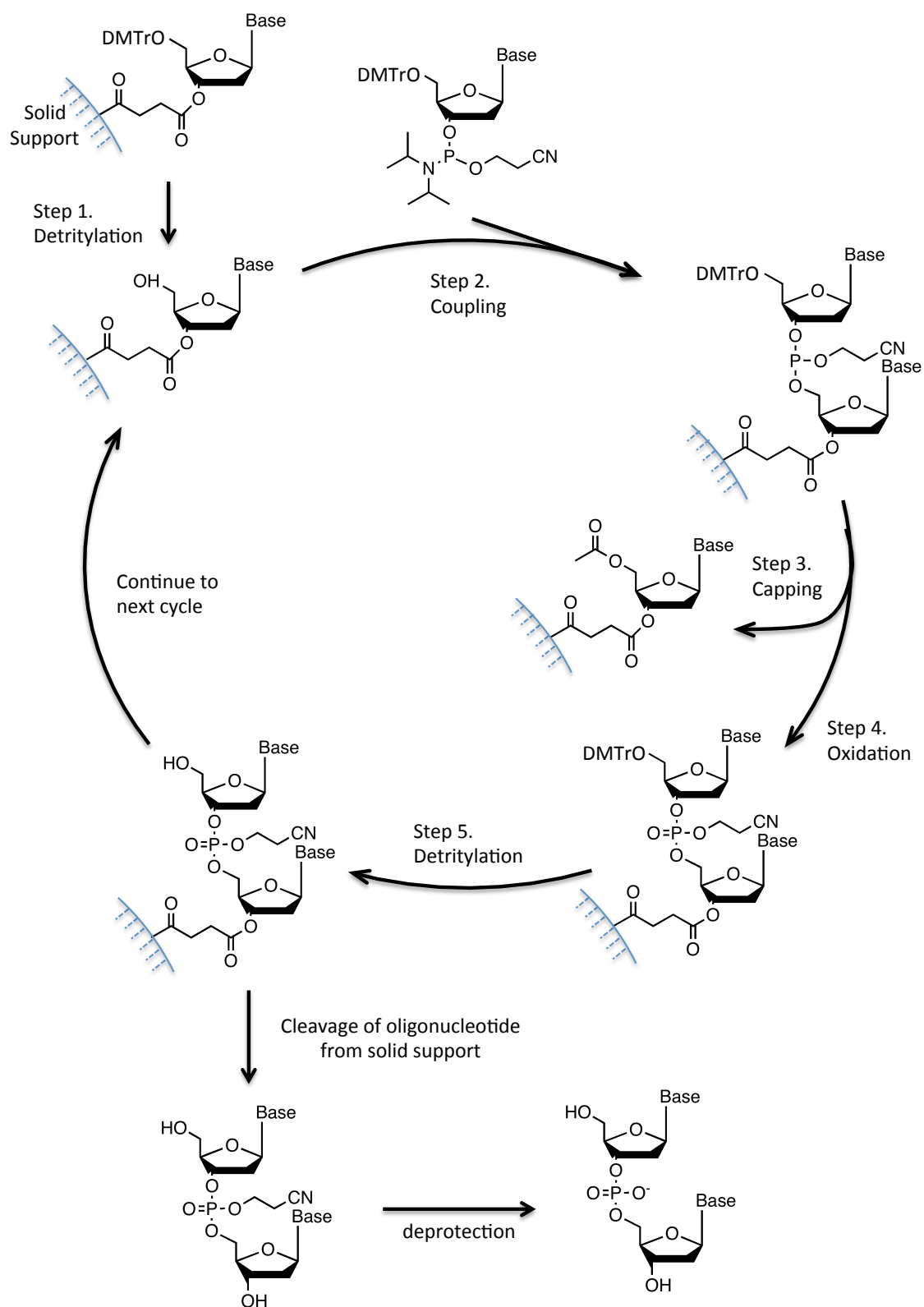
Scheme. 1. 1 Reaction cycle for preparation of oligonucleotides by phosphoramidite method.

Functional Nucleic Acids

By estimating the organic synthesis of oligodeoxynucleotide, arbitrary DNA sequences are now easily obtained. Moreover, various functional nucleic acid produced by organic synthesis are easily incorporated into DNA strands. DNA follows the restrictive Watson-Crick rule for hybridization and is a highly predictable assembling unit to form addressable nanostructures. Functional nucleic acids with remarkable recognition and catalytic properties make the DNA nanostructures a good template for patterning other molecules, studying biological molecular interactions in nano-scale precision, sensing with unique properties, serving as selective drug release, as well as driving the motions of nanodevices.

1) Aptamers

   Single-stranded DNA or RNA oligonucleotide that adopt specific three-dimensional conformations for targeting distinct molecules are called aptamers [15]. Aptamers strongly bind to their target molecules with high affinity and selectivity by intermolecular binding forces such as hydrogen bonds, electrostatics, and van der Waals force. For example, a thrombin aptamer (5'-TGGTTGGTGTGGTTGG-3') has high binding affinity to thrombin and forms G-quadruplex in the presence of potassium ion [16]. Aptamers that have advantages over antibodies have already made substantial contributions in various diagnostic assays concerning the specific immune reactions routinely used in clinics; by maintaining high binding affinity and specificity, aptamers are easily synthesized, and convenient to keep and have less immunogenicity. Because of the *in vitro* selection of aptamers, they can bind essentially to any target of choice, while antibodies cannot be obtained for small molecules, toxic molecules or molecules with low immunogenicity. Moreover, in DNA nanotechnology, aptamers are ready to be engineered in DNA nanotechnology.

2) DNAzyme

 DNAzyme has a DNA strand having catalytic activity similar to a ribozyme, which overturns the fundamental concept of enzymes [17]. DNAzyme compared to ribozyme, despite the lack of the 2'-hydroxy group, has also been evolved to catalyze a diverse range of reactions, including RNA cleavage [18], DNA cleavage [19], RNA ligation [20], DNA ligation [21], and enzymatic activities such as peroxidases [22]. In contrast to the thermal unstable protein enzymes, DNAzymes are robustly stable under ambient temperatures. Furthermore, it is difficult to conjugate protein enzymes to other functionalities or biomolecules. By comparison, DNAzymes, for their intrinsic properties of nucleic acids, are simple to directly label themselves with the desired target through chemical modification, DNA hybridization. DNAzymes are also isolated by *in vitro* selection. Depending on the nature of each catalytic reaction, various methods have been designed to perform the selection. The selection followed the similar basic processes similar to those of aptamer SELEX: reaction, separation, and amplification. And thus autonomous selection is possible.

3) Functional artificial nucleic acid

 Functional artificial nucleic acids, which played an important role in the development of DNA nanotechnology were realized by the progress of organic synthesis chemistry. Nucleic acid has been roughly divided into a sugar part and a base part, and various types of artificial nucleic acids with improvements to each part have been reported. For example, locked nucleic acid (LNA) is modified with an extra bridge connecting the 2' oxygen and 4' carbon, and peptide nucleic acid (PNA) has a peptide bond instead of phosphate [23,24]. These artificial nucleic acids have high interaction with native DNA and RNA since LNA has a strictly specified structure and PNA has no negative charge in the linker part. Thus, LNA is used to increase the sensitivity and specificity of expression in DNA microarrays

[25], FISH probes [26], quantitative PCR probes [27] and other molecular biology techniques based on oligonucleotides. PNA were used in diagnostic assays [28] and antisense therapies [29].

Many functional nucleic acids with a customized base part have been reported. These can be applied to DNA devices with various external stimulation responsive artificial nucleic acids such as sensing pH, temperature, photo, and so forth. Photoresponsive artificial nucleic acids are useful and their activities have been regulated the wavelength and power of photoirradiation easily.

Caged nucleic acids are photoresponsive functional nucleic acids, protected by a photo-removable protecting group [30]. The ODN including caged nucleic acids inhibit the double strand formation of DNA/RNA, but caged nucleic acids that remove the protecting group by photoirradiation can form a double stranded formation. Many applications using caged nucleic acid have been reported since all native bases have caged artificial compound. Heckle et al, reported that the function of siRNA including caged nucleic acids was regulated by photoirradiation [31]. Moreover, the inhibition of expression of nerve predisposing factor in the embryos of zebra fish were successfully achieved using morpholinos ODN including four caged compounds as reported by Deiters [32].

In reversibility, azobenzen and psoralen modified nucleic acid have photoreversibility. In forming a double strand, azobenzen underwent photoregulation since photoisomerization of *cis-trans* occurred by photoirradiation [33]. The ODN containing psoralen was crosslinked to the complementary strand by photoirradiation so a stable duplex was formed [34]. These photoreversible functional nucleic acids were used for photoregulation of the antisense effect, creation of photo-driven nanomachines, and creation of stable DNA nanostructures [35-37].

The reaction represented by the thymidine dimer that forms a [2+2] cyclobutane ring by the photostimulation is very interesting. Through, subsequent research,

various artificial nucleic acids that form the [2+2] cyclobutane ring by photostimulation have been reported. In 2004, Ihara and coworker reported "Photochemical Ligation of DNA Conjugates through Anthracene Cyclodimer Formation and Its Fidelity to The template Sequence" in *J. Am. Chem. Soc.* [38] In this paper, the ODNs that modify anthracene at the 5'-end or 3-end, respectively, were ligated by 366 nm photoirradiation on template mediated [2+2] cyclobutan ring (Fig. 1.2A). This photochemical ligation was only dimerized in the presence of the adjacent sequence template by the photoirradiation, and was applicable to gene analysis. [39]. These artificial nucleic acids have ligation type mediated [2+2] cyclobutane formation. Photocrosslinking type artificial nucleic acids are introduced as follows.

In 2008, Yoshimura and Fujimoto reported a photoresponsive artificial nucleotide "3-cyanovinylcarbazole nucleotide (^CNVK)," which is photocrosslinked to pyrimidine onto complementary ODN or ORN via [2+2] photocycloaddition by photoirradiation at 366 nm for a few seconds (Fig. 1.2D) [40,41]. This photocrosslinking reaction of ^CNVK is applicable to the selection of miRNAs, SNPs genotyping, and antisence strategy [42-44]. As other examples, Asanuma et al, reported the photocrosslinking of DNA duplex using p-stilbazole moieties (Fig. 1.2B) [45].
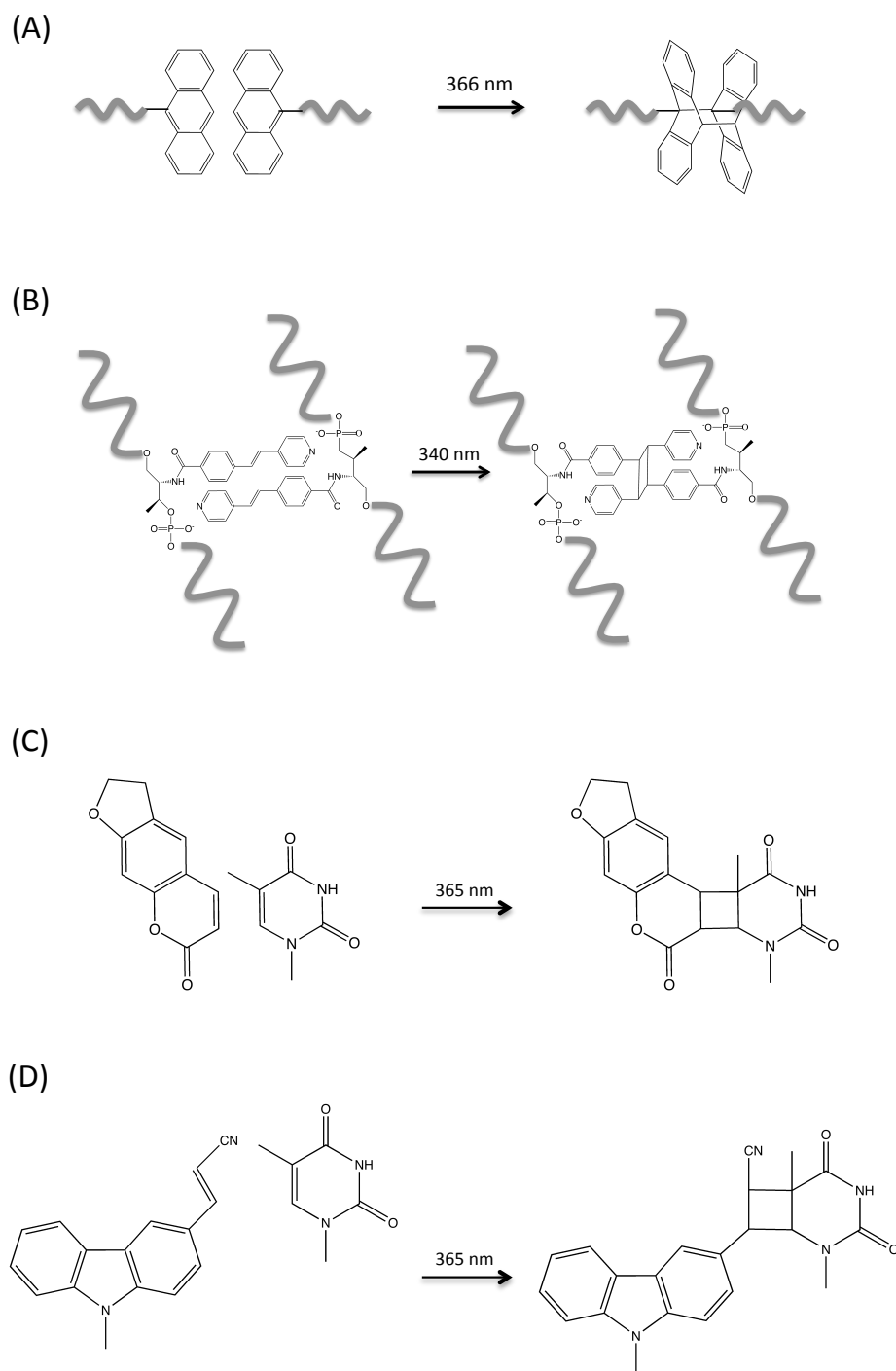
Figure. 1.2 The photoresponsive artificial nucleotide mediated [2+2] cyclobutane ring (A) anthracene modified ODN (B) *p*-stilbazole modified ODN (C) psoralen (D) 3-cyanovinylcarbazole

DNA Nanotechnology

DNA nanotechnology is a branch of nanotechnology that uses the unique molecular recognition properties of DNA and other nucleic acids to create designed, controllable structures out of DNA. In this field, DNA is regarded not only as a carrier of genetic information but also as a type of structurally precise nanomaterial. In double stranded DNA, the distance between bases is 0.34 nm, and the distance between one turn in the helix is 10.5 bp (3.5 nm). The diameter of the B-form DNA is 2 nm. Thus, a DNA structure is defined as a nanomaterial. These merits allow construct of a DNA structure by sequence design. Taking these features together, DNA molecules can be used as versatile nanoscale building blocks for the construction of artificial supermolecular nanostructures with tailorable functions. Nucleic acid design is the process of generating a set of nucleic acid base sequences that will associate into a desired conformation. Nucleic acid design is central to the field of DNA nanotechnology and DNA computing. There are many possible sequences of nucleic acid strands that will fold into a given secondary structure, but many of these sequences will have undesired additional interactions that must be avoided. In addition, there are many tertiary structure considerations that affect the choice of secondary structure for a given design. The sequence of a monomer is designed to favor the desired folded or associated structure and to disfavor alternate structures. However, nucleic acid design has the advantage of being a much computationally simpler problem, since the simplicity of Watson-Crick base pairing rules leads to simple heuristic methods that yield experimentally robust designs.

However, it has been reported that DNA forms various high dimensional structures without Watson-Crick interaction. The thrombin aptamer [46] was reported to form G-quadruplex in the presence of potassium ions and the nucleic acid sequences that have catalystic activity called DNAzyme [47] and RNAzyme [48]. The existence of nucleic acid sequences with unique functions expands the capability of DNA nanotechnology, and various DNA devices using them have been reported.

DNA Nanostructures

In the early 1980s, Nadrian Seeman proposed an innovative method of exploiting unique molecular recongnition properties for nanoconstruction [49-53]. He constructed a nanostructure composed of deoxynucleotide on a nano-scale using holiday junction (Fig. 1.3A). This area grew rapidly in the 1990s, partially because of the industrial availability of chemically synthesized DNA molecules with arbitrary sequences. Nowadays, it is possible to order almost all components required for the nanotechnology. Another reason for the rapid development of DNA nanotechnology is the invention and commercialization of atomic force microscopy (AFM). AFM is a type of scanning probe microscopy (SPM); it can readily probe almost any sample deposited on a flat surface and perform measurements in three dimensions, X, Y, and Z, thereby enabling the visualization of three-dimensional images of a given sample. AFM and more recently developed technology provide a powerful set of toolbox for in-depth characterization of self-assembled DNA nanotechnology.

After that the many types of DNA structure have been reported using various DNA motifs such as double-crossover (DX) [50], triple-crossover (TX) [54], DNA paranemic crossover (PX) [55] and T-motif [56] (Fig. 1.3B). The DNA motif design relies on the operation of reciprocal exchange, the switching of the connections between DNA strands in two different double helices to produce a new connectivity. It is important to recognize that this is not an operation performed in the laboratory; it is done on paper or with a computer, and then the strands corresponding to the results of the operation are synthesized. Owing to the polar nature of DNA backbones, the operation can be performed between strands of the same polarity or between strands of opposite polarity. If only single reciprocal exchange is performed, there is no difference, because the two products are simply conformers of each other; however, if two or more operations are performed, different topologies result. Often a different ease of formation accompanies the two different topologies; empirically, the best behaved molecules are those in which exchange takes place between strands of opposite polarity.

The earliest DNA construction was best described as a topological species, rather than a geometrical species because the earliest DNA motifs, i.e., branched junctions, were not robust but could be described as floppy if they were ligated [57,58]. Thus both the linking and branching topologies of these molecules were well-defined because these features could be established as gels, but their detailed structures were not fixed. Idealized pictures of the first two structures, a cube [59] and a truncated octahedron [60], each with two double helical turns between vertices, are reported. All nicks in these molecules were sealed, and they were characterized topologically by denaturing gel electrophoresis. One of the issues with these structures is that they were not deltahedrons (polyhedrons whose faces are all triangles); deltahedrons, such as tetrahedrons [61], octahedrons [62], and icosahedrons [63], have all been produced in the last ten years [63, 64]. In addition, a protein has been encapsulated within a tetrahedron [65]. The larger species have been characterized by electron microscopy. Other polyhedrons, such as DNA buckyballs (truncated icosahedrons), have been produced by carefully exploiting the interplay between junction flexibility and edge rigidity.

The topological features of the early constructs also led to the development of a single-stranded DNA topology. A crossover in a knot or a catenane can be regarded as being equivalent to a half-turn of DNA can be exploited accordingly [66]. Thus, it has proved fairly simple to produce a variety of knotted molecules from single-stranded DNA [67], as well as a number of specially linked catenanes. Some of these constructs have been used to characterize the topology of holiday junctions [68]. By using left-handed Z-DNA, it is possible to produce nodes of both signs in topological products. This aspect of DNA topology was exploited to produce the first Borromean rings from DNA. An RNA knot was used in discovering that E. coli DNA topoisomerase III can act as an RNA topoisomerase [69].
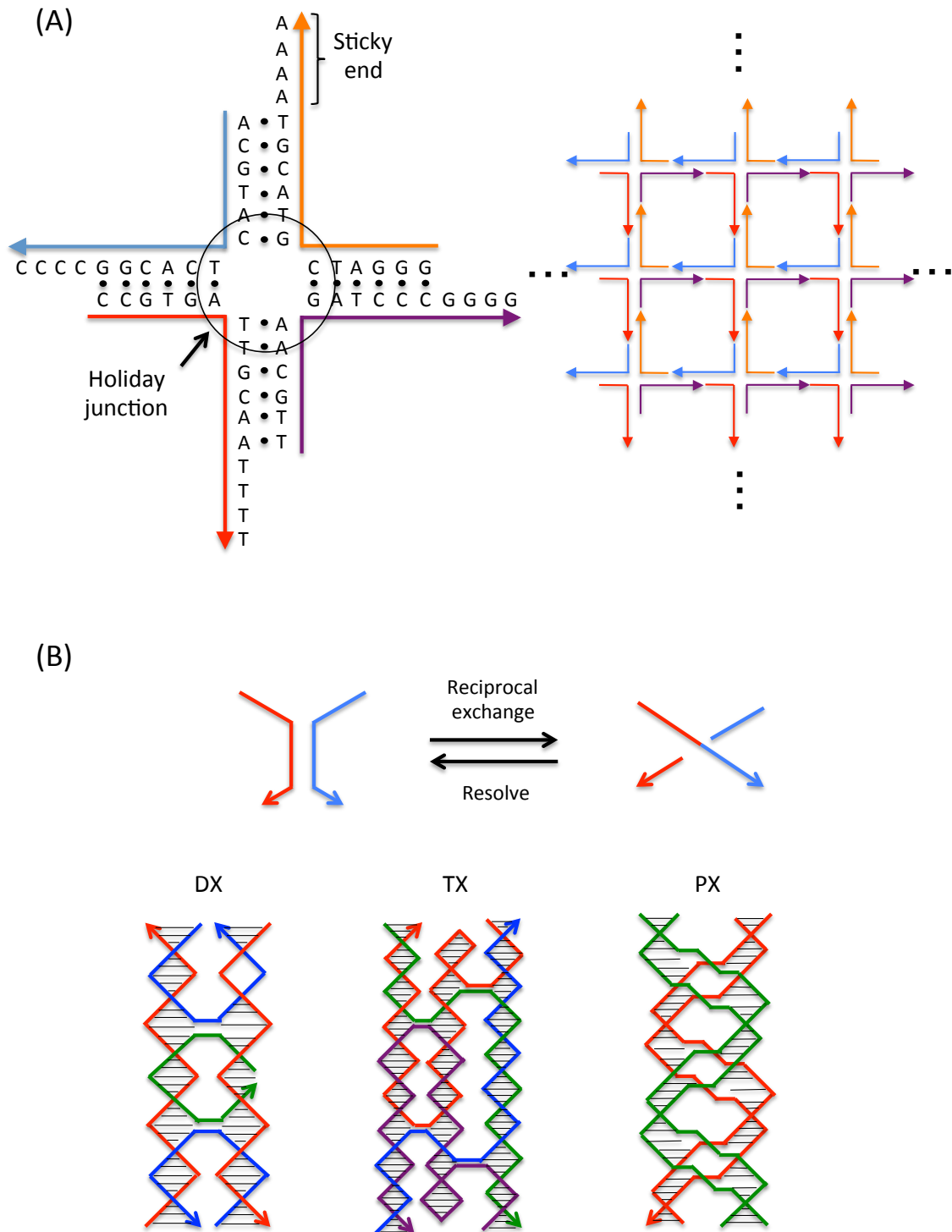
Figure 1. 3 (A) Self-assembly of branched DNA molecules to form larger tile structure. (B) DNA motif generation by reciprocal exchange and double-crossover, triple-crossover, and paranemic-crossover DNA motif.

DNA origami

Since the report on the creation of a DNA nanostructure by Nadrian Seeman 30 years ago, DNA has been considered a powerful material for nano-scale fabrication. Based on Watson-Crick interaction and programmable sequencing, the given sets of designed oligonucleotides are able to form a specific man-made DNA motif at a size of sub- 10 nm. However, building submicron finite nanostructures with full addressability and higher complexity is a challenges for this tile-based fabrication strategy. In addition, the design of tiles follows strict sequence optimization rules, and the strands used for tile preparation should be highly purified and precisely equimolar.

In 2006, the invention of DNA origami [70] by Rothemund greatly increased the complexity and size of man-made DNA nanostructures as well as largely simplified the design and preparation processes. The DNA origami method involves raster filling the desired shape with a long single stranded scaffold with the help of hundreds of short staple ODN to hold the scaffold. The scaffold sequence does not need a specific design, because the success of DNA origami is ensured by strand displacement reaction, in which a longer region of complementarity between the staple and the scaffold stabilizes the staple-scaffold interaction over the scaffold's secondary structure. Rothemund selected genomic DNA from the virus M13mp18 with more than 7,000 bases as the scaffold. More than 200 staple strands were used to help fold and different shapes could be assembled from different sets of staple strands, such as smiles, stars, and disks. DNA origami was provided a breakthrough in structural DNA nanotechnology (Fig. 1. 4A).

DNA computing

This field was initially developed by Lenard Adleman at the University of Southern California, in 1994 [71]. Adleman demonstrated a proof of concept use of DNA as a form of computation that solved the seven–point Hamiltonian path problem. Since the initial Adleman experiments, advances have been made and various turning machines have proven to be constructible (Fig. 1.4B). Unfortunately, massive parallelism in

molecular computing could not compete directly with silicon computers due to the inherently slow operations such as DNA hybridization and electrophoresis. Instead, the DNA computing has changed its direction from performance competition to the study of autonomous computing models in which computation takes place spontaneously after the molecular ingredients have been mixed in.

In 2003, researchers from the Weizmann Institute of Science in Rehovot, Israel, unveiled a programmable molecular computing machine composed of enzymes and DNA molecules instead of silicon microchips [72]. On April 28, 2004, the construction of a DNA computing couple with an input and output module that would theoretically be capable of diagnosing cancerous activity within a cell, and releasing an anti-cancer drug upon diagnosis was reported in the journal of *Nature* [73].

DNA molecules have become essential molecules for realizing molecular logic circuits, because DNA molecules facilitate digitalization properties and high selectivity. In addition, DNA hybridization plays an essential role in guaranteeing high-yield reaction products and suppressing crosstalk between molecules when building multi-variable and multi-stage molecular logic gate. Examples of DNA based molecular logic gates include: finite-state automata using restriction enzymes [74], single-molecule finite-state automata based on DNA polymerization, [75] various types of DNA memory [76-78], and DNAzyme-based logic gates [79]. Moreover, a DNA logic gate using nucleic acid not only a native-base but also artificial-base nucleic acid has been [80]. In order to implement hundreds of logic gates in a single DNA hybridization reaction, toehold mediated branch migration has been developed. Recently, Rondelez developed dynamic oscillators using logic gates that combine DNA polymerization with nicking enzyme and exonuclease [81].

DNA computers have also been constructed using the concept of toehold mediated strand exchange. In this system, an input DNA strand binds to a sticky end, or toehold, on another DNA molecule, which allows it to displace another strand segment from the molecule, which is central to many dynamic DNA devices built to date. Toehold

mediated strand exchange enables control over the kinetics of molecular rearrangement, allowing the engineer to program when and where specific steps take place in a molecular machine.
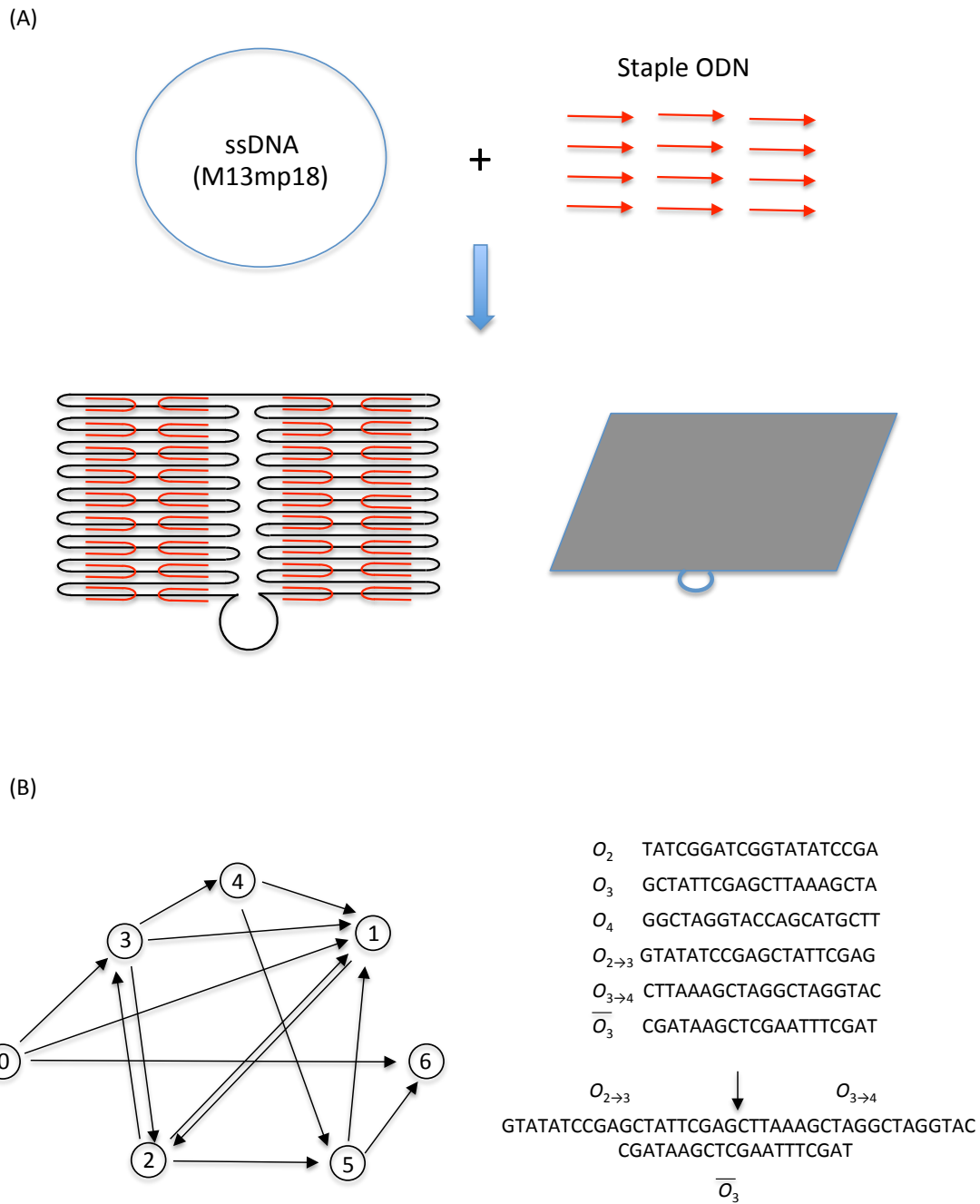
(A)

(B)

Figure. 1. 4 (A) The design principle of DNA origami nanostructure using ssDNA and many staple ODNs (B) DNA motif generation by reciprocal exchange and double-crossover, triple-crossover, and paranemic-crossover DNA motif.

DNA molecular machines

DNA structures that act as building blocks of DNA nanomachines are the simplest and most suitable materials for creating DNA molecular machines. The molecular recognition mechanisms and dynamic properties of these building blocks are described for the elucidation of the design principles of DNA nanomachines. According to driving mechanisms, the DNA nanomachines are divided into two categories. One is buffer-dependent DNA nanomachines, which are triggered by changes in the environment, such as metal ions, pH, and protons. The other is DNA strand fueled nanomachines, in which moving forces are generated through the hybridization of carefully designed DNA strands. A variety of DNA based nanomachines with different functions have been constructed, such as tweezers [82], rotors [83], and walkers [84].

The first example of DNA-based nanomechanical devices was motivated by ethidium inos used as intercalators to induce branch point migration in a four-way junction structure. It is proposed that transition from the B to Z structure drives the motion of the junction. B and Z form DNA are the only conformation of DNA that have been directly observed in functional organisms. The B-Z transition can be realized by alternating purine and pyrimidine sequences in the presence of certain cations such as hexamminecobalt. Seeman et al, demonstrated the first rotary nanomechanical device that was based on B-Z transition triggered by the addition of $[Co(NH3)6]^{3+}$ [85]. This super molecular mechanical device consists of two rigid DNA DX molecules connected by 4.5 double-helical turns. One domain of each DX molecule is attached to the connecting helix. The two unconnected domains of the DX molecule lie on the same side of the central axis in buffer conditions favoring B-DNA, while in the Z-DNA promoting condition, these domains switch to opposite sides of the helix. Each tile of the DX molecules carries a fluorophore, the relative proximity of which is measured to detect the relative repositioning of the domains by means of FRET. The B-Z transition is triggered by changing the concentration of $[Co(NH3)6]^{3+}$ from 0 to 0.25 mM. When the B-Z transition occurs, FRET measurements showed an increase in the separation

between the fluorophores consistent with the expected relative rotation of the tiles by 3.5 turns (Fig. 1.5A).

DNA tweezers are the first report of DNA nanomachines that are not only made from but also driven by fuel DNA strands. In 2000, Bernard Yurke et al, reported a DNA machine that constructed molecular tweezers out of DNA [86]. The DNA tweezers contain three strands: A, B and C. Strand A latches onto half of strand B and half of strand C, and so it joins them all together. Strand A acts as a hinge so that the two arms of strand AB and AC can move. The structure floats with its arms open wide. They can be pulled shut by adding a fourth strand of DNA programmed to stick to both of the dangling, unpaired sections of strand B and C. The closing of the tweezers was proven by tagging strand A at either end with light-emitting molecules that do not emit light when they are close together (Fig. 1.5B).

Sherman and Seeman reported the first DNA walker consisting of two feet connected by a flexible single-stranded scaffold [87]. Each foot is a DNA duplex with a single-stranded extension that is capable of pairing with a complementary strand, called a foothold, equipped on TX molecules, which is referred to as a footpath. The two feet of the bipedal walker are initially attached to the adjacent footpaths by two set strands, each of which has eight base toeholds allowing the set strand to be removed by the unset strand. In the presence of the unset strand that specifically releases the leading foot from the foothold, the leading foot is lifted and connected to the footpath only through the flexible linker. As for the leading foot taking a step forward, the set strand complementary to the leading foot and the next foothold is added to the solution. Consequently, the leading foot moves a 2 nm step along the footpath, leaving an unoccupied foothold in the middle of the two feet. Flexible linkers that are sufficiently long to extend across two footholds ensure the motion. Then similar unset and set operations are used to move the trailing foot ahead. Now the bipedal walker accomplishes an inchworm link movement and is ready to take the next step. More evolved DNA walkers [88-90] were reported, in 2010 Lund et al, reported a molecular

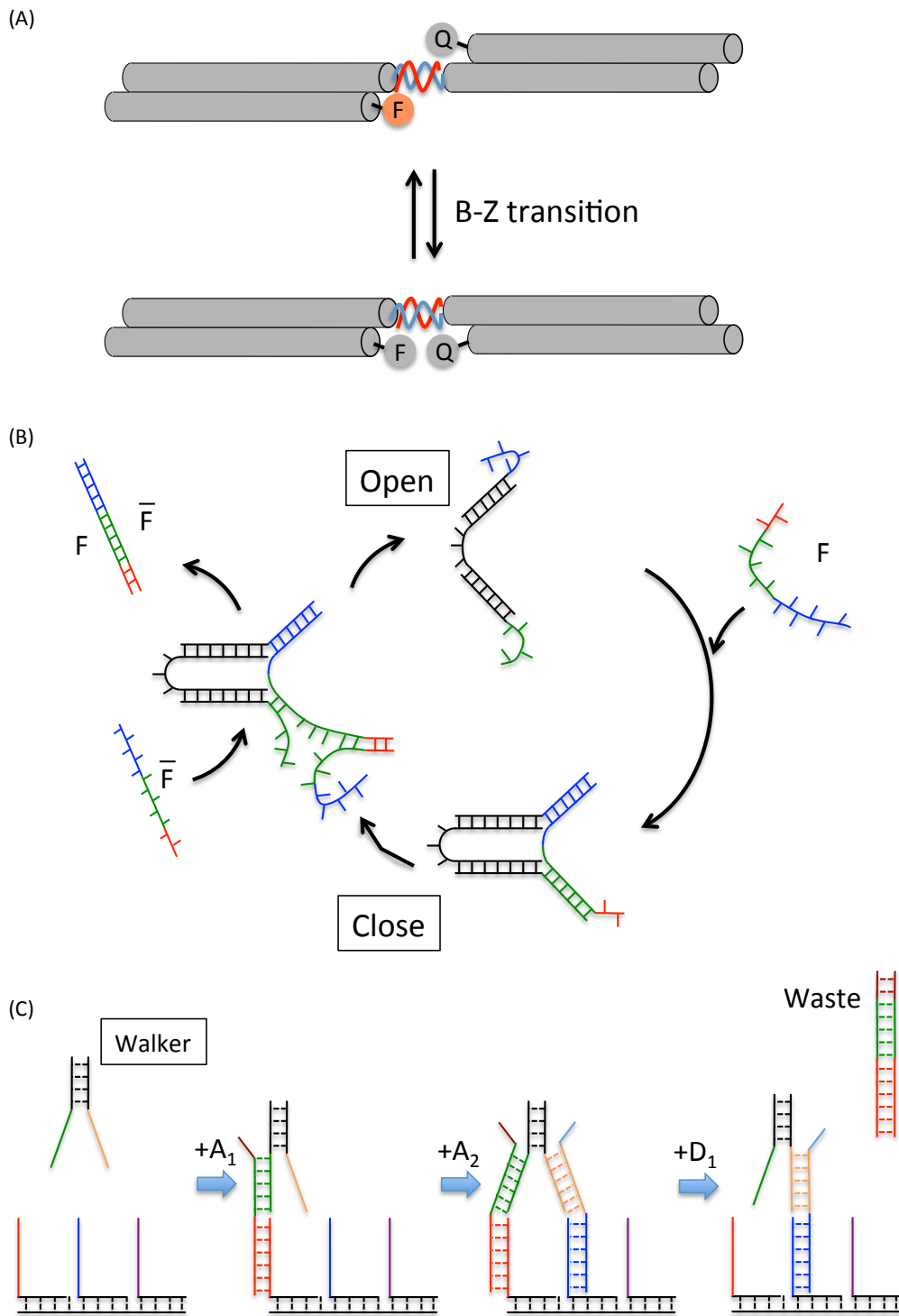spider as a closer step to creating molecular robots [91] (Fig. 1.5C).

Figure. 1.5 (A) Design of the B-Z nanomechanical device. (B) Construction and operation of the molecular tweezers (C) Design of bipedal DNA walker locomotion.

Many projects have attempted to create like a robots ultilizing nucleic acids, proteins, and peptides [92]. The minimum component of a DNA molecular machine is a sensor that senses the external environment, a processer that outputs the power or information based on the sensing information, an actuator that outputs the power or information, and a structure that includes them.

1) Structure

DNA robot requires a compartment in which to integrate multiple DNA devices. The DNA nanostructures explained above and artificial liposomes can be used for this purpose. The DNA structure can specify the size and position correctly as a scaffold, By regulating the form on the nanoscale, reporting the 3D structure, and using two or more origami in a DNA origami method, it is possible to produce large-scale compartments [93,94]. These advantages are based on combining each DNA device bottom-up in a sequence specific manner. Intention of the molecule by DNA hydrogel has also become possible, and discharge of the intention molecule by the dissolution of DNAgel by a DNA strand displacement has also been enabled [95, 96].

2) Sensors

Sensing devices capable of detection, amplification, and conversion of input signals are required for molecular robots to detect weak input signals in noisy environments. In order to realize the sensing devices, molecular robots use DNA/RNA fragments, aptamers and DNA logic gates as information molecules, molecular switches and control logics, respectively. In DNA logic gates, DNA/RNA fragments work as information molecules that carry digitalized information encoded in nucleic acid sequences, DNA/RNA fragments also work as high S/N ratio detectors due to the high selectivity to complementary strands. Aptamers are nucleic acid sequences that recognize specific small molecules. Moreover, artificial nucleic

acids provide molecular robots with a mean of sensing environmental parameters such as the pH, ion concentration and temperature to molecular robot.

3) Intelligence

"Intelligence" is a keywords distinguishes robots and is the most important component in a molecular robot. The processing of sensing information is required as reality intelligence and networking of sensing information is required, ultimately. The intelligence of molecular robots may not exceed the intelligence of bacteria at the first stage. However, we believe that once molecular robots gain such facilities, they will gain knowledge autonomously, and it will only be a matter of time before we see the emergence of more and more intelligent molecular robots.

4) Actuator

Many DNA actuators have been proposed so far, including DNA tweezers, DNA walkers, DNA spiders, and DNA motors. It is possible to control DNA walkers by mean of DNAzymes and DNA strand displacement. The DNA actuators mentioned above are driven by DNA strand displacement and enzymatic reactions. The objectives of actuators are to achieve certain motions at the micro-level. In order to function as a DNA robot's actuator, it is necessary to give a concentration gradient to a substance or to carry a molecule to the target site. The action and discharge of a molecule are performed to influence the surrounding environment.

Objective of this study

Detection, regulation, and manipulation of a nucleic acid has been enabled by the development of DNA nanotechnology. DNA photocrosslinking technology is a useful tool for detection, manipulation, and regulation of DNA or RNA. The 3-cyanovinylcarbazole nucleotide (^{CNV}K) has high phoresponsive ability, whereby the ODN containing ^{CNV}K is photocrosslinked to complementary with 366 nm for a few seconds. We realized the creation of [2+2] photocyclization using ^{CNV}K by the change of structure, creation of a covalent band, and as it has high photoresponse ability, those behaviors were adapted to DNA nanotechnology to create an the application that has a function unrealizable only with a native base.

In Chapter 1, I describe the photopolymerization of oligodeoxynucleotides (ODN) by 3-cyanovinylcarbazole (^{CNV}K) mediated DNA photocrosslinking. DNA is an anion biopolymer that has an important function *in vivo*, and it was configured A, T, G, and C as monomer compounds. Enzymes such as ligase and polymerse play a role in the polymerization of DNA. However, the photopolymerization of ODN using thymidine dimer, required long photoirradiation and a degree of polymerizations. We demonstrated the photopolymerization of ODN by DNA photocrosslinking using ^{CNV}K.
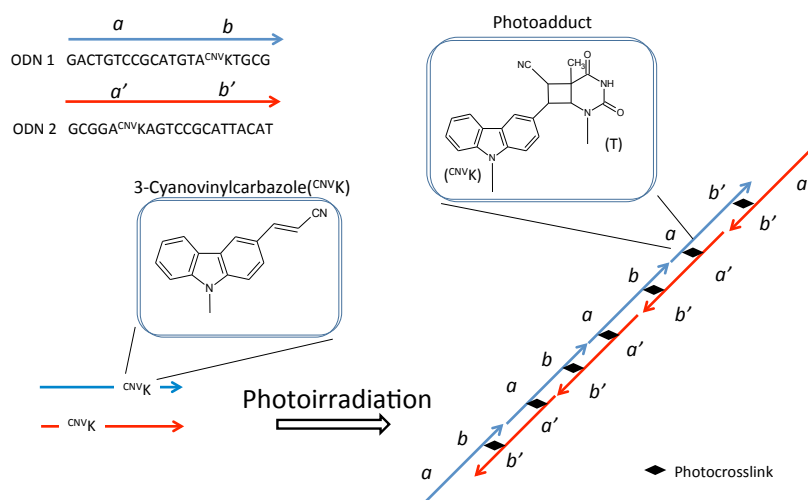
Figure. 1.6 Schematic illustration of photopolymerization of ODNs using photocrosslinking reaction.

In Chapter 2, I describe the creation of a DNA array structure equipped with heat resistance by ultrafast photocrossinking. As formation of the DNA structures was maintained by the hydrogen bonds of the Watson-Crick interaction, they can be used only at temperatures lower than melting temperature in solution. I focused on the creation of a covalent bond using the photocrosslinking reaction with ^{CNV}K, and adapted the photocrosslinking reaction to the DNA structure. I evaluated the thermal stability of DNA structures containing ^{CNV}K before and after 366 nm UV-exposure by denaturing PAGE and melting curve.
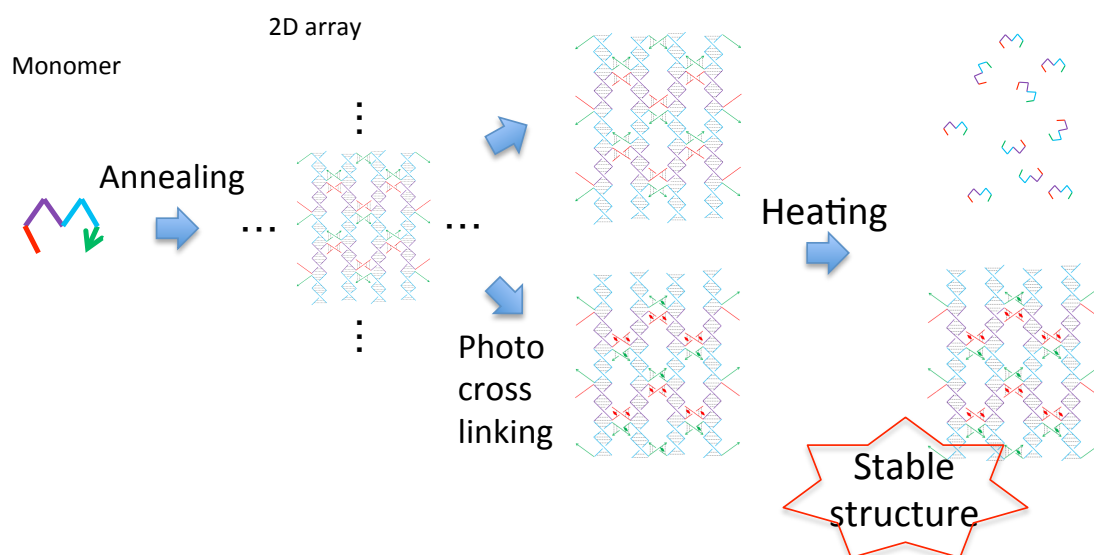
Figure. 1.7 Schematic diagram of creation of DNA array structure equipped with heat resistance using 3-cyanovinylcarbazole.

In Chapter 3, I describe 19F-NMR chemical shift imaging via photocrosslinking reaction using trifluorothymidine and 3-cyanovinylcarbazole. The photocrosslinking change the spatial vicinity and electron environment of target thymidine so that I demonstrated the chemical shift imaging of nucleic acid was demonstrated using the photocrosslinking reaction of ^{CNV}K. The ^{TF}T was selected as 19F-labeled DNA from the viewpoint of the structure (fluorine was near the cyclobutan ring) and sensitivity (it has three equivalent fluorine).
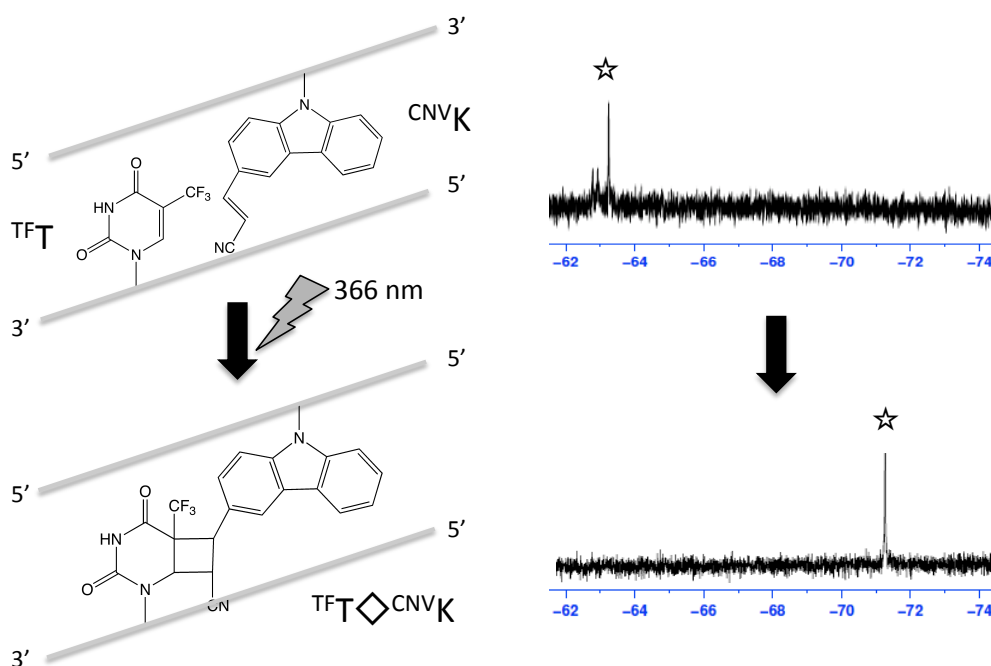
Figure. 1.8 Schematic diagram of the chemical shift imaging using DNA photocrosslinking.

31

In Chapter 4, I describe accelerated DNA strand displacement by ultrafast photocrosslinking reaction using ^{CNV}K. The DNA strand displacement was basic reaction for construction of the DNA circuit so acceleration was required following the scale-up of the DNA circuit. However, the branch migration in DNA strand displacement was an equilibrium reaction in each hybridization and dissociation of Watson-Crick base pairing. The photochemical regulation of DNA strand displacement by DNA photocrosslinking was demonstrated since the equilibrium reaction let to a non-equilibrium.
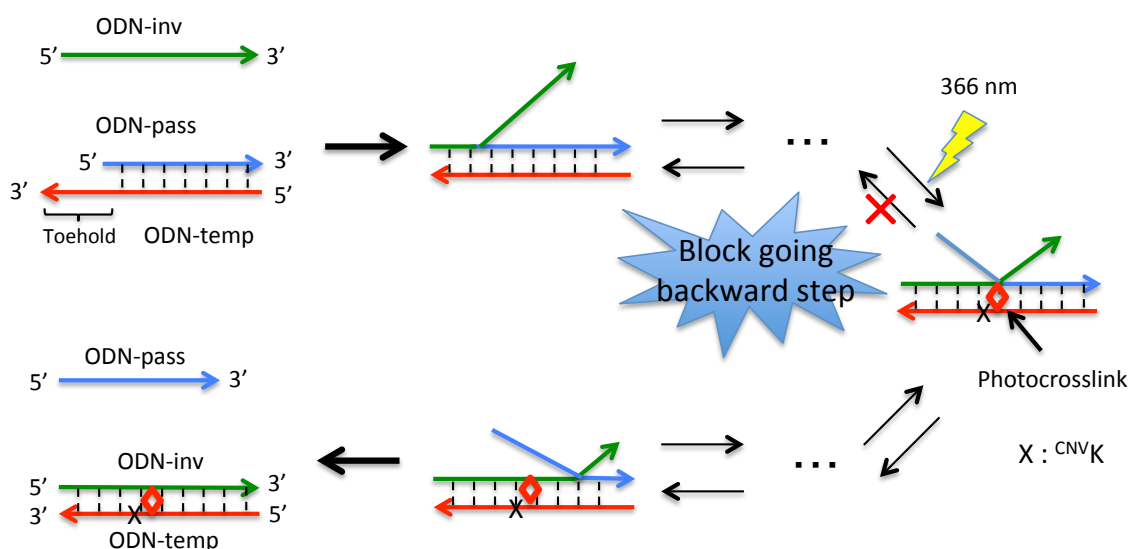
Figure. 1.9 Schematic diagram of photochemical regulation of DNA strand displacement using DNA photocrosslinking.

In Chapter 5, I describe the cleavage reaction of photocrosslinking using ^{CNV}K assisted branch migration. As the photosplitting reaction of ^{CNV}K was required the 312 nm UV-exposure and heating, the UV-light and heating became barriers in using photoreactions with ^{CNV}K *in vivo*. Heating is required because the photoreaction of ^{CNV}K assumes a photostationary state in a wide range wavelengths, so it was necessary to dissociate photosplitted ODN. Therefore, I demonstrated that the photosplitting of photocrosslinked DNA using branch migration instead of heating.
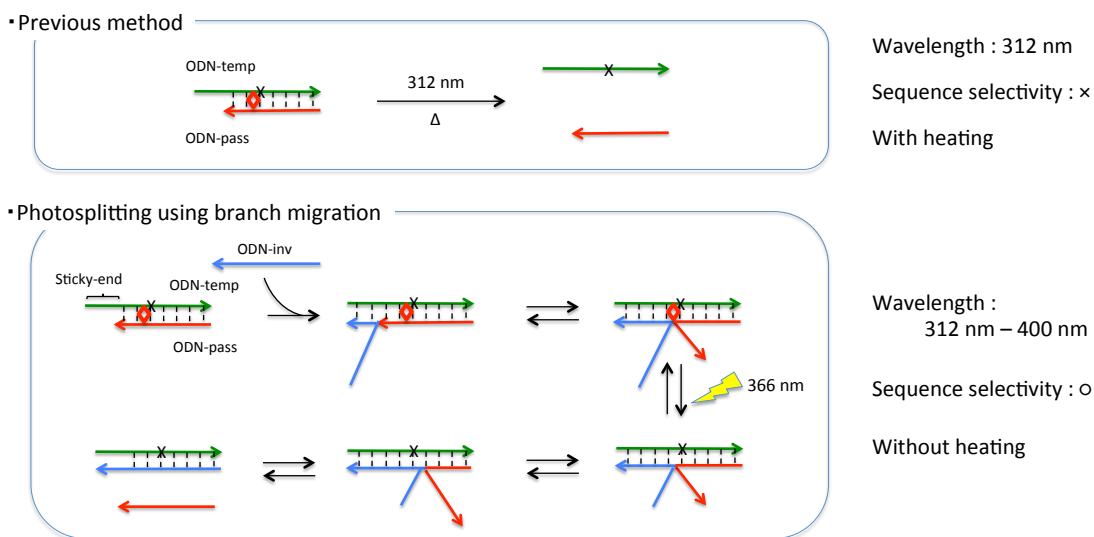
Figure. 1.10 Schematic diagram of photosplitting using branch migration.

In Chapter 6, I describe the template for reversible photochemical ligation of oligodeoxynucleotides. Template directed chemical ligation has been used and, especially, photochemical ligation has many useful characteristics. Previous photochemical ligation required long-term photoirradiation so that artificial nucleotides were required to have high photoresponsive ability.

I reported photoresponsive artificial nucleotide 5-carboxydeoxyuridine (^{CV}U), and demonstrated the photochemical ligated a longer ODN from four smaller different ODNs with ^{CV}U and it has template dependency.
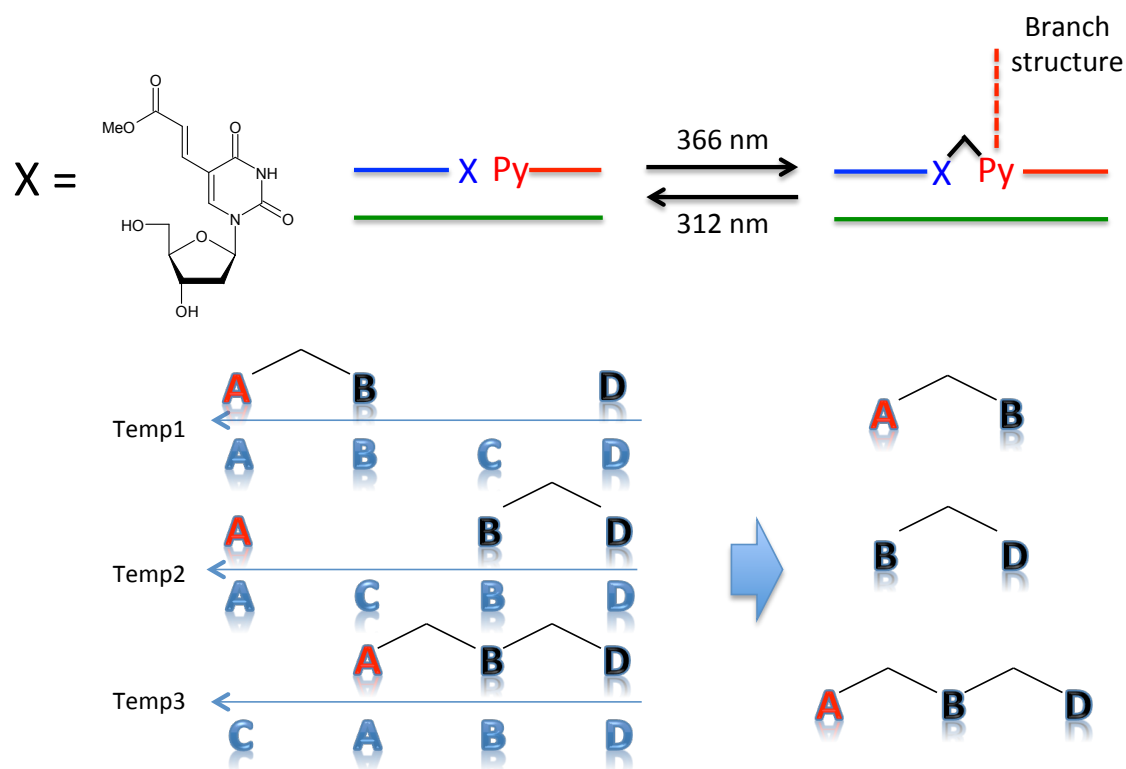
Figure. 1.11 Schematic drawing of template directed photochemical ligation of oligonucleotide.

Reference

1. Ralf D, Discovering DNA: Friedrich Miescher and the early years of nucleic acid research. *Hum. Genet.*, **2008**, 122, 565-581.

2. Jones M E, Albrecht K, A biographical sketch. *Yale. J. Biol. Med.*, **1953**, 26, 80-97.

3. Soyfer V N, The concequence of political dictatorship for Russian science. *Nat. Rev. Genet.*, **2001**, 2, 723-729.

4. Simoni R D, Hill R L, Vaugha M, The Structure of Nucleic Acids and Many Other Natural Products: Phoebus Aaron Levene, *J. Biol. Chem.*, **2002**, 277, 11.

5. Hall K, William Astbury and the biological significance of nucleic acids 1938-1951, *Stud. Hist. Phlios. Biol. Biomed. Sci.*, **2011**, 42, 119-128.

6. Watson J D, Crick F H, A Structure for Deoxyribose Nucleic Acid, *Nature*, **1953**, 171, 737-738.

7. Crick F H, On Proteine Synthesis, *Symp. Soc. Exp. Biol. XII.*, **1958**, 139-163.

8. Sanger F, Nicklen S, Coulson A R, DNA sequencing with chain-terminating inhibitors, *Proc. Natl. Acad. Sci.,* **1977**, 74, 5463-5467.

9. Integration of cytogenetic landmarks into the draft sequence of the human genome. *Nature,* **2001**, 15, 953-958.

10. The sequence of the human genome, *Science*, **2001**, 16, 1304-1351.

11. Letsinger R L, Mahadeven V, Olgonucleotide synthesis on a polymer support. *J. Am. Chem. Soc.*, **1965**, 87, 3526-3527.

12. Letsinger R L, Mahadeven V, Stepwise synthesis of oligodeoxyribonucleotides on an insoluble polymer support. *J. Am. Chem. Soc.*, **1966**, 88, 5319-5324.

13. Matteucci M D, Caruthera M H, The synthesis of oligodeoxypyridines on a polymer support. *Tetrahedron Lett.,* **1980**, 21, 719-722.

14. Matteucci M D, Caruthers M H, Studies on nucleotide chemistry iv: Synthesis of deoxyoligonucleotides on a polymer support. *J. Am. Chem. Soc.,* **1981**, 103, 3185-319.

15. Ellington A D, Szostak J W, Invitro selection of RNA molecules that bind specific ligands. *Nature*, **1990**, 346, 818-822.

16. Bock L C, Griffin L C, Latham J A, Vermaas E H, Toole J J, Selection of single-stranded DNA molecules that bind and inhibit human thrombin. *Nature*, **1992**, 355, 564-566.

17. Kruger K, Grabowski P J, Zaug A J, Sands J, Gottschling D E, Cech T R, Self-Splicing RNA auto-excision and auto-cyclization of the ribosomal –RNA intervening sequence of tetrahedrona. *Cell*, **1982**, 31, 147-157.

18. Santoro S W, Joyce G F, Sakthivel K, Gramatikova S, Barbas C F, RNA cleavage by a DNA enzyme with extended chemical functionality. *J. Am. Chem. Soc.*, **2000**, 122, 2433-2439.

19. Carmi N, Balkhi S R, Breaker R R, Cleaving DNA with DNA. *Proc. Natl. Acad. Sci.*, **1998**, 95, 2233-2237.

20. Flynn-Charlebois A, Wang Y M, Prior T K, Rashid I, Hoadley K A, Coppins R L, Wolf A C, Silverman S K, Deoxyribozymes with 2'-5' RNA ligase activity. *J. Am. Che. Soc.*, **2003**, 125, 2444-2454.

21. Cuenoud B, Szostak J W, A DNA metalloenzyme with DNA-ligase activity. *Nature*, **1995**, 375, 611-614.

22. Travascio P, Bennet A J, Wang D Y, Sen D, A ribozyme and catalytic DNA with peroxidase activity: active sites versus cofactor-binding sites. *Chem. Biol.*, **1999**, 6, 779-787.

23. Kumar R, Singh S K, Koshkin A A, Rajwanshi V K, Meldgaard M, Wengel J, The dirst analogues of LNA (Locked nucleic acids) phosphorothioate-LNA and 2'-thio-LNA. *Bioorg. Med. Chem. Lett.*, **1998**, 8, 2219-2222.

24. Nielsen P E, Egholm M, Berg R H, Buchardt O, Sequence-selective recognition of DNA by strand displacement with a thymine-substituted polyamide. *Science*, **1991**, 254, 1497-1500.

25. Tolstrup N, Nielsen P S, Kolberg J G, Frankel A M, Vissing H, Kauppinen S, OligoDesign: Optimal design of LNA (locked nucleic acid) oligonucleotide capture probes for gene expression profiling. *Nucleic. Acids. Res.*, **2003**, 31, 3758-3762.

26. Cerqueria L, Azevedo N F, Almeida C, Jardim T, Keevil C W, Vieria M J, DNA mimics for the rapid identification of microorganisims by fluorescence in situ hybridization (FISH). *Int. J. Mol. Sci.*, **2008**, 10, 1944-1960.

27. Reynisson E, Josefsen M H, Krause M, Hoorfar J, Evalution of probe chemistries and platforms to improve the detection limit of real-time PCR. *J. Microbiol. Methods.*, **2006**, 66, 206-216.

28. Karras J G, Maier M A, Lu T, Watt A, Manoharan M, Peptide nucleic acids are potent modulator s of endogenous pre-mRNA splicing of the murine interleukin-5

receptor-chain. *Biochemistry*, **2001**, 40, 7853-7859.

29. Mologni L, Marchesi E, Nielsen P E, Gambacorti-passerini C, Inhibition of promyelocytic leukemia (PML)/retinoic acid receptor-alpha and PML expression in acute promyelocytic leukemia cells by anti-PML peptidenucleic acid. *Cancer. Res.*, **2001**, 61, 5468-5473.

30. Hobartner C, Silverman S K, Modulation of RNA Tertiary Folding by incorporation of caged Nucleotides. *Angew. Chem. Int. Ed.*, **2005**, 44, 7305-7309.

31. Mikat V, Heckel A, Light-dependent RNA interference with nucleobase-caged siRNAs. *RNA,* **2007**, 13, 2341-2347.

32. Deiters A, Garner R A, Lusic H, Govan J M, Dush M, Nascone-Yoder N M, Yoder J A, Photocaged Morpholino Oligomers for the Light-Regulation of gene Function in Zebrafish and Xenopus Enbryos. *J. Am. Chem. Soc.,* **2010**, 132, 15644-15650.

33. Yamana K, Yoshikawa A, Nakano H, Synthesis of a new photoisomerizable linker for connecting two oligonucleotide segments. *Tetrahedron Lett*, **1996**, 37, 637-640.

34. Lee B L, Blake K R, Miller P S, Interaction of psoralen-derivatized oligonucleotide methylphosphonates with synthetic DNA containing a promoter for T7 RNA polymerase. *Nucleic. Acdis. Res.*, **1988**, 16, 10681-10697.

35. Kamiya Y, Asanuma H, Light-driven DNA nanomachine with a photoresponsive molecular engine. *Acc. Chem. Res.*, **2014**, 47, 1663-1672.

36. Liang X, Wakuda R, Fujioka K, Asanuma H, Photo-regulation of DNA transcription by using photoresponsive T7 promoters and clarification of its mechanism. *FEBS. J.,* **2010**, 277, 1551-1561.

37. Liu J, Geng Y, Pound E, Gyawall S, Ashton J R, Hickey J, Woolley A T, Harb J N, Metallization of branched DNA origami for nanoelectronic circuit fabrication. *ACS. Nano.*, **2011**, 5, 2240-2247.

38. Ihara T, Fujii T, Mukae M, Kitamura Y, Jyo A, Photochemical ligation of DNA conjugates through anthracene cyclodimer formation and its fidelity to the template sequence. *J. Am. Chem. Soc.,* **2004**, 126, 8880-8881.

39. Ihara T, Mukae M, Tabara M, Kitamura Y, Jyo A, Photochemical ligation between anthracene-DNA conhugates and its analytical application to gene analysis. *Nucleic. Acids. Symp. Ser. (Oxf).,* **2005**, 49, 41-42.

40. Yoshimura Y, Fujimoto K, Ultrafast Reversible Photocrosslinking Reaction Toward in Situ DNA Manipulation, *Org. Lett.*, **2008**, 10, 3227-3230.

41. Fujimoto K, Yamada A, Toshimura Y, Tsukaguchi T, Sakamoto T, Details of the ultra-fast DNA photocrosslinking reaction of 3-cyanovinylcarbazole nucleotide; Cis-trans isomeric effect and the application for SNP based genotyping. *J. Am. Chem. Soc.*, **2013**, 135, 16161-16167.

42. Fujimoto K, Kishi S, Sakamoto T, Genometric Effect on the Photocrosslinking Reaction between 3-cyanovinylcarbazole Nucleoside and Pyrimidine based in DNA/RNA Heteroduplex. *Photochemistry and Photobiology*, **2013**, 8, 1095-1099.

43. Fujimoto K, Kaoru Konishi-Hiratsuka, Sakamoto T, Quick, Selective and Reversible Photocrosslinking Reaction between 5-methylcytosine and 3-cyanovinylcarbazole in DNA Double Strand. *Int. J. Mol. Sci.,* **2013**, 14, 5765-5774.

44. Shigeno A, Sakamoto T, Yoshimura Y, Fujimoto K, Quick Regulation of mRNA Functions by a Few Seconds of Photoirradiation. *Organic & Biomolecular Chemistry*, **2012**, 10, 7820-7825.

45. Kashida H, Doi T, Sakakibara T, Hayashi T, Asanuma H, p-Stilbazole moieties as artificial base pairs for photocrosslinking of DNA duplex. *J. Am. Chem. Soc.,* **2013**, 135, 7960-7966.

46. Griffin L C, Tidmarsh G F, Bock. L C, Toole J J, Leung L L, In vivo anticoagulant of a novel nucleotide-based thrombin inhibitor and demonstration of regional anticoagulation in extracorporeal circuits. *Blood.*, **1993**, 81, 3271-3276.

47. Breaker R R, Joyce G F, A DNA enzyme that cleaves RNA, *Chem. Biol.*, **1994**, 1, 223-220.

48. Beaudry A A, Joyce G F, Directed evolution of an RNA enzyme. *Science*, **1992**, 257, 635-641.

49. Seeman N C, Nucleic acids junctions and lattices. *J. Theor. Biol.*, **1982**, 99, 237-247

50. Seeman N C, DNA in a material world. *Nature*, **2003**, 421, 427-431.

51. Seeman N C, An overview of structural DNA nanotechnology. *Mol. Biotechnol.*, **2007**, 37, 246-257.

52. Seeman N C, Nanomaterials based on DNA. *Annu. Rev. Biochem.*, **2010**, 79, 65-87.

53. Krishnan Y, Simmel F C, Nucleic acid based molecular devices. *Angew. Chem. Int. Ed.*, **2011**, 50, 3124-3156.

54. Seeman N C, Nanotechnology and the double helix. *Scientific American*, **2004**, 290, 64-75.

55. Seeman N C, DNA engineering and its application to nanotechnology. *Trends. Biotechnol.*, **1999**, 17, 437-443.

56. Seeman N C, Structual DNA nanotechnology: growing alone with Nano Letters. *Nano. Lett.*, **2010**, 10, 1971-1978.

57. Ma R –I, Kallenbach N R, Sheardy R D, Petrillo M K, Seeman N C, 3-Arm nuclei acid junctions are flexible. *Nucl. Acdis. Res*., **1986**, 14, 9745-9753.

58. Petrillo M L, Newton C J, Cunningham R P, Ma R –I, Kallenbach N R, Seeman N C, The ligation and flexibility of 4-arm DNA junctions. *Biopolymers,* **1988,** 27, 1337-1352.

59. Chen J, Seeman N C, The synthesis from DNA of molecue with the connectivity of a cube. *Nature*, **1991**, 350, 631-633.

60. Zhang Y, Seeman N C, The construction of a DNA truncated octahedron. *J. Am. Chem. Soc.,* **1994**, 116, 1661-1669.

61. Goodman R P, Schaap I A T, Tardin C F, Erben C F, Berry R M, Schmidt C F, Turberfield A J, Rapid chiral assembly of rigid DNA building blocks for molecular nanofabrication. *Science,* **2005**, 310, 1661-65.

62. Shih W M, Quispe J D, Joyce G F, DNA that folds into a nanoscale octahedron. *Nature*, **2004**, 427, 618-621.

63. Douglas S M, Dietz H, Liedl T, Hogborg B, Graf F, Shih W M, Self-assembly of DNA into nanoscale three-dimensional shape. *Nature*, **2009**, 459, 414-418.

64. He Y, Ye T, Su M, Zhang C, Ribbe A E, Jiang W, Mao C, Hierarchical self-assembly of DNA into symmetric supermolecular polyhedron. *Nature*, **2008**, 452, 198-201.

65. Erben C M, Goodman R P, Turberfield A J, Single molecule protein encapsulation in a rigid DNA cage. *Angew. Chem. Int. Ed.*, **2006**, 45, 7414-7417.

66. Andersen E S, Dong M, Nielsen M M, Jahn K, Subramani R, Mamdouh W, Golas M M, Sander B, Stark H, Olivera CLP, Pedersen J S, Birkedal V, Besenbacher F, Gothelf K V, Kjiems J, Self-assembly of a nanoscale box with a controllable lid. *Nature*, **2009**, 459, 73-76.

67. Seeman N C, The design of single-stranded nucleic acid knots. *Molec. Eng.*, **1992**, 2, 297-307.

68. Du S M, Stollar B D, Seeman N C, A synthetic DNA molecule in three knotted topologies. *J. Am. Chem. Soc.,* **1995**, 117, 1194-1200.

69. Mao C, Sun W, Seeman N C, Assembly of Borromean rings form DNA. *Nature*, **1997**, 386, 137-138.

70. Rothemund P W, Folding DNA to create nanoscale shapes and patters. *Nature*, **2006**, 440, 297-302.

71. Adleman L M, Molecular computational of solutions to combinational problems. *Science*, **1994**, 266, 1021-1024.

72. Lovgren S, Computer made form DNA and Enzyme, *National Geograhic,* **2003**-02-24.

73. Benson Y, Gil B, Ben-Dor U, Adar R, Shapiro E, An autonomous molecular computer for logical control of gene expression. *Nature*, **2004**, 429, 423-429.

74. Benenson Y, Paz-Elizur T, Adar R, Keinan E, Livneh Z, Shapiro E, Programmable and autonomous computing machine made of biomolecules. *Nature*, **2001**, 414, 430-434.

75. Sakamoto K, Kiga D, Komiya K, Gouzo H, Yokoyama S, Ikeda S, Sugiyama H, Hagiya M, State Yransitions by molecules. *Biosystems*, **1999**, 52, 81-91.

76. Takinoue M, Suyama A, Hairpin-DNA Memory Using Molecular Addressing. *Small*, **2006**, 2, 1244-1247.

77. Qian L, Winfree E, Bruck J, Neural network computation with DNA strand displacement cascades. *Nature*, **2011**, 475, 368-372.

78. Stojanovic M, Stefanovic D, A Deoxyribozyme-based Molecular Automaton. *Nature Biotechnology*, **2003**, 21, 1069-1074.

79. Ogasawara S, Fujimoto K, Autonomous DNA computing Machine based on Photochemical Gate Transition. *J. Am. Chem. Soc.*, **2008**, 130, 10050-10051.

80. Montagnue K, Plasson R, Sakai Y, Fujii T, Rondelez Y, Programming an in vitro DNA oscillator using a molecular networking strategy. *Mol. Syst. Biol.*, **2011**, 466, 1-7.

81. Liang X G, Nishioka H, Takenaka N, Asanuma H, A DNA nanomachine powered by light irradiation. *ChemBioChem*, **2008**, 9, 702-705.

82. Yurke B, Yurberfield A J, Mills A P, Simmel F C, Neumann J, A DNA-fuelded molecular machine made of DNA. *Nature*, **2000**, 406, 605-608.

83. Shin J S, Pierce N A, A synthesis DNA walker for molecular transport. *J. Am. Chem. Soc.*, **2004**, 126, 10834-10835.

84. Mao C D, Sun W Q, Shen Z Y, Seeman N C, A nanomechanical device based on

the B-Z transition of DNA. *Nature*, **1999**, 397, 144-146.

85. Ogura Y, Nishimura T, Tanida J, Self-contained photonically-controlled DNA tweezers. *Appl. Phys. Express.*, **2009**, 2, 25004-25006.

86. Sherman W B, Seeman N C, A precisely controlled DNA biped walking device. *Nano. Lett.*, **2004**, 1203-1207.

87. Yin P, Yan H, Daniell X G, Turberfield A J, Reif J H, A unidirectional DNA walker that moves autonomously along a track. *Angew. Chem. Int. Ed.*, **2004**, 43, 4906-4911.

88. Yin P, Choi H M T, Calvert C R, Pierce N A, Programming biomolecular self-assembly pathways, *Nature*, **2008**, 451, 318-322.

89. Omabegho T, Sha R, Seeman N C, A bipedal DNA Brownian motor with coordinated legs. *Science*, **2009**, 324, 67-71.

90. Lund K, Manzo A J, Dabby N, Michelotti N, Johnson-Buck A, Nahgreave J, Taylor S, Pei R, Stojanovic M N, Walter N G, Winfree E, Yan H, Molecular robots guided by prescriptive landscapes, *Nature*, **2010**, 465, 206-210.

91. Murata S, Konagaya A, Kobayashi S, Saito H, Hagiya M, Molecular Robotics: A New Paradigm for Artifacts. *New Generation Computing*, **2013**, 31, 27-45.

92. Anderson E S, Dong M, Nielsen M M, Jahn K, Subramani R, Mamdouh W, Golas M M, Sander B, Stark H, Oliveria C L, Pedersen J S, Birkedal V, Besenbacher F, Gothelf K V, Kjems J. Self-assembly of a nanoscale DNA box with a controllable lid. *Nature*, **2009**, 459,73-76.

93. Zhao Z, Liu Y, Yan H, Organizing DNA origami tiles into larger structures using preformed scaffold frames. *Nano. Lett.*, **2011**, 11, 2997-3002.

94. Lee J B, Peng S, Yang D, Roh Y H, Funabashi H, Park N, Rice E J, Chen L, Long R, Wu M, Luo D, A mechanical metamaterial made form a DNA hydrogel. *Nat. Nanotechnol.*, **2012**, 12, 816-820.

95. Um S H, Lee J B, Park N, Kwon S Y, Umbach C C, Luo D, Enzyme-catalysed assembly of DNA hydrogel. *Nat. Materials.*, **2006**, 5, 797-801.

96. MicroRNA Functions by a Few Seconds of Photoirradiation. *Organic & Biomolecular Chemistry*, **2012**, 10, 7820-7825.

Chapter 1.

Rapid Photopolymerization of Oligonucleotides by

3-Cyanovinylcarbazole mediated DNA Photocrossling

1.1. Introduction

A photopolymer is a molecule that changes its chemical properties and molecular weight by photoirradiation. Photopolymerization is a widely used technology in applications for photoresist, dental treatment, and 3D-image print materials [1-3]. The monomer residues such as polyvinyl cinnamate and acrylate epoxides are polymerized by photoirradiation [4,5]. Researches on investing new materials for application with high sensitivity and size regulation have received much attention in recent years.

DNA is one of the most important biopolymers in living cells. This biopolymer is consists four deoxynucleotides such as adenine(A), thymine(T), guanine(G), and cytosine(C), and forms a helical duplex structure in cell. Two DNA polymers with complementary base sequences can be paired following the strict Watson-Crick rule, A-T and G-C, resulting in the formation of the DNA double helix. The structure and conformation of DNA can be rationally programmed by the sequence design [6,7]. It was possible to regulate the structure on the nano-scale as shown in the DX tile and DNA origami reported by Seeman and Rothemund [8-12]. However, these structures are self-assembled by the hydrogen bond without the covalent bond.

In contrast, a polymerization method from short DNA strand using enzyme and thymine dimer has been reported. A long DNA strand was created from a short oligodeoxynucleotide (ODN) strand or monomer residues by the ligase and polymerase [13-16]. In 1982, Lewis and Hanawalt reported the ligation of ODNs by pyrimidine dimers using photoirradiation [17,18]. A nucleic acid polymer based on the photodimerization of pyrimidine base units was also reported toward photoresists [19]. When the research was first strand, this photopolymerization based on thymidine dimer required long photoirradiation, and the number of polymerization was negligible. Later, some photoresponsive artificial nucleotides based on the thymidine dimer were reported to be photopolymerized from ODNs with a shorter photoirradiation time [20,21].

We have already reported on the photoresponse in artificial nucleotide 3-cyanovinylcarbazole (^{CNV}K), which can photocrosslink to a complementary DNA

strand via [2+2] photocycloaddition between ^{CNV}K and pyrimidine base in a complementary strand with 1 second of 366 nm irradiation [22,23]. We demonstrated the photopolymerization of ODNs using ^{CNV}K irradiation at 366 nm and photodegradation of photopolymerized DNA irradiation at 312 nm. We also demonstrated the feasibility of photopolymerized DNA-RNA hetero-duplex incorporating micro RNA (miRNA) in a sequence specific manner.

1.2. Materials and Method

General

^{1}H NMR spectra were measured with AVANCE III NMR 400 (Bruker, 400 MHz) spectrometer. Mass spectra were recorded on a Voyager-DE PRO-SF, Applied Biosystems. Irradiation was performed by UV-LED (OMRON, ZUV, 366 nm, 1.6 W/cm^{2}). HPLC was performed on a Chemcobond 5-ODS-H column (10 × 150 mm, 4.6 × 150 mm) or a Chemcosorb 5-ODS-H column (4.6 × 150 mm) with a JASCO PU-980, HG-980-31, DG-980-50 system equipped with a JASCO UV 970 detector at 260 nm. The reagents for the DNA synthesizer such as A, G, C, T-β-cyanoethyl phosphoramidite, and CPG support were purchased from Glen Research. Calf intestine alkaline phosphatase (AP) was purchased from Promega. Nuclease P1 was purchased from Yamasa.

3-Iodocarbazole

In an 1 L two neck flask was placed carbazole(8.0 g, 47.9 mmol) and ethanol(700 mL). The mixture was stirred at 65°C and added iodine(6.08 g, 23.9 mmol), sodium periodate(3.75 g, 11.9 mmol), and sulfuric acid (2.48 mL) in ethanol(100 mL)were added after the solved. The reaction was monitored by TLC(Hex:AcOEt=4:1) to confirmed the loss of raw materials, and an ethanol solution(100 mL) of NaOH(3.0 g) was added there to neutralization. Ethanol was removed, and then reaction solution was extracted two times with chloroform. The extract was washed two times with water. The organic phase was dried over Na$_2$SO$_4$, and the solvent was removed. The residue was purified by column chromatography (HexH:AcOEt=4:1), and thus 3-Iodocarbazole (1.83 g, 42%) was obtained as a white powder. 3-Iodocarbazole: ^{1}H NMR (DMSO-d$_6$) δ 11.4 (s, 1H), 8.49 (d, 1H, J=1.7 Hz), 8.14 (d, 1H, J=8.0 Hz), 7.62 (dd, 1H, J=8.4, 1.7 Hz), 7.48 (d, 1H, J=8.0 Hz), 7.40 (m, 1H), 7.33 (d, 2H, J=8.4 Hz), 7.16 (m, 1H).

3-Cyanovinylcarbazole

In an 80 mL glass vessel was placed palladium acetate(498mg, 2.21 mmol), DMF(9.72 mL), 3-Iodocarbazole(6.5 g, 22.2 mmol), tributylamine(5.28 mL, 2,21 mmol), and acerylonitrile(10.3 mL, 55.5 mmol). The vessel was sealed and placed into the microwave cavity. Initial microwave irradiation of 60 W was used, the temperature being ramped from room temperature to the desired temperature of 160°C. Once this was reached, the reaction mixture was held at this temperature for 10 min. After allowing the mixture to cool to room temperature. After the reaction mixture was evaporated, the residue was chromatograph on a silica gel using hexane/AcOEt (3:1 v/v) an elute to give 3-cyanovinylcarbazole(4.21 g, 19.3 mmol) as white powder. ^{1}H-NMR(400 MHz, DMSO) δ 11.6 (s, 1H), 8.44 (s, 1H), 8.11 (d, 1H, J = 8.0 Hz), 7.75 (d, 1H, J =16.5 Hz), 7.69-7.72 (m, 1H), 7.40-7.52 (m, 3H), 7.19-7.24 (m, 1H), 6.36 (d, 1H, J = 16.7 Hz).

3-Cyanovinylcarbazole-1'-β-deoxyriboside-3',5'-di-(p-toluoyl)ester

To a solution of potassium hydroxide(3.48 g, 62 mmol) and Tris[2-(2-methoxyethoxy)ethyl]amine(0.18 mL, 0.57 mmol) in Acetonitrile(200 mL) was added 3-cyanovinylcarbazole(4.2 g, 19.3 mmol) at room temperature and the reaction mixture was stirred at room temperature for 30 min. To this reaction mixture was added chlorosugar(7.71 g, 19.8 mmol) at room temperature and stirred for 3 hours. After the reaction mixture was evaporated, the residue was chromatographed on a silica gel using chloroform as eluted to give 3-cyanovinycarbazole-1'-β-deoxyriboside-3',5'-di-(p-toluoyl)ester(8.1 g, 14.2 mmol) as yellow oil. ^{1}H-NMR(400 MHz, CDCl$_3$) δ 8.09 (s, 1H), 8.02 (d, 2H, J = 8.4 Hz), 7.89 (d, 2H, J = 8.4 Hz), 7.62-7.65(m, 1H), 7.62 (d, 1H, J = 8.8 Hz), 7.49 (d, 1H, 16.5 Hz), 7.25-7.31 (m, 7H), 7.17-7.20(m, 1H), 6.68 (dd, 1H, J = 9.3, 5.8 Hz), 5.78 (m, 1H), 5.76 (d, 1H, J = 16.5Hz), 4.91 (dd, 1H, J = 12.4, 2.7 Hz), 4.78(dd, 1H, J = 12.4, 3.3 Hz), 34.55-4.57 (m, 1H), 3.09-3.20 (m, 1H), 2.45-2.52 (m, 1H), 2.45 (s, 3H), 2.44 (s, 3H).

3-Cyanovinylcarbazole-1'-β-deoxyriboside

To a solution of 3-cyanovinycarbazole-1'-β-deoxyriboside-3',5'-di-(p-toluoyl)ester (8.1 g, 14.2 mmol) in methanol(580 mL), was added 0.5 M methanolic sodium methoxide (85 mL, 43 mmol) and chloroform (52 mL) at room temperature and the reaction mixture was stirred at room temperature for 2 h. After the reaction mixture evaporated, the residue was chromatographed on slica gel using $CHCl_3/CH_3OH$ (9:1 v/v) as elutet to giva 3-cyanovinylcarbazole (4.2 g, 12.6 mmol) as a white powder. ^{1}H-NMR (400 MHz, $CDCl_3$) δ 8.12 (d, 1H, J = 1.7 Hz), 8.06 (d, 1H, J = 7.7 Hz), 7.59 (d, 1H, J = 9.1 Hz), 7.43-7.57 (m, 4H), 7.26-7.31 (m, 1H), 6.64 (dd, 1H, J = 8.2, 6.9 Hz), 5.87 (d, 1H, J = 16.5 Hz), 4.77-4.82 (m, 1H), 3.95-4.06 (m, 3H), 2.95 (dt, 1H, J = 14.0, 8.2 Hz), 2.30 (ddd, 1H, J = 14.0, 6.9, 3.3 Hz).

5'-O-(4,4'-dimethoxytrityl)-3-Cyanovinylcarbazole-1'-β-deoxyriboside

To a solution of 3-cyanovinylcarbazoe-1'-β-deoxyriboside(4.2 g, 12.6 mmol) in pyridine (30 mL) was added a solution of 4,4'-dimethoxytrityl chloride(5.11 g, 15.1 mmol) and 4-(dimethylamino)pyridine (0.3 g, 2.5 mmol), in pyridine (30 mL) at room temperature and the reaction mixture was stirred at room temperature for 24 h. After the reaction mixture was evaporated, the residue was chromatographed on a silica gel usgin $CHCl_3/CH_3OH$ (99:1 v/v) as eluent to give 5'-O-(4,4'-dimethoxytrityl)-3-Cyanovinylcarbazole-1'-β-deoxyriboside (6.0 g, 9.43 mmol) as yellow powder. ^{1}H-NMR (400 MHz, $CDCl_3$) δ 8.07 (d, 1H, J = 1.7 Hz), 8.02-8.05 (m, 1H), 7.71 (d, 1H, J = 8.5 Hz), 7.62-7.65 (m, 1H), 7.45-7.52 (m, 3H), 7.33-7.37 (m, 4H), 7.25-7.28 (m, 4H) 7.12 (dd, 1H, J = 8.8, 1.7 Hz) 6.61 (dd, 1H, J = 8.2, 6.3 Hz) 5.77 (d, 1H, J = 16.7 Hz) 4.80-4.82 (m, 1H), 4.05-4.07 (m, 1H), 3.77 (s, 3H), 3.76 (s, 3H), 3.56-3.58 (m, 2H), 2.89 (dt, 1H, J = 13.8, 8.2 Hz), 2.23 (ddd, 1H, J = 13.8, 6.3, 2.7 Hz), 1.98 (d, 1H, J = 3.6 Hz).

5'-O-(4,4'-dimethoxytrityl)-3-Cyanovinylcarbazole-1'-β-deoxyriboside-3'-O-(cyanoethoxy-N,N-diisopropylamino)phosphoramidite

5'-O-(4,4'-dimethoxytrityl)-3-Cyanovinylcarbazole-1'-β-deoxyriboside (6.0 g, 9.43

mmol) in seal bottle was dissolved in Acetnitrile and coevaporated three times in *vacuo*. After substituted with argon, 2-cyanoethyl *N,N,N,N'*-tetraisopylphosphorodiamidite (2.9 mL, 9.43 mmol) in acetonitrile (9.8 mL) and 0.45 M 1*H*-tetrazole in acetonitrile (22 mL, 9.43 mL) were added, and the reaction mixture was stirred at room temperature for 2h. Then the reaction mixture was extracted with AcOEt, which was washed with a saturated aqueous solution of NaHCO$_3$, and water. The organic layer was collected, dried over anhydrous sodium sulfate, filtered, and evaporated to dryness under reduced pressure. Then, the crude in sealed bottle was dissolved in acetonitrile and coevaporated three times, and was used for automated DNA synthesizer without further purification.
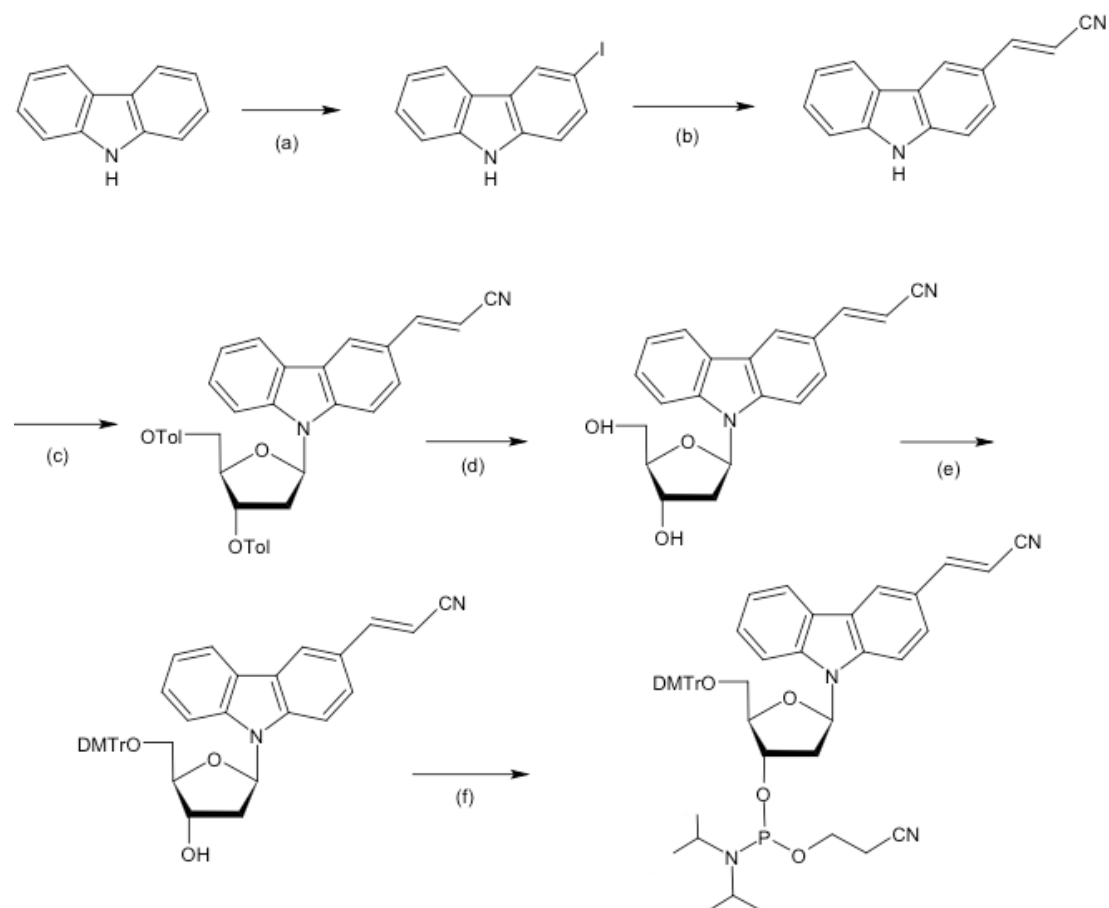
Scheme 2.1. Synthesis of the phosphoramidite of 3-Cyanovinylcarbazole Nucleoside; (a) I$_2$, NaiO$_4$, H$_2$SO$_4$, in MeOH, 65°C (b) acrylonitrile, PdOAc, tributylamine in DMF, 160°C, 60W (c) Cl-sugar, KOH, TDA-1, in MeCN (d) CH$_3$ONa in MeOH (e) DMTrCl, DMAP, in pyridine (f)

Phosphorodiamidite, BTT, in MeCN

DNA sequences, synthesis and purification

Oligonucleotides were prepared by β-(cyanoethyl) phosphoramidite method on controlled pore glass supports (1 mmol) using DNA synthesizer. Strands containing ^{CNV}Ks were synthesized using the cyanoethylphosporamidite of ^{CNV}K that was synthesized according to the previous reported method[20]. After automated synthesis, the oligomer was detached from the support by soaking in concentrated aqueous ammonia for 1 h at room temperature. Deprotection was conducted by heating the concentrated aqueous for 4 h at 65°C concentrated aqueous ammonia was then removing it by speedvac, and the crude oligomer was purified by reverse phase HPLC and lyophilized.

Photoirradiation condition of photopolymerization and photodegradation

Each ODNs including ^{CNV}K was dissolved to 12.5 μM in annealing buffer (10 mM MgCl$_2$, 20 mM Tris-acetate (pH 7.0), 1 mM, EDTA). After mixting, the solutions were photoirradiated at 366 nm UV-rays on ice using a UV-LED illuminator. The 312 nm photoirradiation was performed under the heating at 50°C using a transilluminator.

Denaturing polyacrylamide gel electrophoresis

For analysis of the sizes of photopolymerized DNA structure by gel electrophoresis, sample solutions were diluted by 8M Urea in formamide and heated at 90°C for 5 min. Loading samples were prepared with an appropriate amount of 6×loading buffer [36% (v/v) glycerol, 30 mM EDTA and 0.05% (w/v) each of bromophenol blue and xylene cyanol] and loaded onto gels prepared with 10% polyacrylamide (29:1, polyacrylamide: bisacrylamide) containing 8 M Urea and running buffer (1×TBE). 25 bp DNA Ladder Maker (Promega) was used. The gels were run at 150 V on a gel electrophoresis apparatus (Bio-RAD). After electrophoresis, the gels were stained with SYBRgold (Molecular Probe) and imaged on an Imaging System LAS-3000 (FUJIFILM Inc.).

Agarose gel electrophoresis

3 µl of each same DNA was electrophoresed on a 3 % agarose gel at 100 V in TAE buffer at constant current for 30 min with Mupid-2plus(Mupid). 100 bp DNA Ladder Maker (CosmoBio) was used. After electrophoresis, the gels were stained with ethidium bromide (Wako) and imaged on LAS-3000

Circular dichroism spectrum

Circular dichroism spectrum were determined in 0.1 cm path length cells using a J-720 spectrophotometer (JASCO), equipped with a thermoelectric temperature controller.

Photopolymerization incorporating miRNA

12.5 µM Probe ODN and 12.5 µM miRNA was dissolved in annealing buffer and photoirradiated at 25°C or 37°C for 120 s.

Synthesis of pyrene labeled ODN

The amino-modifer ODN was synthesized using 3'-PT amino-modifier C3 CPG and 5'-PT amino-modifier C3-TFA (Glen research) with an automated DNA synthesizer. Then, purified ODN were conjugated with the pyrene at the amino end by overnight incubation in 0.1 M sodium bicarbonate /sodium carbonate buffer (pH 8.5) mixted with a 15-fold excess of the succinimidyl ester of 1 pyrene acetic acid dissolved in dimethyl sulfoxide(DMSO). The unconjugated pyrene was removed by ethanol precipitation of DNA, repeated three times. The crude sample was purified by HPLC.

Measurement of pyrene excimer

The fluorescence spectrum were recorded on a JASCO FP-6000 at 50°C. An excitation wavelength of 340 nm was used, and excitation and emission slit was 3 nm. The sample was diluted by buffer including 4 M Urea, 1 M NaCl, and 50 mM Na_2PO_4 (PH 7.4).

1.3. Results and Discussion

In this study, we have used a photoresponsive artificial nucleotide ^{CNV}K, which can crosslink to complementary strand by a few photoirradiation. The ^{CNV}K was synthesized according to scheme and various modified ODNs were prepared according to standard phosphoramidite chemistry, on a DNA synthesizer. ODNs containing ^{CNV}K were purificated by HPLC and characterized by MALDI-TOF-MS. Those ODN sequences were designed to construct 1D DNA structure with two strands, the DNA strand ODN 1 (5'-GACTGTCCGCATGTA ^{CNV}KTGCG-3') and ODN 2 (5'-GCGGA^{CNV}KAGTCCG CATTACAT-3') including ^{CNV}K. This ^{CNV}K photocrosslinked to thymidine in a complementary strand, and ODN 1 were separated into two domains *a* and *b* whose sequence are complementary sequence of $\bar{a}$ and $\bar{b}$ domains in strand ODN 2. In this strategy, each strand was hybridized with the other strand and this propagates the next chain reaction of hybridized and photocrosslinking events between alternating ODN 1 and 2 to form a nicked double helix (Fig. 2.1A).

To confirm the photopolymerization of ODNs, two ODNs including ^{CNV}K were photoirradiated at 366 nm, and analyzed by denaturing PAGE and agarose gel electrophoresis. As Fig. 2.1B, only monomer band was observed in Lane 1 because the 1D DNA structure had been broken by denaturing condition. The bands having low mobility compared with the monomer band appeared and the moblitiy of these bands decreased depending on the photoirradiation time, suggesting that the start monomer ODN 1 and 2 were photopolymerized via a photocrosslinking between ^{CNV}K and thymidine. The photopolymerized process was completed by irradiation for 2 second, and the size of the photopolymerized ODN was 500±300 bp. The rate of photopolymerization using ^{CNV}K was 250 bp per second, which was approximately 125-fold faster than extension rate of the enzymatic method [7].

51

(A)

(Strand ODN 1)

(Strand ODN 2)

5' *a* *b* 3'
GACTGTCCGCATGTAXTGCG

+

5' $\overline{a}$ $\overline{b}$ 3'
GCGGAXAGTCCGCATTACAT

Photopolymerization at 366 nm

a *b* *a* *b* *a* *b*
... GACTGTCCGCATGTAXTGCGGACTGTCCGCATGTAXTGCGGACTGTCCGCATGTAXTGCG ...
CTGAXAGGCGTACATTACGCCTGAXAGGCGTACATTACGCCTGAXAGGCGTACATTACGC
$\overline{a}$ $\overline{b}$ $\overline{a}$ $\overline{b}$ $\overline{a}$ $\overline{b}$

Photodegration at 312 nm

(B)

Photoirradiation at 366 nm

M 0 0.1 0.2 0.3 0.4 0.5 1 2 5

100 nt
75 nt
50 nt
25 nt

Lane 1 2 3 4 5 6 7 8 9 10

(C)

Photoirradiation at 312 nm

M 0 1 3 5 10 30 60 120 300 600 900 1800

100 nt
75 nt
50 nt
25 nt

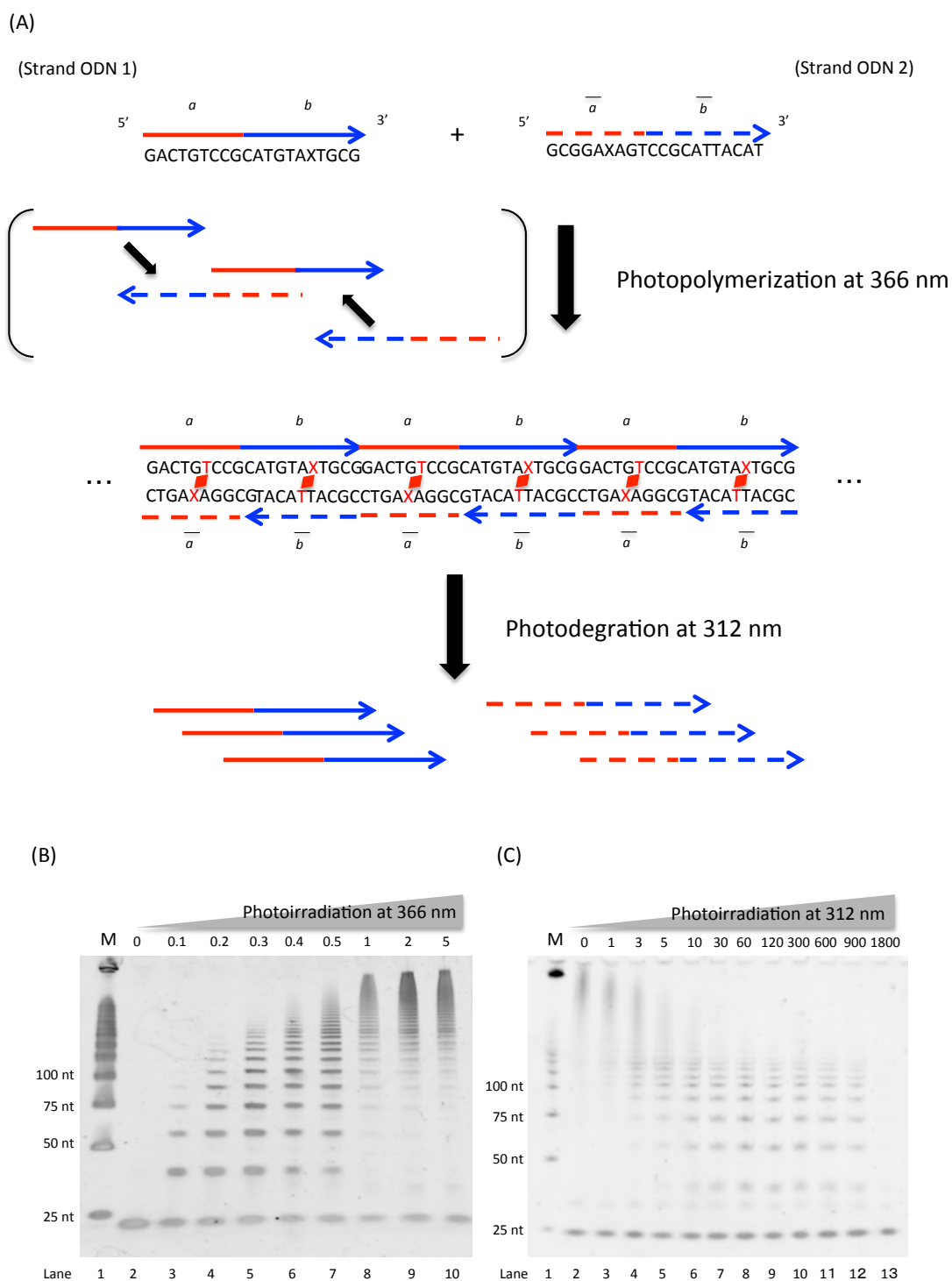Lane 1 2 3 4 5 6 7 8 9 10 11 12 13

Figure. 2.1 The photopolymerization of ODNs using ^{CNV}K by photoirradiation at 366 nm and photodegraded by photoirradiation at 312 nm. (A) Reaction scheme of photopolymerization and photodegraded. (B) The denaturing PAGE analysis of photopolymerization of ODNs;(C) The denaturing PAGE analysis of photodegraded.

The ultrafast reversible photocrosslinker ^{CNV}K was photosplitted by irradiation at 312 nm. So we confirmed the photoreversibility of photopolymerized ODNs by analyzed denaturing PAGE (Fig. 2.1C). The band of photopolymerized ODN disappeared depending on the photoirradiation time and the only monomer was observed in Lane 13 after photoirradiation at 1800 s, suggesting that this photopolymerized DNA was reversible degraded to monomer ODN by photosplitting.

Next, the conformation of this photopolymerized ODN was examined by CD spectrum measurement. The CD spectrum had a negative cotton effect at 255 nm and positive effect at 285 nm, suggesting that photopolymerized ODN had B-form the same as the negative DNA duplex. Moreover, this photopolymerized ODN was measured by CD spectrum at 20°C, 30°C, 40°C, 50°C, and 60°C to examine the thermal stability. The cotton effect of photopolymerized ODN at 255 nm was not reduced compared with the cotton effect of starting ODN 1 and ODN 2, so that its B-form was maintained by heating at 60°C. These results suggest the conformation of photopolymerized ODN was stable B-form DNA caused form [2+2] cycloaddition between ^{CNV}K and thymidine created by photocrosslinking reaction.

Next, we demonstrated the feasibility of sequence specific photopolymerization of DNA or RNA for rapid sensing of nucleic acids. In this study, we used five miRNA that belong to the miRNA 200 Family as target strands. The probe ODNs were designed to polymerized only in the presence of target miRNA by photoirradiation (Fig. 2.2A). For the positive detection of the SNPs, a probe ODN complementary to each miRNA sequence was designed and each probe ODN has two ^{CNV}Ks that photocrosslinked to two target miRNAs, respectively. To examine the photopolymerization incorporating the miRNA in a sequence specific manner, we demonstrated the photopolymerization in all combinations (5 probes x 5 miRNAs). The samples were photoirradiated at 366 nm for 120 seconds and analyzed by denaturing PAGE. The band intensity of the denaturing PAGE result was normalized by the sum of the band intensity. The normalized band intensity of each number of polymerized is shown in Fig. 2.2B.

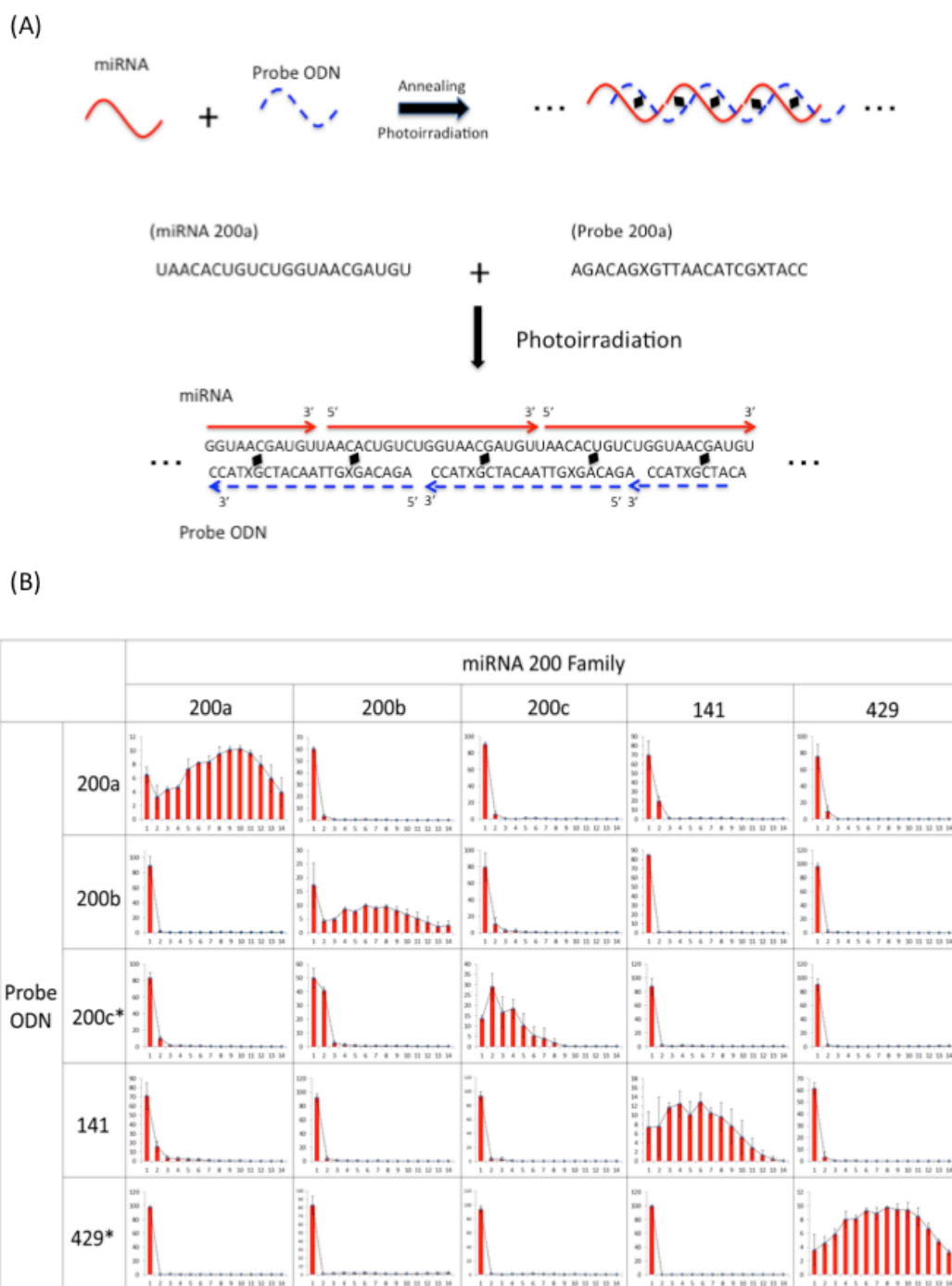**Figure. 2.2** The photopolymerization incorporating miRNA in sequence specific manner (A)Scheme of photopolymerization incorporating miRNA (B) The number of polymerization of photopolymerization ODNs in all combination (5 probes and 5 miRNAs). The abscissas axis shows the number of polymerization and ordinat axis shows the normalized band intensity * is photoirradiated at 37°C, non-sigh is photoirraidated at 25°C.

In case of probe ODN 200a, the photopolymerization reaction was advanced in the presence of miRNA 200a. However, only monomer and dimer were observed in the presence of other miRNAs. And, all probes were photopolymerized incorporation of miRNA only in the presence of target miRNA, respectively. The result clearly shows that the sequence specific photopolymerization incorporating miRNA.

However, the confirmation of photopolymerization by denaturing PAGE is cumbersome so that we design the pyrene modifier probe to image existence of target miRNA by fluororescence. In the presence of target miRNA, the excimer fluorescence was observed since the pyrene-modifier probes were polymerized and two pyrene molecules come to a very near position. In the absent of target miRNA, the monomer emission was observed since the pyrene-modifer probes were not photopolymerized (Fig. 2.3A). The pyrene-modifier probe for 200a was mixed each miRNAs and photopolymerized at 366 nm.

We measured the fluorescence emission spectra of a pyrene-modifier probe at an excitation wavelength of 340 nm in a buffer solution containing various miRNAs. When no target miRNA was present, monomer emission peaks were observed, but there were no observable excimer emissions. On the other hand, in the presence of target miRNA, excimer emission peaks were observed at approximately at 475 nm (Fig. 2.3B). The ratio of excimer emission (475 nm) and monomer emission (397 nm) under each miRNA are compared in Fig. 2.3C. Large excimer emission was observed only in the presence of target miRNA and its excimer emission was 6-fold that of other miRNAs. The results show that photopolymerization incorporating miRNA is processed in a sequence specific manner and this sequence specific photopolymerization is applicable for detecting miRNA.
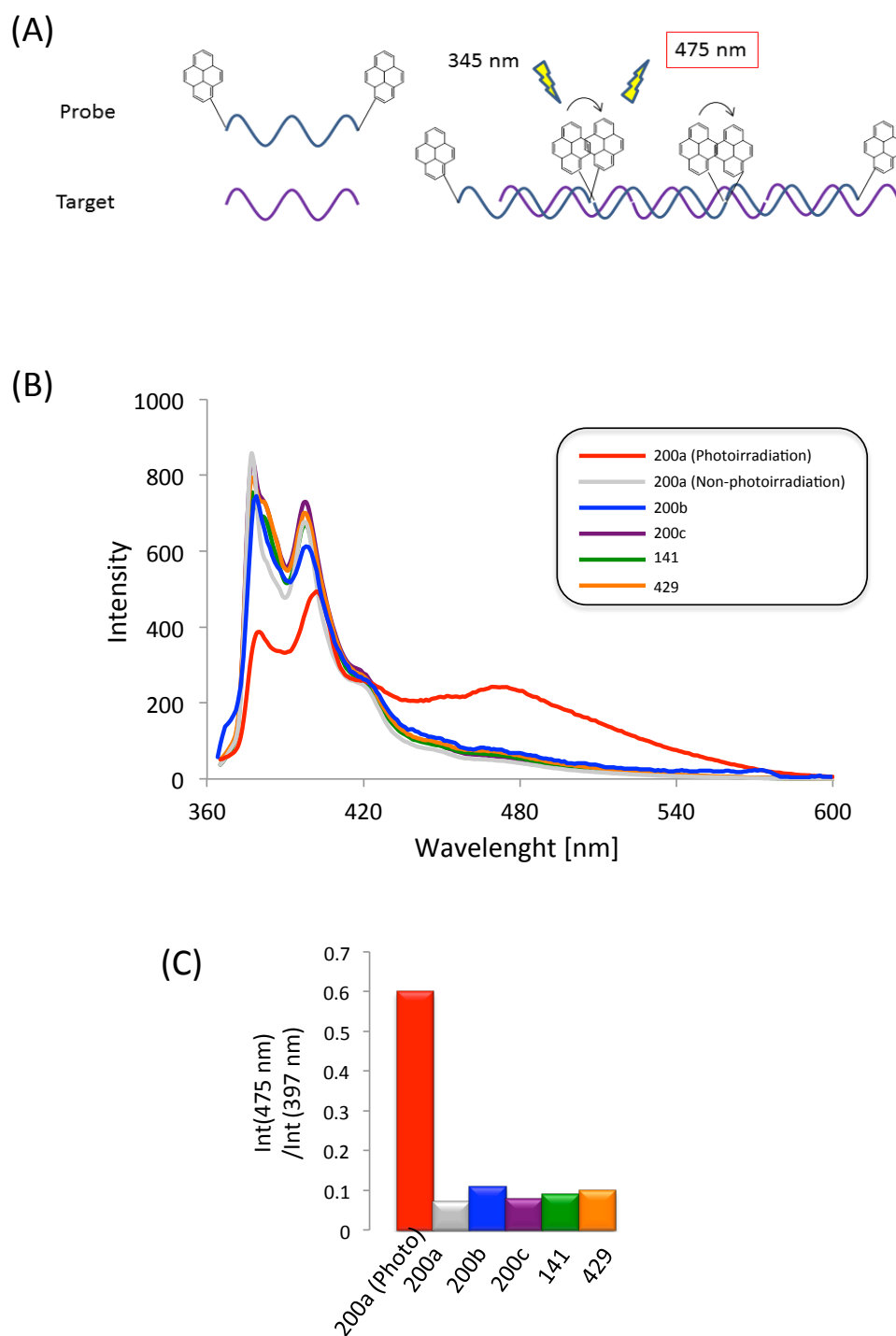
Figure. 2.3 (A) Strategy of sensing miRNA using pyrene modifier probe by excimer emission. (B) Fluorescence spectrum of pyrene modified 1D DNA structure. (C) The ration of excimer fluorescent (475 nm) and monomer fluorescent (397 nm).

1.4. Conclusion

We propose ultrafast photopolymerization of ODNs using ^{CNV}K as the photoresponse artificial nucleoside. These results show that a stable DNA photopolymer was successfully created from short ODNs rapidly by 366 nm irradiation, and its photopolymer was degraded to start short ODNs by 312 nm irradiation. And, this photopolymerization can create a DNA-RNA hetero polymer incorporating miRNA in a sequence specific manner. Development of this technology might provide us with new interesting material for DNA nanotechnology and DNA engineering. Moreover, this rapid sequence specific photopolymerization incorporating miRNA will also be used for miRNA sensing, and this technology might provide us with diagnostic tool and nucleic acid medicine for the treatment of diseases.

1.5. Reference

1. Sheridan J T, Gleeson M R, Close C E, Lelly J V, Optical response of photopolymer materials for holographic data storage applications. *J. Nanosci. Nanotechnol*., **2007**, 7, 232-242.

2. Leprince J G, Palin W H, Hadis M A, Devaus J, Leloup G, Progress in dimethacrylate-based dental composite technology and curing efficiency. *Dent. Mater*., **2013**, 29, 139-156.

3. James V C, Elsa R. Photopolymer Materials and Processes for Advanced Technologies. *Chem. Matter*., **2014**, 26, 533-548.

4. Jordan O P, Marquis-Weible F, Characterization of photopolymerization by a Holographic technique applied to a acattering hydrogel. *Appl. Opt*., **1996,** 35, 6146-6150.

5. Nakamura Y, Yamaguchi M, Kitoyama A, Iko K, Okubo M. Internal stress of epoxy resin modified with acrylic polymers producted by in situ UV radiation polymer. *Appl. Polym. Sci*., **1990**, 39, 1045-1060.

6. Seeman N C, Nucleic acid junctions and lattices. *J. Theor. Biol*., **1982**, 99, 237-247.

7. Adleman L M, Molecular Computation of Solution to Combinational Problems. *Science*, **1994**, 266, 1021-1024.

8. Fu T J, Seeman N C, DNA double crossover structures. *Biochemistry*, **1993**, 32, 3211-3220.

9. Seeman N C, DNA in a material world. *Nature*. **2003**, 421, 427-431.

10. Rothemund P W, Folding DNA to create nanoscale shapes and patterns. *Nature*, **2006**, 440, 297-302.

11. Marsh T C, Vesenka J, Henderson E, A new DNA nanostructure the G-wire imaged by scanning probe microscopy. *Nucleic. Acids. Res.,* **1995**, 23, 696-700.

12. Yan H, Park S H, Flnkelstein G, Reif J H, Labean T H, DNA-templated self-assembly of protein array and highly conductive nanowires. *Science*, **2003**, 301, 1182-1184.

13. Karthikeyan G, Chary K V R, Rao B J, Fold-back structures at the distal end influence DNA slippage at the proximal end during mononucleotide repeat expansions. *Nucleic. Acids. Res*., **1991**, 27, 3851-3858.

14. Ogata N, Miura T, Elongation of tandem repetitive DNA by the DNA polymerase of the hyperthermophilic archaeon Thermococcus litoralis at a hairpin-coil transitional state a model of amplification of a primordial simple DNA sequence. *Biochmistry*, **2000**, 39, 13993-14001.

15. Paiva A M, Sheaedy R D, The influence of Sequence Context and length on the Kinetics of DNA Duplex Formation form Complementary Hairpin Prossessing Repeats. *J. Am. Che. Soc.*, **2005**, 127, 5581-5585.

16. Tanaka A, Yasutaka M, Ijiro K, Immobilizing and stretching of poly(dG)-poly(dC) synthesized by klenow fragment exo- on substrates by LB method. *Colloids and Surface A*, **2006**, 284, 246-249.

17. Gerald L C, Paul W D, William A H, Cyclobutane Pyrimidine Dimers and (6-4) Photoproducts Block Polymerization by DNA Polymerase I. *Biochemistry*, **1985**, 24, 5723-5728.

18. Lewis R J, Hanawalt P C, Ligation of oligonucleotides by pyrimidine dimers. *Nature*, **1982**, 298, 393-396.

19. Inaki Y, Moghaddam M J, Kanabara K, Takemoto K, Pyrimidine Polymers as High Resolution, High Sensitivity Deep-UV Photoresists. *J. Photopolymer. Sci. Tec.,* **1988**, 1, 28-35.

20. Ogasawara S, Fujimoto K, A Novel Method to Synthesized Versatile Multiple-Branched DNA(MB-DNA) by Reversible Photochemical Ligation. *ChemBioChem*, **2005**, 10, 1756-1760.

21. Nakamura S, Ogasawara S, Matsuda S, Saito I, Fujimoto K, Templated Directed Reversible Photochemical Ligation of Oligonuclotides. *Molecules*, **2012**, 17, 163-178.

22. Yoshimura Y, Fujimoto K, Ultrafast reversible Photocrosslinking Reaction Toward in Situ DNA manipulation. *Org. Lett.*, **2008**, 10, 3227-3230.

23. Fujimoto K, Yamada A, Yoshimura Y, Tsukaguchi T, Sakamoto T, Details of the ultra-fast DNA photocroslinking reaction of 3-cyanovinylcarbazole. *J. Am. Chem. Soc.,* **2013**, 135, 16161-16167.

Chapter 2.

Creation of DNA array structure equipped with heat

resistance by ultrafast photocrosslinking

2.1. Introduction

DNA is a promising candidate to serve as a building material on a nanometer-scale. The specificity of the A-T and G-C hydrogen bonded Watson-Crick interaction provides a means to construct diverse DNA constructions of programmed base sequences, which makes DNA a useful construction biomaterial for nanometer-scale applications. DNA motifs [1,2] and a DNA origami method [3] have been reported that allow the creation of various DNA structures such as DNA nanowire [4], and two- or three-dimensional DNA nanostructures [5,6,7]. These DNA nanostructures have been used for applications such as nanopatterning [8], monitoring enzymatic reaction [9], conformation changes [10], and computing systems [11]. In recent attempts to make a molecular robot [12] using DNA, RNA and protein, the DNA nanostructure required thermal resistance because a more practical function is realized by stepwise assembly of a functional DNA structure. However, DNA nanostructures can be used only at temperatures as low as ～ 55°C or less in solution [13] because they melt beyond this temperature. In order to create practical DNA applications and DNA nanodevices, greater temperature resistance is required. Thermal stability has been improved in DNA duplex by enzymatic ligation method [14], crosslinking method [15], and using artificial nucleotides such as PNA [16] and LNA [17]. The enzymatic ligation method and chemical crosslinking reaction which requires the addition of another reagent such as adequate salt and activator must be performed under controlled buffer conditions and were not performed in extremely tight space. On the other hand, photochemical reaction was manipulated by photoirradiation without a buffer condition and its reaction was performed in an extremely tight space. In previous reports, a photochemical reaction such as photochemical ligation with 3-carboxyvinyldeoxyuridine [18] and photocrosslinking with 8-methoxypsoralen [19] was used to improve the thermal stability of the DNA nanostructure. However, in those reports, the photochemical reaction needed to a long irradiation time or its reaction was photocrosslinked at random. To overcome such problem, we reported that an ultrafast photocrosslinker 3-cyanovinylcarbazole [20]

(^{CNV}K), oligodeoxynucleotide containing ^{CNV}K can photocrosslink to a complementary DNA strand via [2 + 2] photocycloaddition between ^{CNV}K and pyrimidine base in a complementary strand with 1 s of 366 nm irradiation. In this study, we demonstrated the thermal stability of a 2D DNA array that was covalently connected by photocrosslinking with ^{CNV}K. Moreover, the influence of inserting position of ^{CNV}K has on structure was investigated.

2.2. Materials and Method

General

^{1}H NMR spectra were measured with AVANCE III NMR 400 (Bruker, 400 MHz) spectrometer. Mass spectra were recorded on a Voyager-DE PRO-SF, Applied Biosystems. Irradiation was performed by UV-LED (OMRON, ZUV, 366 nm, 1.6 W/cm^2) or 2 W transilluminator (FUNAKOSHI, TR-312R/J, 312 nm). HPLC was performed on a Chemcobond 5-ODS-H column (10 × 150 mm, 4.6 × 150 mm) or a Chemcosorb 5-ODS-H column (4.6 × 150 mm) with a JASCO PU-980, HG-980-31, DG-980-50 system equipped with a JASCO UV 970 detector at 260 nm. The reagents for the DNA synthesizer such as A, G, C, T-β-cyanoethyl phosphoramidite, and CPG support were purchased from Glen Research. Atomic force microscopy we

AFM imaging

For atomic force microscopy (AFM) imaging in air, a 2 μl sample and 10μl tetrahydrofuran drop was spotted on freshly cleaved mica (Veeco) and left to adsorb onto the surface for 3 min. Then the mica surface was washed with 100 μl of water three times and dried by blowing nitrogen. An atomic force micrograph was obtained by tapping mode in air on a NanoScope3D (Veeco).

Denaturing polyacrylamide gel electrophoresis

For analysis of the sizes of DNA nanostructures by gel electrophoresis, sample solutions were diluted by 8M Urea in formamide and heated at 70°C for 5 min. Loading samples were prepared with an appropriate amount of 6×loading buffer [36% (v/v) glycerol, 30 mM EDTA and 0.05% (w/v) each of bromophenol blue and xylene cyanol] and loaded onto gels prepared with 10% polyacrylamide (29:1, polyacrylamide: bisacrylamide) containing 8 M Urea and running buffer (1×TBE). 25 bp DNA Ladder Maker (Promega) was used. The gels were run at 150 V on a gel electrophoresis apparatus (Bio-RAD). After electrophoresis, the gels were stained with SYBRgold

(Molecular Probe) and imaged on an Imaging System LAS-3000(FUJIFILM Inc.).

Agarose gel electrophoresis

3 μl of each sample DNA was electrophoresed on a 2 % agarose gel at 100 V in TAE buffer at constant current for 30 min with Mupid-2plus(Mupid). 100 bp DNA Ladder Maker (CosmoBio) was used. After electrophoresis, the gels were stained with ethidium bromide (Wako) and imaged on LAS-3000(FUJIFILM Inc.)

UV-melting study

Ultraviolet melting curves were determined in 1 cm path length cells using a V-630 Bio UV–Visible spectrophotometer (JASCO), equipped with a thermoelectric temperature controller. Absorbance versus temperature profile was measured at 260 nm with a heating rate of 0.5 °C/min. Experiments were generally conducted at a concentration of 2.5 μM diluted 10 times after annealing and photoirradiation.

2.3. Results and Discussions

Based on the sequence that was constructed by 2D DNA array by one strand [21], the DNA strands ODN 2 to ODN 5 including ^{CNV}K were designed to create a DNA array structure equipped with heat resistance (Fig. 3.1A). Those DNA strands including ^{CNV}K contain four palindromic segments, which are 6-, 10-, 10-, and 6-based-long, respectively, each at the central two 10-base-long segments, resulting in long, pseudo continuous duplexes with dangling, single-stranded, 6-base-long overhangs every 10 base pairs along the DNA duplexes (Fig. 3.1B). ODN 2 and ODN 3 included one ^{CNV}K in first and second segment, respectively, ODN 4 included two ^{CNV}Ks in second and third segments, and ODN 5 was including two ^{CNV}Ks in the first and forth segments.

Construction of photocrosslinked DNA array made of ODN 5 was annealed and photoirradiated at 366 nm for 120 s. First, a photocrosslinked DNA array made of ODN 5 was observed by atomic force microscopy (AFM) under air. The result is shown in Fig. 3.1C, the size of this structure was 150 nm × 150 nm and the height was about 1 nm which is consistent with the height of DNA duplex in air (Fig. 3.1C).

Next, to confirm the formation of photocrosslinking onto a 2D DNA array made of ODN 5, the 2D DNA arrays that which were irradiated each time were analyzed by denaturing PAGE (Fig. 3.2A). Surprisingly, this photocrosslinked DNA array was stable under the denaturing condition, which allowed to analysis of the DNA structure by denaturing PAGE. The monomer band was observed in Lane 2, and dimer and tetramer bands were observed in Lane 3 to 6 as the irradiation time became long. Finally, at a in photoirradiation time of over 60 s, various bands were concentrated at the high molecular weight band considered to be issued from the 2D DNA array. The result dovetailed with the result of AFM, and this 2D DNA array was stable by photocrosslinking under the denaturing.

(A)

Entry	The Sequence of ODN(5'-3')
ODN 1	CCATGG-ACTGGCCAGT-GGTTCGAACC-TGATCA
ODN 2	CCATG**X**-ACTGGCCAGT-GGTTCGAACC-TGATCA
ODN 3	CCATGG-ACTG**X**CCAGT-GGTTCGAACC-TGATCA
ODN 4	CCATGG-ACTG**X**CCAGT-GGTTCG**X**ACC-TGATCA
ODN 5	CCATG**X**-ACTGGCCAGT-GGTTCGAACC-TG**X**TCA

(X = ^CNVK)
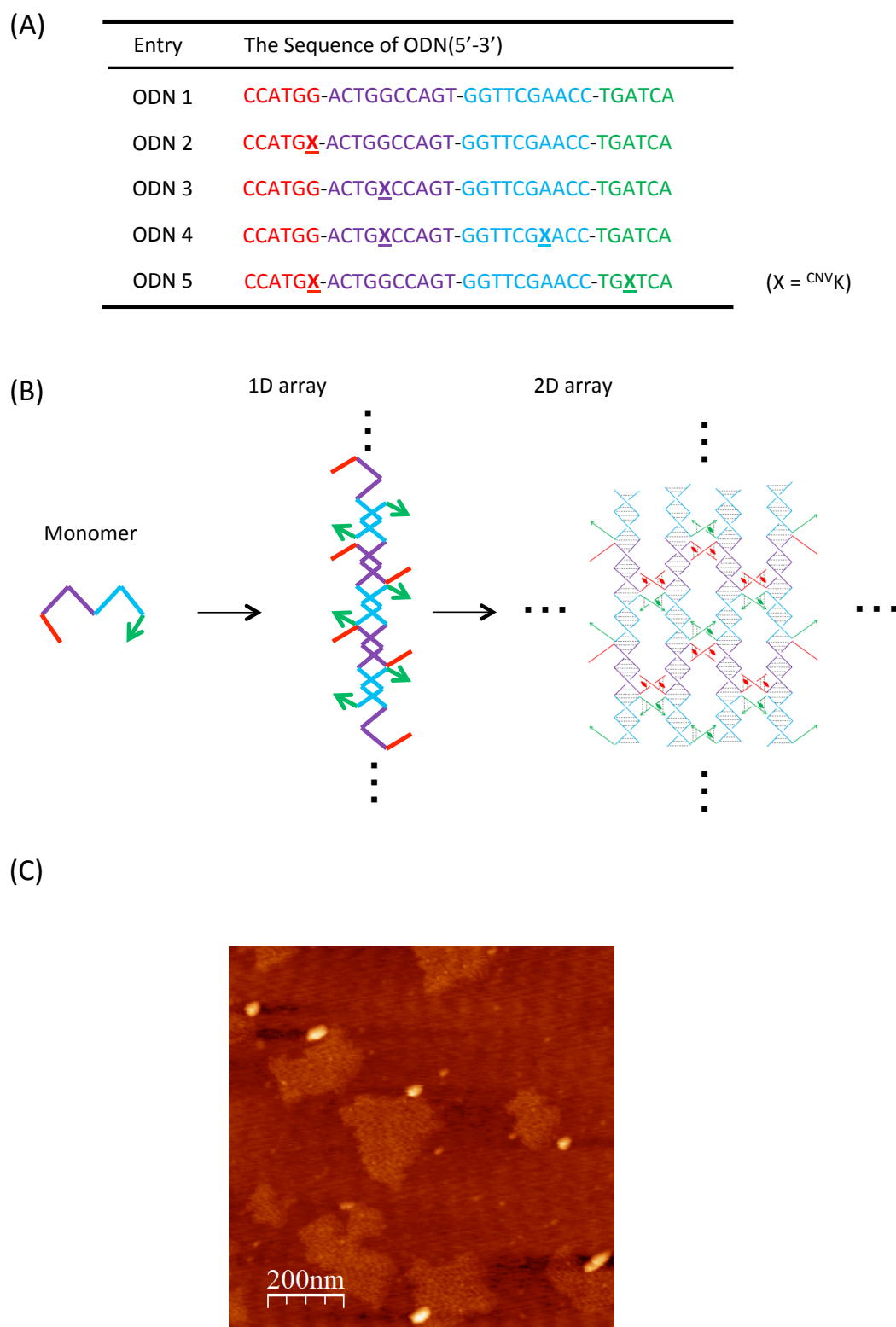
(B)

1D array   2D array

Monomer

(C)

200nm

Figure. 3.1 (A) The sequence of ODN (B) Schematic illustration of photocrosslinking DNA array (C) AFM imaging of photocrosslinked DNA array made from ODN 5.

The arrays made of ODN 1 to ODN 5 were analyzed by 3% agarose gel electrophoresis. The size of the DNA array depended on the position and number of inserting ^{CNV}K, and the breadth of the size distribution of the DNA array was decreased by photocrosslinking. The result which photoirradiated DNA array made of ODN 5 is smaller than that of ODN 1 in agarose was supported by AFM imaging. This result was issued from local instability which generated by that ^{CNV}K have no hydrogen-bonding interaction between native base such as A, T, G, and C. Those results suggested the number of ^{CNV}K and inserting position were influenced the size of the DNA array. Next, in order to conduct more detailed analysis, before and after photoirradiated DNA arrays were analyzed by denaturing PAGE (Fig. 3.2B). The band corresponding to monomer ODN was lost after a few seconds of photoirradiation in all ODNs including ^{CNV}K, which suggested all ODNs were efficiently used to construct the DNA array by photocrosslinking neighboring DNA. In the case of the array made of ODN 1, only the monomer band was observed under the denaturing condition regardless of before or after photoirradiation in Lane 2 and 3. In the case of the 2D DNA arrays made of ODN 2 and 3, dimer bands were observed after photoirradiation. In case of the DNA arrays made of ODN 4 or ODN 5, bands of high molecular weight were observed after photoirradiation. While ODN 4 and 5 had two ^{CNV}Ks, the array made of ODN 4 had two high molecular weight bands. The band of high molecular weight was considered to be a pseudo continuous duplex as a 1D DNA array and 2D DNA array. On the other hand, the array made of ODN 5 had one high molecular weight band. These results suggest that the size and conformation of the DNA array were regulated by the inserting position of ^{CNV}K and the stability of the photocrosslinked DNA array was improved.

(A)

(B)
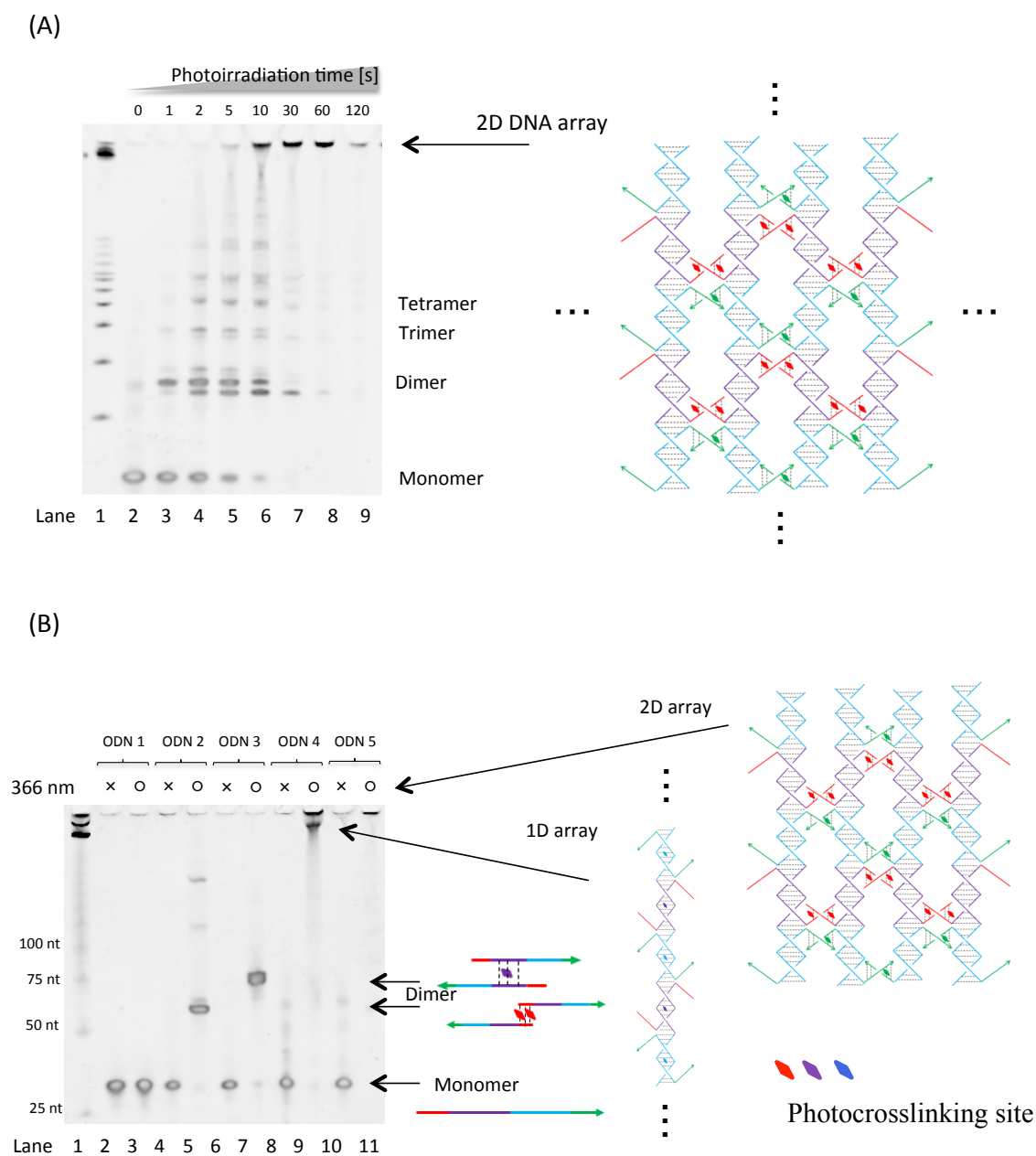
Figure. 3.2 (A) Denaturing PAGE analysis of DNA array made of ODN 5; Lane 1 is 25 bp DNA Ladder Maker, Lane 2 to Lane 9 are samples irradiated with 366 nm light for 0, 1, 2, 5, 10, 30, 60, and 120 seconds, respectively. (B) The Denaturing PAGE analysis of each DNA array before and after photoirradiation; Lane 1 is 25 bp DNA Ladder Maker; Lane 2 and 3 are ODN 1 before and after photoirradiation, respectively; Lane 4 and 5 are ODN 2 before and after photoirradiation; Lane 6 and 7 are ODN 3 before and after photoirradiation; Lane 8 and 9 are ODN 4 before and after photoirradiation; Lane 10 and 11 are ODN 5 before and after photoirradiation.

The effect of photocrosslinking on the thermal stability of 2D DNA arrays was examined by thermal denaturing profile. The photocrosslinked DNA array was reduced hyperchromic change that accompanies denaturation [22], it decreased to 30% of hyperchromic change of the non-photocrosslinked DNA array. Photocrosslinked DNA array made of ODN 5 was not broken on heating at 80ºC, it was acquired heat resistance which is at least over 40ºC compared to non-photoirradiated DNA array made of ODN 5. The photoirradiated DNA array made of ODN 4 was also acquired heat resistance as a result of reducing hyperchromic change that accompanies denaturation. Melting profiles of photocrosslinked DNA array made of ODN 4 and 5 show appreciation of the absorbance near 50ºC and 40ºC, this is because that the segments non-including ^{CNV}K were dissociation. Moreover, we measured the melting curve heating to cooling profile (Fig. 3.3B). The thermal cooling profile had the same curve as the thermal heating profile in photocrosslinked DNA array. On the other hand, in the non-photocrosslinked DNA array, the thermal cooling profile had a different curve to that of the thermal heating profile. This result suggests that the photocrosslinked DNA array was maintains its structure and returns to its original structure by rapid cooling. However, the non-photocrosslinked DNA array was broken under the heating condition so that it cannot return to its original structure by rapid cooling.

These results suggest that thermal stability of the DNA array was dramatically improved by photocrosslinking. The thermal stability on DNA array including ^{CNV}K by photocrosslinking was improved by making a covalent bond between the DNA strands by photoirradiation.

(A)

(B)
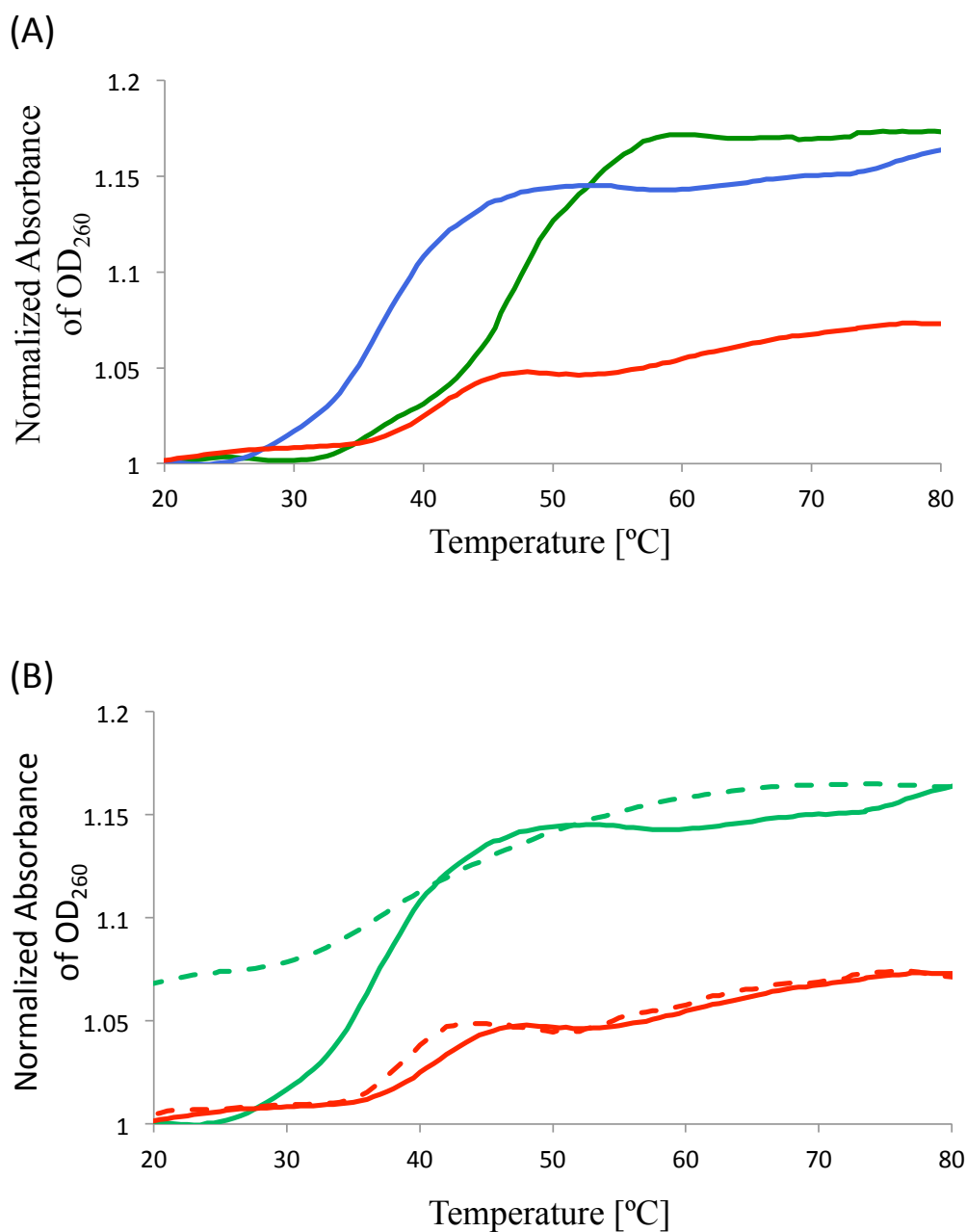
Figure. 3.3 (A) Thermal denaturing of DNA structure; The green line is the DNA array made of ODN **1**. The blue line is the non-photoirradiated DNA array made of ODN 5. The red line is the photoirraidated DNA array made of ODN 5. (B) The thermal reversibility of DNA array structure; The green line is the non-photocrosslinked DNA array made of ODN 5 and the red line is photocrosslinked one of ODN 5. Solid line is the melting curve of 20°C to 80°C, and dot line is one of 80°C to 20°C.

2.4. Conclusion

In conclusion, we created DNA array structures equipped with heat resistance by ultrafast photocrosslinking with ^{CNV}K. The simple DNA array became a very stable structure which is not broken under conditions of heating and denaturing by photocrosslinking. Moreover, the inserting position and number of ^{CNV}K allow regulation of the size and conformation of the DNA array. This method equips DNA array with heat resistance by photocrosslinking applied to DNA nanostructures. This knowledge is useful for making practical DNA nanodevices and stepwise assembly for various applications.

2.5 Reference

1. Fu T J, Seeman N C, DNA double-crossover molecules. *Biochemistry*, **1993**, 32, 3211–3220.

2. Seeman N C, Liu F, Mao C, Yang X, Wenzler L A, Sha R, Sun W, Shen Z, Li X, Qi J, Zhang Y, Fu T J, Chen J, Winfree E, Two dimensions and two States in DNA nanotechnology. *J. Biomol. Struct. Dyn.*, **2000**, 17, 253-262.

3. Rothemund P W, Folding DNA to create nanoscale shapes and patterns. *Nature*, **2006**, 440, 297-302.

4. Marsh T C, Vesenka J, Henderson E, A new DNA nanostructure, the G-wire, imaged by scanning probe microscopy. *Nucleic. Acids. Res.*, **1995**, 23, 696-700.

5. Winfree E, Liu F, Wenzler L A, Seeman N C, Design and self-assembly of two-dimensional DNA crystals. *Nature*, **1998**, 394, 539-544.

6. Endo M, Sugiyama H, Three-dimensional DNA nanostructures constructed by folding of multiple rectangles. *Nucleic. Acids. Symp. Ser. (Oxf)*, **2009**, 53, 81-82.

7. Andersen E S, Dong M, Nielsen M M, Jahn K, Subramani R, Mamdouh W, Golas M M, Sander B, Stark H, Oliveira C L, Pedersen J S, Birkedal V, Besenbacher F, Gothelf K V, Kjems J, Self-assembly of a nanoscale DNA box with a controllable lid. *Nature*, **2009**, 459, 73-76.

8. Chhabra R, Sharma J, Ke Y, Kiu Y, Rinker S, Lindsay S, Yan H, Spatially Addressable Multiprotein Nanoarrays Templated by Aptamer-Tagged DNA Nanoarchitectures. *J. Am. Chem. Soc.,* **2007**, 129, 10304-10305.

9. Endo M, Katsuda Y, Hidaka K, Sugiyama H, Regulation of DNA methylation Using Different Tensions of Double Strands Constructed in a Defined DNA Nanostructure. *J. Am. Chem. Soc.*, **2010**, 132, 1592-1597.

10. Sannohe Y, Endo M, Katsuda, Y, Hidaka K, Sugiyama H, Visualization of Dynamic Conformationa; Switching of the G-Quadruplex in a DNA Nanostructure. *J. Am. Chem. Soc.,* **2010**, 132, 16311-16313.

11. Mao C, LaBean T H, Relf J H, Seeman N C, Logical computation using algorithmic self-assembly of DNA triple-crossover molecules. *Nature,* **2000**, 407, 493-496.

12. Murata S, Konagaya A, Kobayashi S, Saito H, Hagiya M, Molecular robotics; A New Paradigm for Artifact. *New generation computing,* **2013**, 31, 27-45.

13. Castro C E, Kilchherr F, Kim D, Shiao E L, Wauer T, Wortmann P, Bathe M, Dietz H, A primer to scaffolded DNA origami. *Nat. Methods.,* **2011**, 8, 221-229.

14. Erie D, Sinha N, Olson W, Jones R, Breslaue K, A dumbbell-Shaped, double-hairpin structure of DNA: a thermodynamic investigation. *Biochemistry,* **1987***,* 26, 7150-7159.

15. Chanq C L, Lando D Y, Fridman A S, Hu C K, Thermal stability of DNA with interstrand crosslinks. *Biopolymers*, **2012**, 97, 807-817.

16. Giesen U, Kleider W, Berdinq C, Geiqer A, Orum H, Nielsen P E, A formula for thermal stability (Tm) prediction of PNA/DNA duplexes. *Nucleic. Acids. Res.,* **1998**, 26, 5004-5006.

17. Christensen U, Jacobsen N, Rajwanshi V K, Wengel J, Koch T, Stopped-flow kinetics of locked nucleic acid (LNA)-oligonucleotide duplex formation: studies of LNA-DNA and DNA-DNA interactions. *Biochem. J.,* **2011**, 354, 481-484.

18. Tagawa M, Shohda K, Fujimoto K, Sugawara T, Suyama A, Heat-resistant DNA Tile Arrays Constructed by Template-directed Photoligation through 5-Carboxyvinyl-2-deoxyuridine. *Nucleic. Acids. Research.*, **2007**, 35, e140.

19. Rajendran A, Endo M, Katsuda Y, Hidaka K, Sugiyama H, Photo-cross-linking-assisted thermal stability of DNA origami structures and its application for higher-temperature self-assembly. *J. Am. Chem. Soc.,* **2011**, 21, 14488-14491.

20. Yoshimura Y, Fujimoto K, Ultrafast Reversible Photocrosslinking Reaction: Toward in Situ DNA Manipulation. *Org. Lett.,* **2007***,* 10, 3227-3230.

21. Zhang C, He Y, Chen Y, Ribbe A E, Mao C, Aligning one-dimensional DNA duplexes into two-dimensional crystals. *J. Am. Chem. Soc.*, **2007**, 21, 14134-14135.

22. Natasa P, Daniel S, Pilch T, Stephen J, Lippard T, Elizabeth A, Redding T, Shari U, Dunhamt T, Kenneth J, Breslauer T, Influence of cisplatin intrastrand crosslinking on the conformation, thermal stability and energetics of a 20-mer DNA duplex. *Proc. Natl. Acad. Sci.,* **1996***,* 93, 7606-7611.

Chapter 3.

19F chemical shift imaging of nucleic acids by ultrafast

DNA photocrosslinking

3.1. Introduction

DNA photocrosslinking technology is an useful for detection, manipulation and regulation of DNA and RNA. The psoralen and its relate derivatives are famous photocrosslinkers and the psoralen-modified oligonucleotide had been used as photodynamic antisense [1-3] and antigene [4] oligonucleotide, and these oligonucleotides successfully regulate the gene expression in a photoresponsive manner. However, the psoralen was required the minitues-scale photoirradiation and the photocrosslinked DNA, via 2+2 cycloaddition between psoralen and thymidine base, were regenerated to the patent DNA by 254 nm irradiation resulting in fatal damage to normal DNA, due to the formation of pyrimidine dimer. We had already reported ultrafast photocrosslinker 3-cyanovinylcarbazole (^{CNV}K) [5,6] which can photocrosslink to pyrimidine base in complementary strand by a few second photoirradiation. And, it was reported the application using ^{CNV}K such as photochemical regulation of antisence effect [7-8], creation of DNA structure equipped with thermal resistance [9-11], and RNA sensing [12-14]. Moreover, we had recently reported the result of structural analysis of photocrosslinking adduct, it report had been described that ^{CNV}K photocrosslinked to a thymine base in the complementary DNA strand through the *trans* isomer of cyanovinyl moiety and cyclobutane formation process is a rate-determining step of the photocrosslinking reaction [6]. And it is surmised the spatial vicinity of target thymidine was drastically changed by photocrosslinking reaction in duplex DNA. So we tried to chemical shift imaging of nucleic acid using photocrosslinking reaction of ^{CNV}K.

Over the past a few decades, magnetic resonance imaging (MRI) [15-17] was established for in vivo imaging technology as same as X-ray computed tomography, positron emission tomography. Especially, 19F-NMR was attention many years to have a large part to favourable NMR properties of the 19F nucleus. Advantages of using spin 19F as a NMR probe is high sensitivity (83% of the proton) and low background combined with 100% natural abundance and a wide chemical shift distribution [18,19].

Addition, various biomolecules such as enzymatic activity [20,21], protein [22], protein aggregation [23], and nucleic acid [24] were imaged by 19F NMR imaging probes. It was many reported nucleic acid sensing using fluorescent molecular probe though 19F NMR imaging probe has advantage *in vivo* permeability. So, we designed 19F-NMR chemical shift imaging using DNA photocrosslinking reaction between [CNV]K and nucleic 19F-labeled pyrimidine base. This decade, conformational equilibria of bistable RNAs, metal ion binding to the TAR RNA, and Mg^{2+} induced folding of the hammerhead ribozyme have been studied by 19F NMR by incorporation of fluorinated nucleotides nucleobases and monitoring changes in their 19F chemical shift. Remarkably, most of the 19F NMR studies of the nucleic acids utilized nucleoside that have been modified with fluorine at the nucleobase, such as 5-fluorouracil ([F]U) [25-29], 5-trifluorothymidine([TF]T) [30], 5-(4,4,4-trifluoro-3,3-bistrifluoromethyl)but-l-ynyl-thymidine ([(CF3)3]T) [31], 5-fluorocytosine ([F]C) [32,33] (Fig. 4.1).
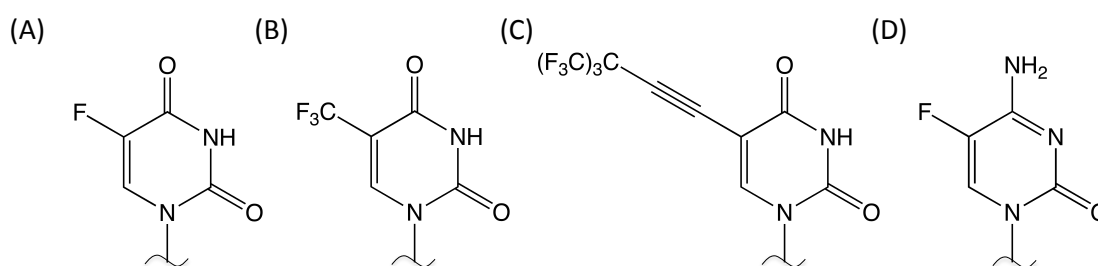
Figure. 4.1 The chemical structure of pyrimidine containing fluorine.

In this report, we present a novel concept for imaging of nucleic acids by 19F-NMR chemical shift imaging. The approach relies on photocrosslinking reaction of [CNV]K and [TF]T, 19F MR signal of [TF]T was drastically change by photocrosslinking because of the change of spatial proximity of trifluoromethyl group and the electron environment which the hybrid orbital of 5-carbon in [TF]T was changed sp2 to sp3. The [TF]T was chosen as 19F-labeled DNA from a viewpoint of structure (fluorine was near the cyclobutan ring) and sensitivity (it has three equivalent fluorine) (Fig. 4.2). Thus, we could monitor the change of 19F MR signal by the DNA photocrosslinking reaction in

19F NMR. And, we designed the miRNA-detection system based on 19F NMR chemical shift imaging.
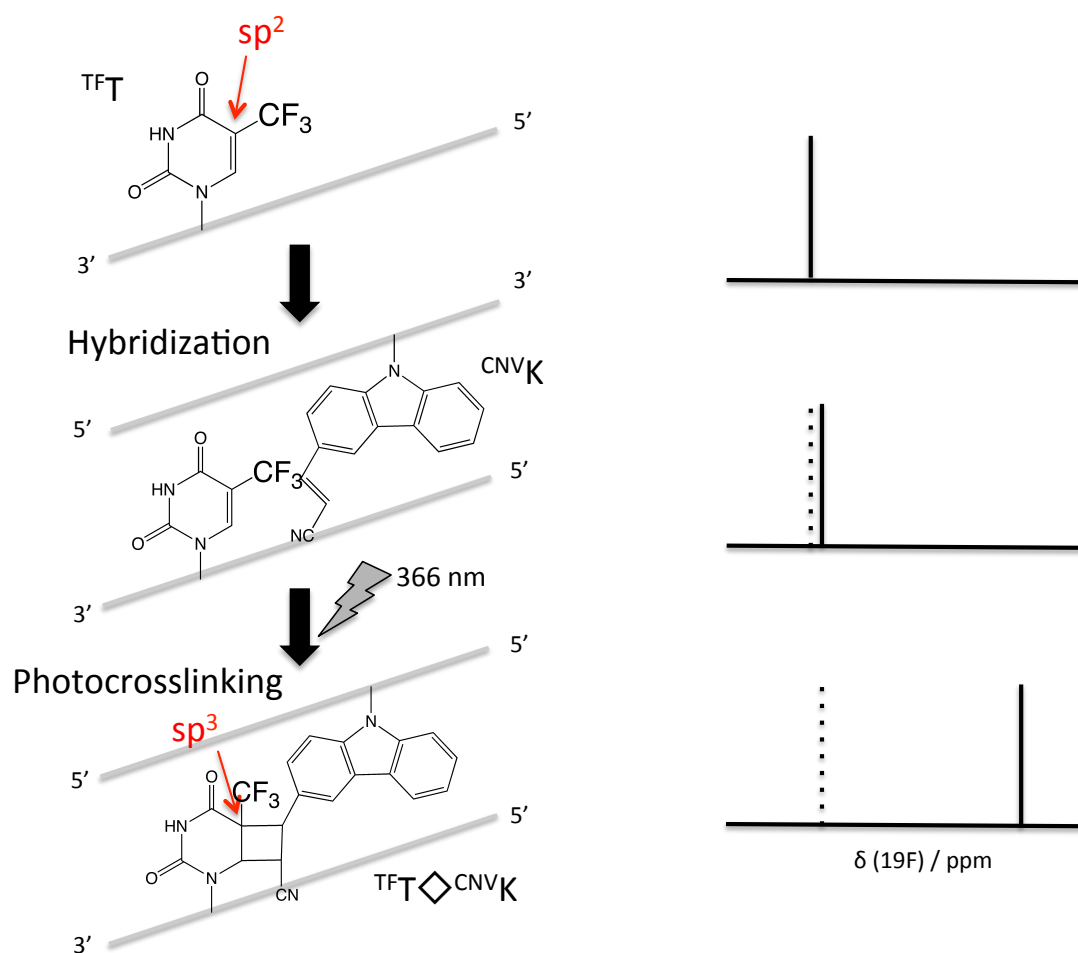

Figure 4.1 Strategy of chemical shift imaging using DNA photocrosslinking.

3.2. Materials and Methods

General

 ^{1}H NMR spectra were measured with AVANCE III NMR 500 (Bruker, 500 MHz) spectrometer. Mass spectra were recorded on a Voyager-DE PRO-SF, Applied Biosystems. Irradiation was performed by UV-LED (OMRON, ZUV, 366 nm, 1.6 W/cm^2). HPLC was performed on a Chemcobond 5-ODS-H column (10 × 150 mm, 4.6 × 150 mm) or a Chemcosorb 5-ODS-H column (4.6 × 150 mm) with a JASCO PU-980, HG-980-31, DG-980-50 system equipped with a JASCO UV 970 detector at 260 nm. The reagents for the DNA synthesizer such as A, G, C, T-β-cyanoethyl phosphoramidite, and CPG support were purchased from Glen Research. Calf intestine alkaline phosphatase (AP) was purchased from Promega. Nuclease P1 was purchased from Yamasa.

5'-O-(4,4'-dimethoxytrityl)-5-trifluoromethyl-deoxyuridine

 To a solution of 5-trifluoromethyl-deoxyuridine(1.0 g, 3.04 mmol) in pyridine (10 mL) was added a solution of 4,4'-dimethoxytrityl chloride(1.23 g, 3.65 mmol) and 4-(dimethylamino)pyridine (0.07 g, 0.6 mmol), in pyridine (10 mL) at room temperature and the reaction mixture was stirred at room temperature for 24 h. After the reaction mixture was evaporated, the residue was chromatographed on a silica gel usgin CHCl$_3$/CH$_3$OH (99:1 v/v) as eluent to give 5'-O-(4,4'-dimethoxytrityl)-3-Cyanovinylcarbazole-1'-β-deoxyriboside (1.2 g, 2.01 mmol) as yellow powder. ^{1}H-NMR (400 MHz, CDCl$_3$) δ

5'-O-(4,4'-dimethoxytrityl)-5-trifluoromethyl-deoxyuridine-3'-O-(cyanoethoxy-N,N-di isopropylamino)phosphoramidite

 5'-O-(4,4'-dimethoxytrityl)-3-Cyanovinylcarbazole-1'-β-deoxyriboside (0.50 g, 0.83 mmol) in seal bottle was dissolved in Acetnitrile and coevaporated three times in *vacuo*. After substituted with argon, 2-cyanoethyl *N,N,N,N'*-tetraisopylphosphorodiamidite

(0.26 mL, 0.83 mmol) in acetonitrile (0.87 mL) and 0.45 M 1*H*-tetrazole in acetonitrile (1.96 mL, 0.83 mL) were added, and the reaction mixture was stirred at room temperature for 3 h. Then the reaction mixture was extracted with AcOEt, which was washed with a saturated aqueous solution of NaHCO$_3$, and water. The organic layer was collected, dried over anhydrous sodium sulfate, filtered, and evaporated to dryness under reduced pressure. Then, the crude in sealed bottle was dissolved in acetonitrile and coevaporated three times, and was used for automated DNA synthesizer without further purification.

DNA sequences, synthesis and purification

Oligonucleotides were prepared by β-(cyanoethyl) phosphoramidite method on controlled pore glass supports (1 mmol) using DNA synthesizer. Strands containing ^{CNV}Ks and ^{TF}Ts were synthesized using the cyanoethylphosporamidite of ^{CNV}K that was synthesized according to the previous reported method. After automated synthesis, the oligomer was detached from the support by soaking in 50 mM K$_2$CO$_3$ in methanol for 1 h at room temperature. Deprotection was conducted by 50 mM K$_2$CO$_3$ in methanol at room temperature for 4 h and neutralization by TCA. The sample was removed the solvent using speedvac, and melts in water, and the crude oligomer was purified by reverse phase HPLC.

19F-NMR spectrum

^{19}F NMR spectra were recorded on Bruker AVANCE III 500 instrument with a 5 nm probe head at 470 MHz for fluorine. The solvent for ^{19}F NMR measurement was 10 mM Tris-HCl buffer (pH 7.6) containing trisfluoroacetic acid (for an internal standard, -75.6 ppm) and 10% (v/v) D$_2$O. Acquisition; 8192 or 16384 times.

3.3. Results and Discussions

To evaluate the photoreactivity of ^{CNV}K to ^{TF}T, an equimolar mixture of ODN 1 containing ^{CNV}K (5'-TGCA^{CNV}KACGT-3') and ODN 2 containing ^{TF}T (5'-ACGTG^{TF}TGCA) was irradiated at 366 nm at 4°C (Fig. 4.2A), and then analyzed by HPLC (Fig. 4.2B). Before photoirradiation, the ODN 1 having a retention time of 29 min and ODN 2 having retention time of 17 min was detected. The new peak having a retention time of 21 min was increased dependent on the photoirraidation time, and the peak of ODN 1 and 2 disappeared by photoirradiation for 2 seconds. The mass analysis of the photoproduct having a retention time of 21 min, whose mass is identified to a mass of d(ODN 1◇ODN 2) (5597.15, calcd. For [(M+H)$^+$], found 5595.84), suggested that the reaction was caused by photoreaction of ODN 1 and ODN 2. And, the photoproduct was enzymatic-degraded, purified by HPLC, and then the photocrosslinked product was analyzed by mass spectrum. The result of the mass of (630.19, calcd for [(M+H)$^+$], found 630.33), suggested that ^{CNV}K can be crosslinked with ^{TF}T. The photocrosslinking rate constant of target ^{TF}T was two-fold lower than that of target T. And, to confirm the reversibility of the photocrosslinking reaction, the photoproduct of ODN 1 and ODN 2 was irradiated at 312 nm and analyzed by denaturing HPLC. The peak of having retention time of 21 disappeared and the peak of having retention time of 17 and 29 was detected, it suggested that the photoproduct was reverted to the original ODN 1 and ODN 2.
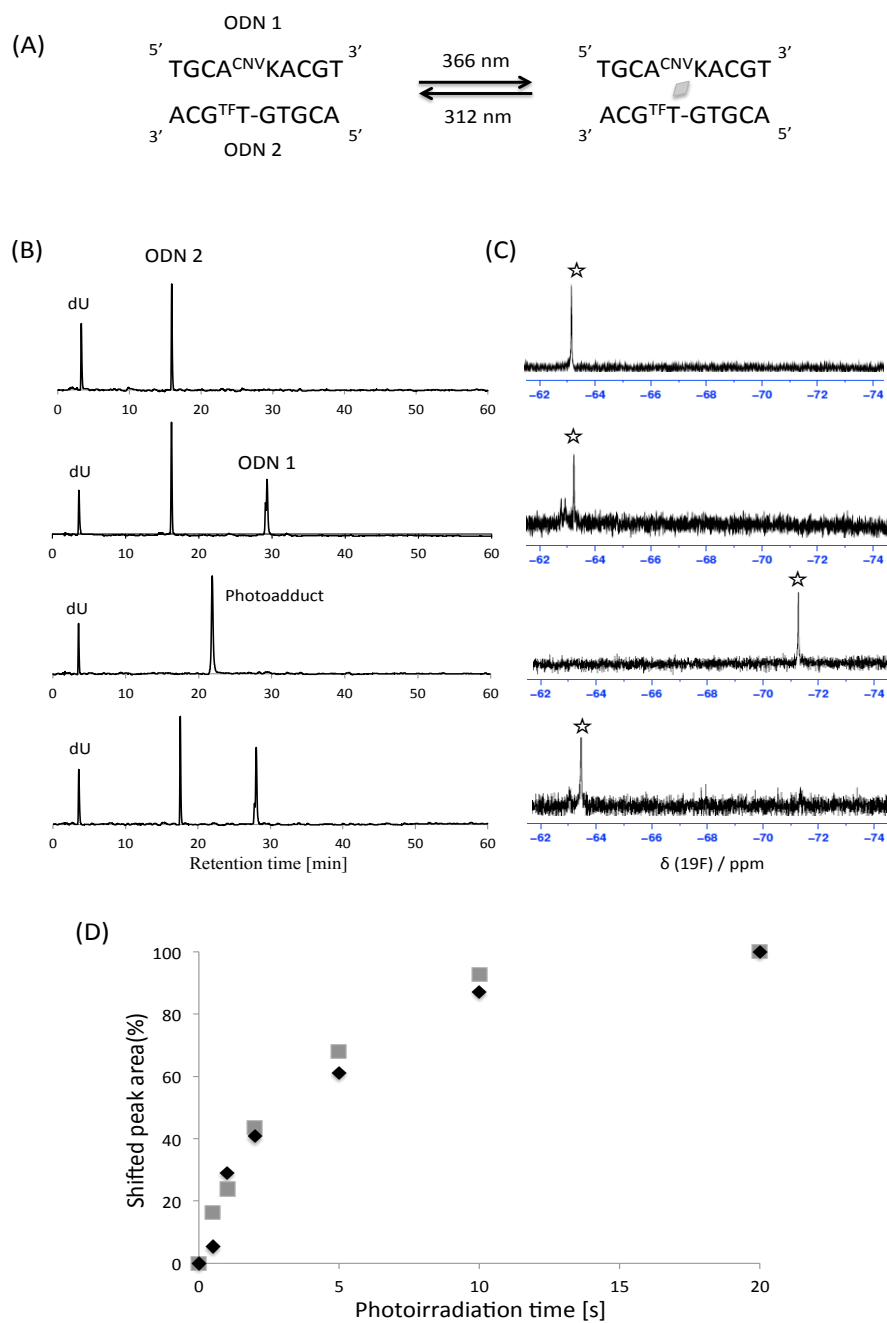
Figure. 4.2 (A) Schematic illustration of reversible photocrosslinking between ODN 1 having ^{CNV}K and ODN 2 having ^{TF}T. (B) The HPLC analysis and (C) 19F-NMR spectrum of 20 μM ssODN, ds ODN, photocrosslinked dsODN, and photosplitted dsODN in 10 mM Tris-HCl (pH 7.6) containing 100 mM NaCl, 100 μM deoxyuridine as an internal standard in HPLC, and 10 μM trifluoroacetic acid as an internal standard in 19F-NMR(-75.6 ppm). (D) The time course of the photocrosslinking rate analyzed HPLC (■) and NMR (◆).

To evaluate the usefulness of change of chemical shift by photocrosslinking with ^{CNV}K for chemical shift imaging based on photocrosslinking reaction, the photoirradiated sample was measured by the 19F MR signal in 19F-NMR to confirm the shift of the 19F MR signal by photocrosslinking (Fig. 4.2C). As shown in Fig. 4.2C, the 19F MR signal of ^{TF}T in single strand DNA was appeared at -63.1 ppm. Then, by addition ODN 1 as the complementary strand including ^{CNV}K, the 19F MR signal shifted to -63.2 ppm, suggesting that it was a 19F MR signal of ^{TF}T in double stranded DNA. After the photoirradiation at 366 nm for 20 s in an NMR tube, the chemical shift of the 19F MR signal in ^{TF}T clearly shifted toward the high magnetic field at -71.2 ppm dependent on the photoirradiation time. The shifted peak of -71.2 ppm was return to -63.2 ppm according to photosplitting of ^{CNV}K and ^{TF}T. The samples after the 19F NMR measurement were analyzed by HPLC and the photocrosslinking rate calculated. In Fig 1D, the photocrossilnking rate calculated by HPLC compared with the shifted peak are calculated by the NMR spectrum and both peak areas were in good agreement, suggesting this chemical shift of the 19F MR signal was induced by the photocrosslinking reaction of ^{CNV}K and ^{TF}T.

This dramatic change of the chemical shift at 8 ppm using the photocrosslinking reaction was 10 times larger than the chemical shift according to the transition single strand to double strand using ^{F}U and $^{(TF)3}$T. This suggests that this wide range chemical shift was capable of imaging the target molecule into a complex system without being influenced by the surrounding sequence.

The ^{CNV}K having reversibility was photocrosslinked by 366 nm photoirradiation and photosplitted by 312 nm irradiation. This 8 ppm chemical shift by photocrosslinking can be reverted to -63.2 ppm by photosplitting. Conventionally, we checked the photocrosslinking reaction by HPLC and denaturing PAGE, which required the change of the sample condition. However, by the 19F NMR chemical shift of the photocrosslinking reaction, we will investigate the photocrosslinking without the change of the sample condition.

Next, we demonstrated a RNA-detection system based on 19F NMR chemical shift imaging that combines the amplification capability of the hybridization chain reaction (HCR). In the absence of target miRNA, both probes are in the closed forms, and the 19F MR signal was not shifted by the photocrosslinking reaction. However, in the presence of target miRNA, it pairs with the sticky end of probe-A, which undergoes an unbiased strand exchange interaction to open the hairpin structure. The newly exposed sticky end of probe-A nucleates at the sticky end of probe-B and opens the hairpin to expose a sticky end on probe-B. This sticky end is identical in sequence to the target. In this way each copy of the miRNA can propagate a chain reaction of hybridization events between alternating probe-A and -B hairpin to form a nicked double strand DNA (Fig. 4.3A). In this time, ^{TF}T is located in the target position of ^{CNV}K so we can observe the 19F MR signal by photocrosslinking only in the presence of target miRNA.

We designed that the DNA hairpin probes including ^{TF}T and ^{CNV}K having a stem of 14 base pairs enclosing an 8 nucleotide loop and the ^{CNV}K was inserted into the hairpin part and ^{TF}T was inserted into the sticky end. First, the 19F MR signal of hairpin probe A and B was measured, and it was observed at approximately -63.2 ppm. Then, by adding the 10 nM miRNA, the hairpin structures were opened by strand exchange interaction and it formed a nicked double strand DNA. However, in this state, the 19F MR signal was observed at -63.2 ppm because of non-photocrosslinking between ^{CNV}K and ^{TF}T (Fig. 4.3C(I)). By the photoirradiation to the nicked double strand, the 19F MR signal shifted to -71.2 ppm at first by the change of the electron environment and the spatial proximity of trifluorothymidine accompanying photocrosslinking (Fig. 4.3C(II)). In this experiment, 10 nM miRNA was successfully detected by the shift of 19F MR signal using DNA photocrosslinking.

Finally, to test the selectivity of 19F NMR chemical shift imaging mediated HCR, we used miRNA200 family having 5 miRNAs as 200a, 200b, 200c, 141, 429 (Fig. 4.3B). The NMR spectrum showed that only miRNA 200a worked as trigger to open the hairpin structure of the probe. Thus, the HCR probe had high selectivity for

complementary miRNA and the chemical shift was successfully performed photoirradiation at 366 nm to nicked duplex DNA. The shifted peak area has an approximately 60% peak, its peak area was over 60 times compared with shifted peak areas at the time of using the expected target miRNA as a trigger. This miRNA-detection system based on chemical shift was capable of detecting the 10 nM target miRNA in a sequence specific manner.

Probe A : TCTGGTAACGATGTTGAAA^{CNV}KCTACATCGTTACCAGACAG^{TF}TGTTA
Probe B : AGG^{TF}TTTCAACATCGTTACCAGATAACA^{CNV}KTGTCTGGTAACGATGT

(B)

Entry	miRNA
200a	UAA**C**ACUG**U**C**U**GGUAA**CGAU**G**U**
200b	UAA**U**ACUG**C**C**U**GGUAA**UGAU**G**A**
200c	UAA**U**ACUG**C**C**G**GGUAA**UGAU**G**GA**
141	UAA**C**ACUG**U**C**U**GGUAA**AGAU**G**G**
429	UAA**U**ACUG**U**C**U**GGUAA**AACC**G**U**

(C)

(D)

Figure. 4.3 (A) Schematic illustration of HCR using DNA photocrosslinking and probe sequence. (B) The sequence of miRNA 200 family (C) The 19F NMR spectrum of the trigger as (I) 200a without photoirradiation, (II) 200a, (III) 200b, (IV) 200c, (V) 141, and (VI) 429 with photoirradiation at 366 nm. (D) The relative shifted peak area in the presence of each miRNA.

3.4. Conclusion

In this chapter, we presented a concept of chemical shift imaging of nucleic acid using DNA photocrosslinking. The 19F MR signal was shifted -63.2 ppm to -71.2 ppm by the change of spatial proximity and electronic state in trifluoromethyl group using DNA photocrosslinking with ^{CNV}K. And, it was successful the detection of 10 nM miRNA using 19F chemical shift imaging mediated HCR in sequence specific manner.

3.5 Reference

1 Higuchi M, Kobori A, Yamayoshi A, Murakami A, Synthesis of antisense oligonucleotides containing 2'-O-psoralenylmethoxyalkyl adenosine for photodynamic regulation of point mutations in RNA. *Bioorg. Med. Chem.*, **2009**, 17, 475-483.

2 Higuchi M, Yamayoshi A, Yamaguchi T, Iwase R, Yamaoka T, Kobori A, Murakami A, Selective photo-cross-linking of 2'-O-psoralen-conjugated oligonucleotide with RNAs having point utations. *Nucleosides. Ncleotides. Nucleic. Acids.*, **2007**, 26, 277-290.

3 Murakami A, Yamayoshi A, Iwase R, Nishida J, Yamaoka T, Wake N, Photodynamic antisense regulation of human cervical carcinoma cell growth using psoralen-conjugated oligo(nucleoside phosphorothioate). *Eur. J. Pharmac. Sci.*, **2001,** 13, 25-34.

4 Giovannangeli C, Diviacco S, Labrousse V, Gryaznov S, Charneau P, Helene C. Accessibility of nuclear DNA to triplex-forming oligonucleotides: the integrated HIV-1 provirus as a target. *Proc. Natl. Acad. Sci. U.S.A.*, **1997**, 94, 79-84.

5 Yoshimura Y, Fujimoto K, Ultrafast reversible photo-cross-linking reaction: toward in situ DNA manipulation. *Org. Lett.,* **2008**, 10, 3227-3230.

6 Fujimoto K, Yamada A, Yoshimura Y, Tsukaguchi T, Sakamoto T, Detail of ultrafast DNA photo-cross-linking reaction of 3-cyanovinylcarbazole nucleoside: cis-trans isomeric effect and the its application for SNP based genotyping. *J. Am. Chem. Soc.,* **2013**, 135, 16161-16167.

7 Shigeno A, Sakamoto T, Yoshimura Y, Fujimoto K, Quick regulation of mRNA functions by a few seconds of photoirradiation. *Org. Biomol. Chem.,* **2012**, 10, 7820-7825.

8 Sakamoto T, Shigeno A, Ohtaki Y, Fujimoto K, Photo-regulation of constitutive gene expression in living cells by using ultrafast photo-cross-linking oligonucleotides. *Biomaterials. Science,* **2014**, 2, 1154-1157.

9 Tagawa M, Shohda K, Fujimoto K, Suyama A, Stabilization of DNA nanostructures by photo-cross-linking. *Soft. Matter.,* **2011**, 7, 10931-10934.

10 Gerrard S R, Hardiman C, Shelbourne M, Nandhakumar I, Noed*é*n B, Brown T, A new modular approach to nanoassembly: stable and addressable DNA nanoconstructs via orthogonal click chemistries. *ACS. Nano.,* **2012**, 6, 9221-9228.

11 Nakamura S, Fujimoto K, Creation of DNA array structure equipped with heat resistance by ultrafastcrosslinking. *J. chem. Tech. Biotech.,* **2014**, 89, 1086-1090.

12 Yoshimura Y, Ohtake T, Okada H, Fujimoto K, A new approach for reversible RNA photocrosslinking reaction: application to sequence-specific RNA selection. *ChemBioChem*, **2009**, 10, 1473-1476.

13 Fujimoto K, Kishi S, Sakamoto K, Geometric effect on photocrosslinking reaction between 3-cyanovinylcarbazole nucleoside and pyrimidine base in DNA/RNA heteroduplex. *Photochemistry and Photobiology*, **2013**, 89, 1095-1099.

14 Nakamura S, Fujimoto K, Rapid photopolymerization of oligonucleotides by 3-cyanovinylcarbazole mediated DNA photocrosslinking. *Journal of photopolymer Science and Technology*. **2014**, 27, 485-490.

15 Z*í*dek L, *Ś*tefl R, Sklen*á*ř V, NMR methodology for the study of nucleic acids. Opin. *Curr.* Struct. Biol., **2001**, 11, 275-281.

16 F*ü*rtig B, Richter C, W*ö*hnert J, Schwalbe H, NMR spectroscopy of RNA. *ChemBioChem*, **2003**, 4, 936-962.

17 Mayer M, James T L, Discovery of ligands by a combination of computational and NMR-based screening: RNA as an example target. *Methods. Enzymo.*, **2005**, 394, 571-587.

18 Tanabe K, Harada H, Narazaki M, Tanaka K, Inafuku K, Komatsu H, Ito T, Yamada H, Chujo Y, Matsuda T, Hiraoka M, Nishomoto S, Monitoring of biological one-electron reduction by 19F NMR using hypoxia selective activation of an 19F labeled indolequinone derivave. *J. Am. Chem. Soc.,* **2009**, 131, 15982-15983.

19 Rastinejad F, Evilia C, Lu P, Studies of nucleic acids and their protein interactions by 19F NMR. *Methods. Enzymol.,* **1995**, 261, 560-575.

20 Mizukami S, Takikawa R, Sugihara F, Hori Y, Tochio H, W*ä*lchi M, Shirakawa M, Kikuchi K, Paramagnetic relaxation-based 19F NMR probe to detect protease activity. *J. Am. Chem. Soc.,* **2008**, 130, 794-795.

21 Mizukami S, Takikawa R, Sugihara F, Shirakawa M, Kikuchi K, Dual-function probe to detect protease activity for fluorescence measurement and 19F NMR. *Angew. Chem. Int. Ed.,* **2009**, 48, 3641-3643.

22 Takaoka Y, Sakamoto T, Tsukiji S, Narazaki M, Matsuda T, Tochio H, Shirakawa M, Hamachi I, Self-assembling nanoprobes that display off/on 19F nuclear magnetic resonance signals for protein detection and imaging. *Nat. Chem.,* **2009**, 1, 557-561.

23 Higuchi M, Iwata N, Matsuba Y, Sato K, Sasamoto K, Saido T C, 19F and 1H NMR detection of amyloid beta plaques in vivo. *Nat. Neurosci.,* **2005**, 8, 527-533.

24 Sakamoto T, Shimizu Y, Sasaki J, Hayakawa H, Fujimoto K. Signal turn-on probe for nucleic acid detection based on 19F nuclear magnetic resonance. Bioorg. *Med. Chem. Lett.,* **2011**, 21, 303-306.

25 Olejniczak M, Gdaniec Z, Fischer A, Grabarkiewicz T, Bielecki L, Adamiak R W, The bulge region of HIV-1 TAR RNA binds metal ions in solution. *Nucleic. Acids. Res.,* **2002**, 30, 4241-4249.

26 Arnold J R P, Fisher J, Structural equilibrium in RNA as revealed by 19F NMR. *J. Biomol. Struct. Dyn.,* **2000**, 17, 843-856.

27 Hammann C, Norman D G, Lilley D M, Dissection of the ion-induced folding of the hammerhead ribozyme using 19F NMR. *J. Proc. Natl. Acad. Sci. U.S.A.,* **2001**, 98, 5503-5508.

28 Chu W-C, Horowitz J, 19F NMR of 5-fluorouracil-substituted transfer RNA transcribed in vitro: resonance assignment of fluorouracil-guanine base pair. *Nucleic. Acids. Res.,* **1989**, 17, 7241-7252.

29 Marshall A G, Smith J L, Nuclear-spin-labeled nucleic acids. 1 19F nuclear magnetic resonance of Escherichia coli 5-fluorouracil-5S-RNA. *J. Am. Chem. Soc.,* **1977**, 99, 635-636.

30 Gmeiner W H, Pon R T, Lown J W, 2'-SCF3 Uridine-A Powerful Label for probing structure and function of RNA by 19F NMR Spectroscopy. *J. Org. Chem.,* **1991**, 56, 3602-3608.

31 Nivrutti B B, Rerhate N B, Pavol C, Drobny D, Snorri T S, A nanofluoro nucleoside as a sensitive 19f NMR probe of nucleic acid conformation. *Org. Lett.,* **2008**, 10, 2745-2747.

32 Kimasauskas S, Szyperski T, Serva S, Wuthrich K, Dynamic modes of the fipped-out cytosine during HhaI methytransferase-DNA interaction in solution. *EMBO. J.,* **1998**, 17, 317-324.

33 Trempe J-F, Wilds C J, Denisov A Y, Pon R T, Damha M J, Gehring K J, NMR solution structure of an oligonucleotide hairpin with a 2F'-ANA/RNA stem:

implications for RNase H specificity toward DNA/RNA hybrid duplexes. *J. Am. Chem. Soc.,* **2001**, 123, 4896-4903.

Chapter 4.

Photochemical regulation of DNA strand displacement by

ultrafast photocrosslinking reaction using ^{CNV}K

4.1. Introduction

DNA strand displacement is an important biological reaction in gene recombination, DNA replication, and the repair of DNA damage. RecA and Rad51 play central roles in DNA strand displacement *in vivo* and these proteins regulate and promote the reaction [1-3].

In the field of DNA nanotechnology, nucleic acids have predictable double-helical structure and generally well-understood thermodynamic and mechanical properties, which makes them excellent enegineering materials. Moreover, toehold-mediated DNA strand displacement is a central reaction to provide dynamics to DNA. The DNA strand displacement between double stranded DNA and single stranded DNA is a basic operation of dynamic DNA nanotechnology to construct DNA logic circuits [6-8], catalysts [9,10], autonomous molecular motors [11-14], and reconfigurable DNA nanostructures [15-17], which is central to many dynamic DNA devices built to date.

Fig. 5.1(A) showed DNA strand displacement in detail. A domain is a set of contiguous nucleotides designed to be either fully bound or fully unbound in stable configurations. A system initially comprises a two-stranded complex containing template and passenger strand and single standed invader strand. The complex has a single stranded overhang called a "toehold". The invader is fully Watson-Crick complementary to the template strand and may bind reversibly to it using the toehold domain. This binding reversibility because the toehold may fray and eventually dissociation. Once the toehold is bound, the "overhanging" branch migration domain of the invader may complex with the template the ranch point of the three-stranded complex moves back and forth. This "three-way branch migration" process has previously been modeled as an unbiased random walk, as each step causes no net change in base pairing. Eventually, the passenger may dissociate, completing strand

displacement. Overall, displacement is thermodynamically driven forward by the net gain in base pairs due to the toehold.
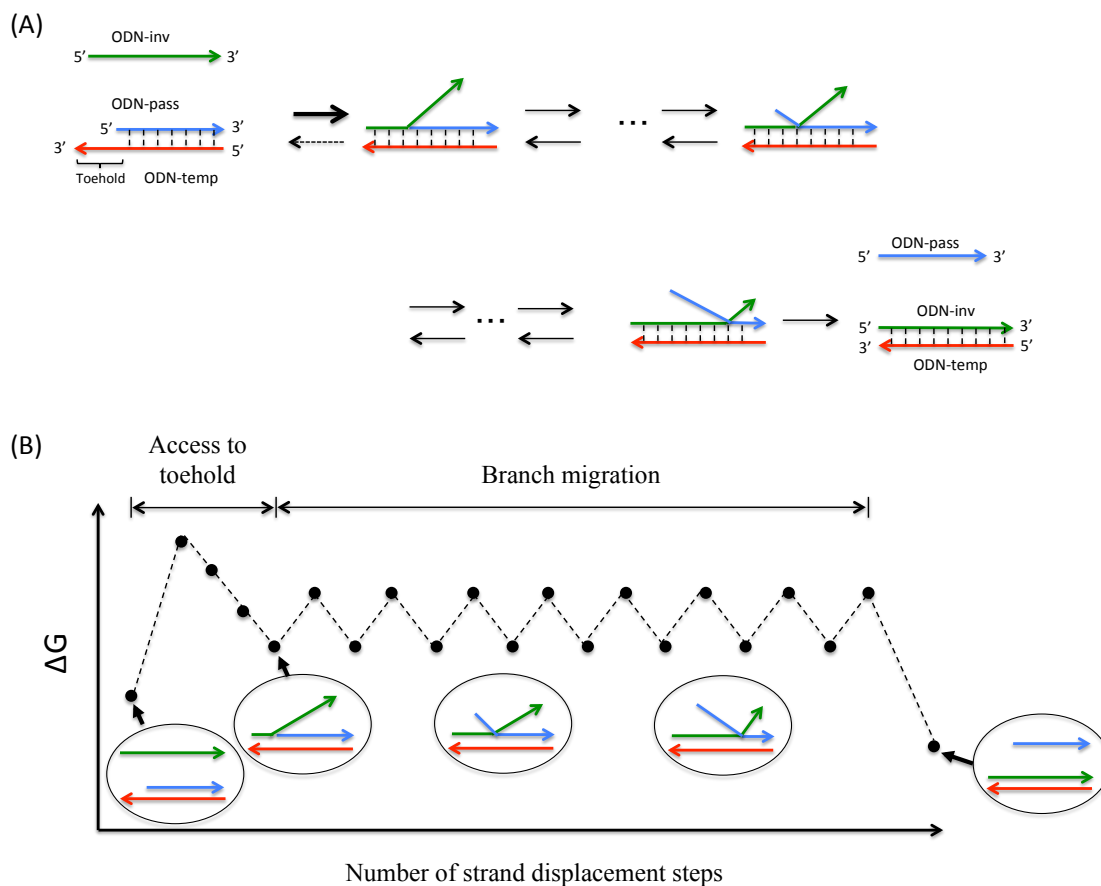

Figure. 5.1 (A) Scheme of toehold mediated DNA strand displacement (B) Imgage of free energy landscape of the intuitive energy landscape model.

Winfree and co-worker considered on the kinetics of toehold-mediated DNA strand displacement by building a simple single-pathway model called the IEL model. The IEL considers an invading strand and a template-passenger complex contained in a virtual box. The state space of the IEL is illustrated in Fig. 5.1B. First state corresponds to the invader being unattached to the template-passenger duplex. Next state represents the formation of a first base pair within the toehold. This access to toehold step has almost no backward reaction so that this step was advanced faster in free energy. From here, each step of branch migration involves replacing a template-passenger

base pair with template-invader base pair. They describe the stepping between these intermediates using a simple effective transition state of raised free energy, so each complete branch migration step is shown as a single tooth of the "saw tooth" pattern. This unknown effective transition state could be potentially as simple as a frayed template-passenger base pair, but could also be more complex. The final stage of successful displacement involves the dissociation of the final base pair between invader and template. This branch migration step is equiblibrium reaction which is hybridize and dissociate in each base so this step is bottoleneck in DNA strand displacement. However, there is an issue with the response speed of the action when the DNA concentration is lower. Acceleration of DNA strand displacement is required for the rapid response of the nanomachines or the logic gate. Maruyama and co-workers have previously demonstrated that cationic comb-type copolymers composed of a polycation backbone and abundant hydrophilic graft chains influence kinetics and thermodynamics of nucleic acid hybridization under physiologically relevant conditions.

 The bottoleneck is branch migration step which has equilibrium reaction in each base and it is expected the acceleration of DNA strand displacement by the change equilibrium reaction into non-equilibrium reaction. The three-way junction have to move only forward by the change hydrogen bond between invader strand and invader strand into covalent bond (Fig. 5.2A). We have reported on ultrafast photocrosslinker 3-cyanovinylcarbazole (^{CNV}K) [26,27], in which ODN containing ^{CNV}K was photocrosslinked to complementary strand by irradiation at 366 nm for a few seconds. In this report, we demonstrate the photochemical acceleration of DNA strand displacement by DNA photocrosslinking using ^{CNV}K. By the DNA photocrosslinking was applyied to DNA strand displacement, the energybarrier becames big in photocrosslinking site.
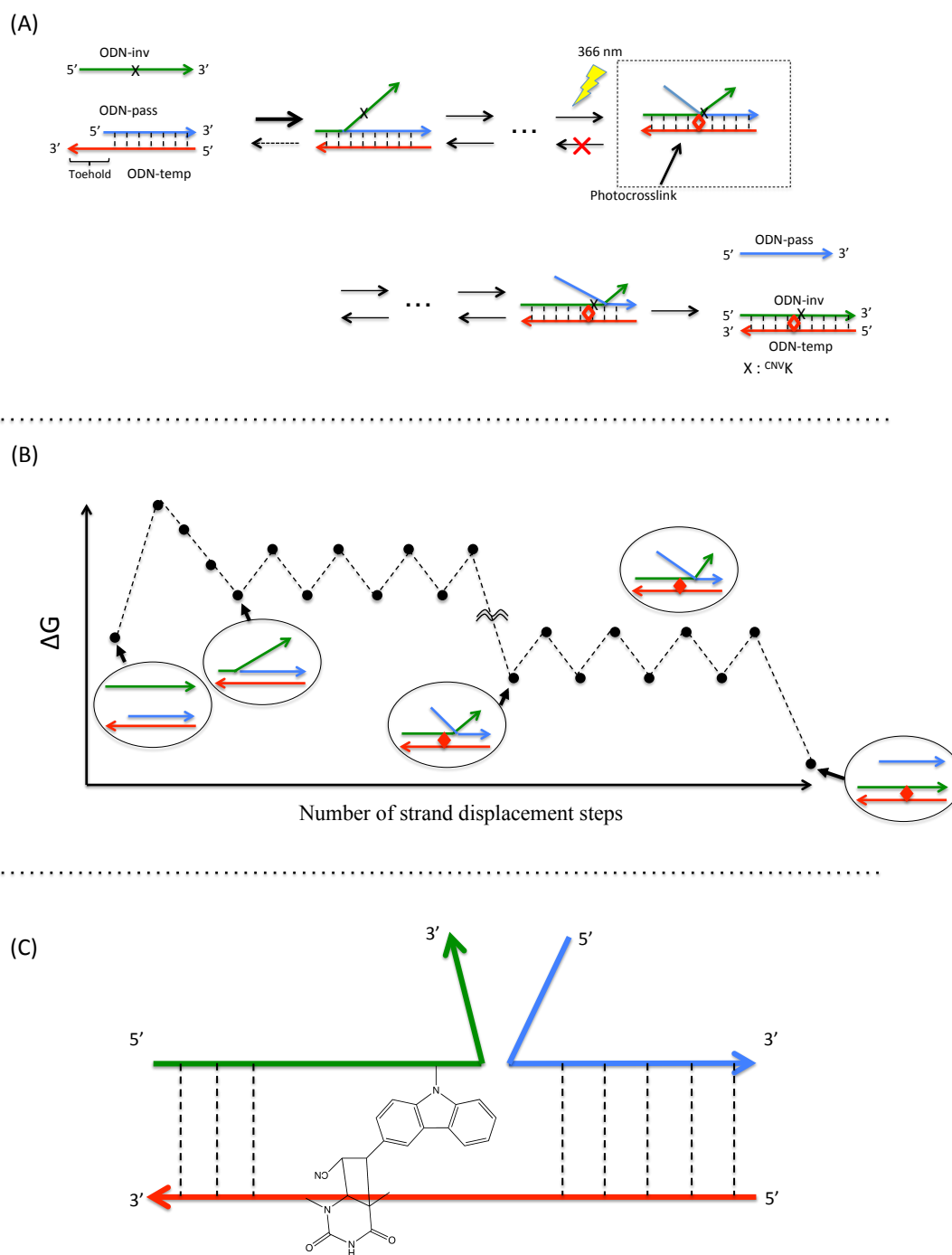
Figure. 5.2 (A) Concept of photochemical regulation of toehold mediated DNA strand displacement (B) Image of free energy landscape of the intuitive energy landscape model (C) Photocrosslink adduct in DNA strand displacement.

4.2. Materials and Methods

General

Mass spectra were recorded on a Voyager-DE PRO-SF, Applied Biosystems. Irradiation was performed by UV-LED (OMRON, ZUV, 366 nm, 1.6 W/cm^2). HPLC was performed on a Chemcobond 5-ODS-H column (10 × 150 mm, 4.6 × 150 mm) or a Chemcosorb 5-ODS-H column (4.6 × 150 mm) with a JASCO PU-980, HG-980-31, DG-980-50 system equipped with a JASCO UV 970 detector at 260 nm. The reagents for the DNA synthesizer such as A, G, C, T-β-cyanoethyl phosphoramidite, and CPG support were purchased from Glen Research. Calf intestine alkaline phosphatase (AP) was purchased from Promega. Nuclease P1 was purchased from Yamasa.

Denaturing polyacrylamide gel electrophoresis

For analysis of the sizes of DNA nanostructures by gel electrophoresis, sample solutions were diluted by 8M Urea in formamide and heated at 70°C for 5 min. Loading samples were prepared with an appropriate amount of 6×loading buffer [36% (v/v) glycerol, 30 mM EDTA and 0.05% (w/v) each of bromophenol blue and xylene cyanol] and loaded onto gels prepared with 10% polyacrylamide (29:1, polyacrylamide: bisacrylamide) containing 8 M Urea and running buffer (1×TBE). The gels were run at 150 V on a gel electrophoresis apparatus (Bio-RAD). After electrophoresis, the gels were imaged by Cy3 fluorescence on an Imaging System LAS-3000(FUJIFILM Inc.).

UV-melting study

Ultraviolet melting curves were determined in 1 cm path length cells using a V-630 Bio UV–Visible spectrophotometer (JASCO), equipped with a thermoelectric temperature controller. Absorbance versus temperature profile was measured at 260 nm with a heating rate of 0.5 °C/min.

FRET assay for real-time monitoring of DNA strand displacement

Cy3/dabcyl-labeled ds DNA (50 nM) was incubated at 25°C with invader strand (60 nM) in 50 mM Cacodylate buffer (pH7.4) conyaining 100 mM NaCl in the absence or presence of photoirradiation. The changein fluorescence intensity of the mixture (total volume 100 μL) in a 0.5×0.5 cm^2 quarz cell was recorder on a JASCO FP-6500 spectrofluprpmeter at excitation and emission wavelengths of 550 nm and 520 nm, respectively, with excitation and emission slits at 3 nm. The degree of DNA strand displscement was calculated using the following equation.

Degree of strand displacement = $([FI]_t - [FI]_0) / ([FI]_\infty - [FI]_0) * 100$

Where $[FI]_0$ is the initial fluorescence intensity and $[FI]_t$ and $[FI]_\infty$ are fluorescence intensities at time t and after the reaction reached equilibrium, respectively. The value of $[FI]_\infty$ was obtained by measuring fluorescence intensity after one day.

4.3. Results and Discussion

I demonstrated a photochemical regulation of DNA strand displacement having 6 nt toehold and 13 nt branch migration by DNA photocrosslinking using ^{CNV}K. The invader strand containing ^{CNV}K was photocrosslink to thymidine in template strand when the three-way junction moves to inserting position of ^{CNV}K, and then the three-way junction have to move forward since the covalent bond blocked. Thus, it is expected that the insertion position of ^{CNV}K is an important factor in the photochemical regulation of DNA strand exchange (Fig. 5.2A). So we synthesized ODN containing ^{CNV}K in the 5'-position (nearest toehold), center-position, and 3'-position of branch migration. The rate of DNA strand exchange was monitored by FRET system using Cy3-labeled template strand as the fluorescence and Dabcyl-labeled passenger strand as Quencher (Table 5.1).

Table. 5.1 The sequence of ODN; The template strand and passenger strand was labeled Cy3 and Dabcyl, respectively. Invader strands with ^{CNV}K inserted in the 5', center, or 3'-position and the native strand were used in this experiment.

Entery	Role	Sequence(5'- to 3')
ODN 1	Template strand	Cy3-AGTAGCTTCATTATCGTAC
ODN 2	Passenger strand	TAATGAAGCTACT-Dabcyl
ODN 3	Invader strand(5')	GTACGATAA^{CNV}KGAAGCTACT
ODN 4	Invader strand(Center)	GTACGATAATGAA^{CNV}KCTACT
ODN 5	Invader strand(3')	GTACGATAATGAAGCTA^{CNV}KT
ODN 6	Invader strand(Native)	GTACGATAATGAAGCTACT

We prepared a series of invader strand inserting ^{CNV}K in different position to estimate the effect of ^{CNV}K on the stability of dsDNA since ^{CNV}K has no Watson-Crick interaction with the native base. Fig. 5.3 shows UV-melting curve of template-passenger and template-invader pairs dsDNA in 50 mM sodium cacodylate buffer (pH7.0) containing 100 mM NaCl. The template-passenger dsDNA was less stabilizing than all template-invader dsDNA so that DNA strand displacement thermodynamically

driven forward by the net gain in base pairs due to the toehold. The dsDNA with ^{CNV}K inserted in the center position has the lowest thermal stability in the other template-invader dsDNAs, and native template-invader dsDNA has the highest thermal stability.
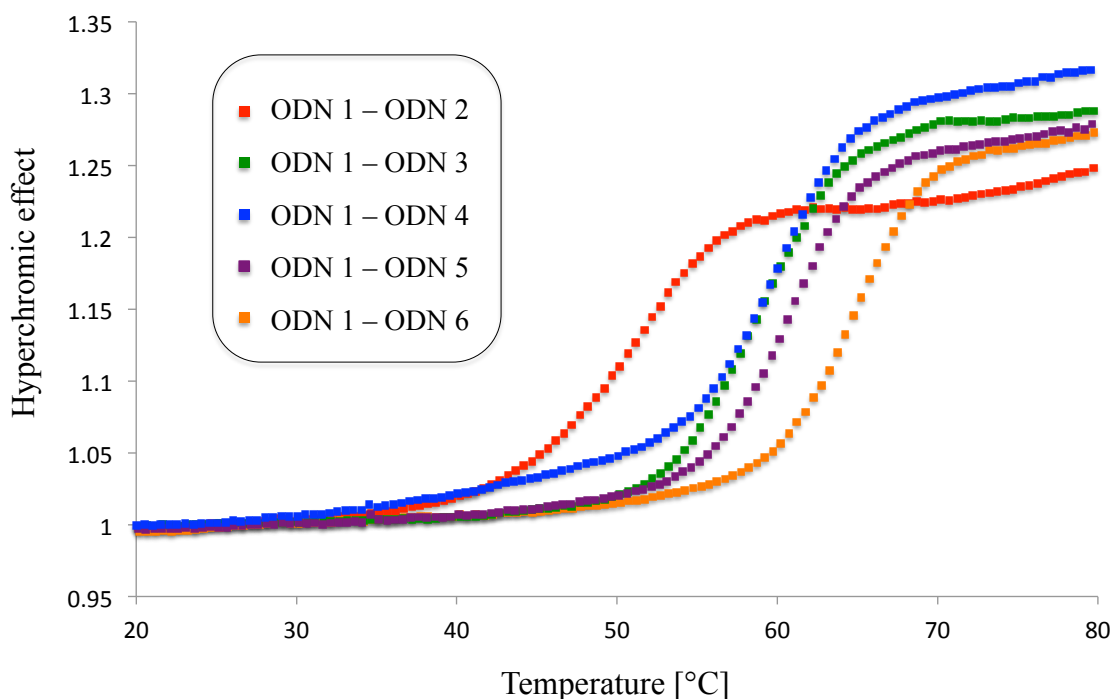

Figure. 5.3 UV-melting curve of template-passenger (red), template-invader containing ^{CNV}K in 3'-side (green), template-invader containing ^{CNV}K in center (blue), template-invader containing ^{CNV}K in 5'-side (purple), and template-invader (yellow).

Next, we examined the acceleration of DNA strand displacement by DNA photocrosslinking using ODN 4 as invader strand. The DNA photocrosslinking was advanced when branch migration move to inserting position so we confirmed photocrosslinking reaction onto DNA stand displacement by denaturing PAGE analysis imaged by Cy-3 fluorescence. The photoirradiation was performed at 25°C after addition of invader strand. A band corresponding to ODN 1 disappeared and a new band corresponding to photoadduct of ODN 1 and ODN 4 appeared as a photoirradiation time (Fig. 5.4B). This result indicated that the photocrosslinking reaction was advanced onto DNA strand displacement. In order to evaluate the kinetic of DNA strand displacement

more quantitatively, we employed a FRET assay using Cy3 and dabcyl as fluorescent molecule and quencher. The extent of DNA strand displacement over time in the absence and presence of photoirradiation is shown in Fig. 5.4C. The rate of DNA strand displacement in the presence of photoirradiation was clearly higher than that in the absence of photoirradiation, indicating that the DNA strand displacement was accelerated by the photocrosslinking reaction using ^{CNV}K.
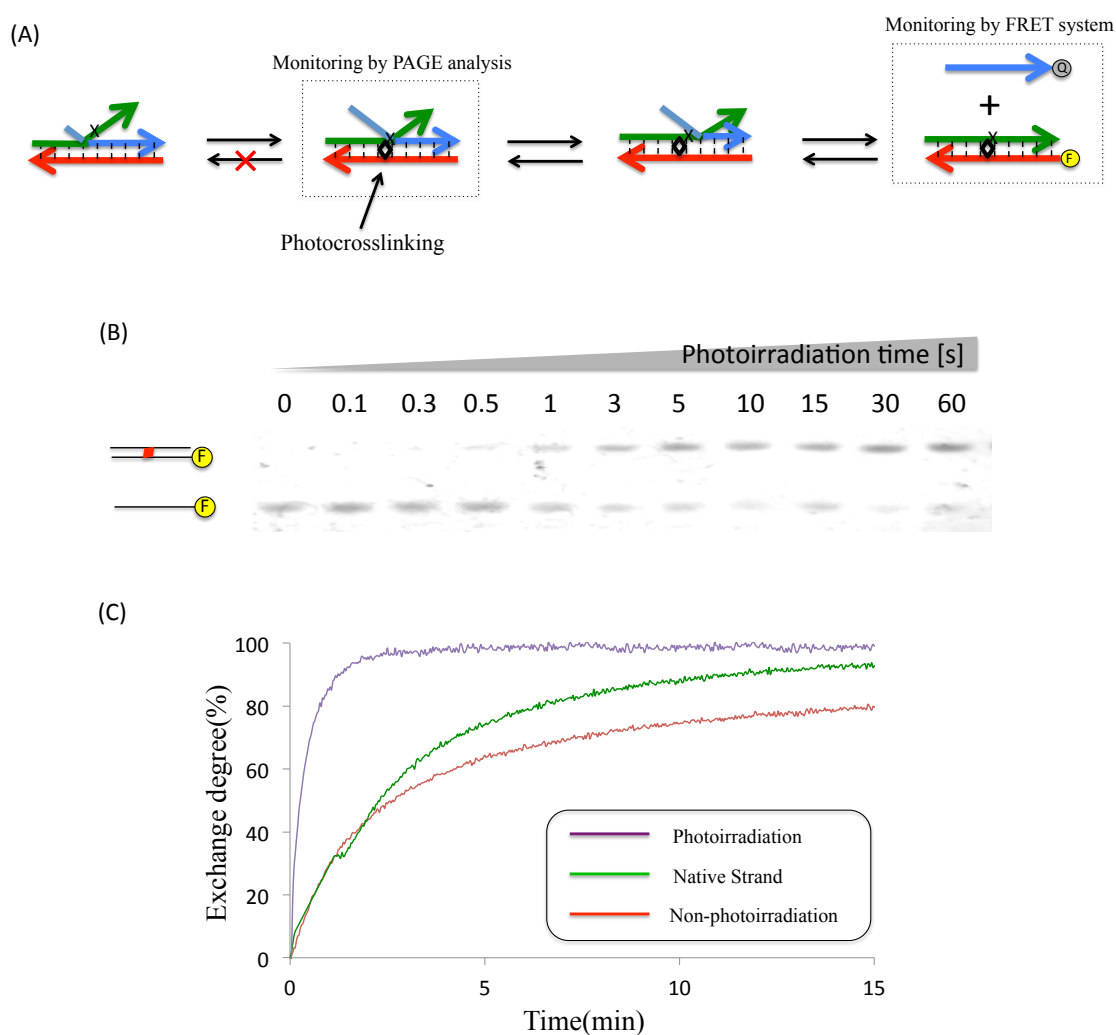

Figure. 5.4 (A) Illustrated monitoring of DNA strand displacement by PAGE analysis and FRET system. (B) The denaturing PAGE analysis on photocrosslinking reaction (C) Time course of DNA strand displacement using ODN 4 as the invader strand with photoirradiation (purple) and without photoirradiation (red) and that using ODN 6 as invader strand.

For the assessment of the effect of photocrosslinking position of ^{CNV}K, ODN 3 and ODN 5 were added as invader strand. The mixture was photoirradiated at 366 nm immediately after addition of invader strand, and the rate of DNA strand displacement was analyzed by FRET (Fig. 5.5). The pseudo first order rate (*k'*) for the DNA strand displacement determinedby FRET are summarized in Table 5.2. For all invader strands containing ^{CNV}K in the presence of photoirradiation, acceleration of the DNA strand displacement was observed, although the acceleration effects were different depending on the photocrosslinking position of ^{CNV}K. The acceleration effects of ODN 4 and ODN 5 were clearly greater than those in the absence of photoirradiation, and ○○ to ○○-fold acceleration effect was observed. On the other hands, a little acceleration effect was acquired using ODN 3 as invader strand. Moreover, the rate of photocrosslinked DNA strand displacement was compaired with one of DNA strand displacemtn using ODN 6. In using ODN 4 and ODN5 as invader strand, the ○○- and ○○- fold acceleration effect was observed. However, in using ODN 3 as invader strand, the rate of photocrosslinked DNA strand displacement was later than one of DNA strand displacement using ODN 6 as invader strand. Those results suggested the DNA strand displacement was accelerated by DNA photocrosslinking and the high acceleration effect requires that ^{CNV}K inserted the number of bases certain degree from toehold.

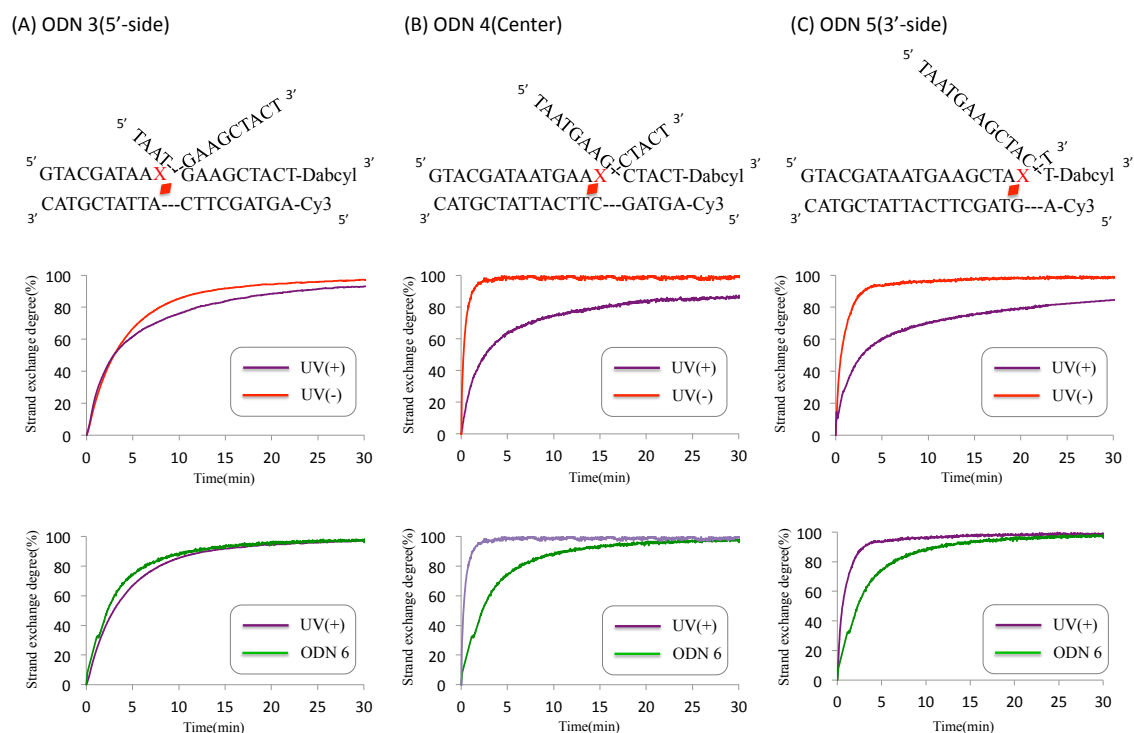(A) ODN 3(5′-side)　　　　　(B) ODN 4(Center)　　　　　(C) ODN 5(3′-side)

Figure. 5.5 The illustrated three-way junction when photocrosslinking and the time course of DNA strand displacement using DNA photocrosslinking. (A) The ODN 3 as invader strand;(B) The ODN 4 as invader strand; (C)The ODN 5 as invader strand.

Table. 5.2 The rate of DNA strand displacement and acceleration effect of DNA strand displacement by DNA photocrosslinking.

Invader strand	Photoirradiation	k/s^{-1}	Acceleration effect
ODN 3	non		
ODN 3			
ODN 4			
ODN 4			
ODN 5			
ODN 5			
ODN 6			

ODN 3 $\overset{\text{2 steps}}{\longleftrightarrow}$ $\overset{\text{10 steps}}{\longleftrightarrow}$ $(2^2+10^2)\cdot K$

ODN 4 $\overset{\text{6 steps}}{\longleftrightarrow}$ $\overset{\text{6 steps}}{\longleftrightarrow}$ $(6^2+6^2)\cdot K$

ODN 5 $\overset{\text{10 steps}}{\longleftrightarrow}$ $\overset{\text{2 steps}}{\longleftrightarrow}$ $(10^2+2^2)\cdot K$

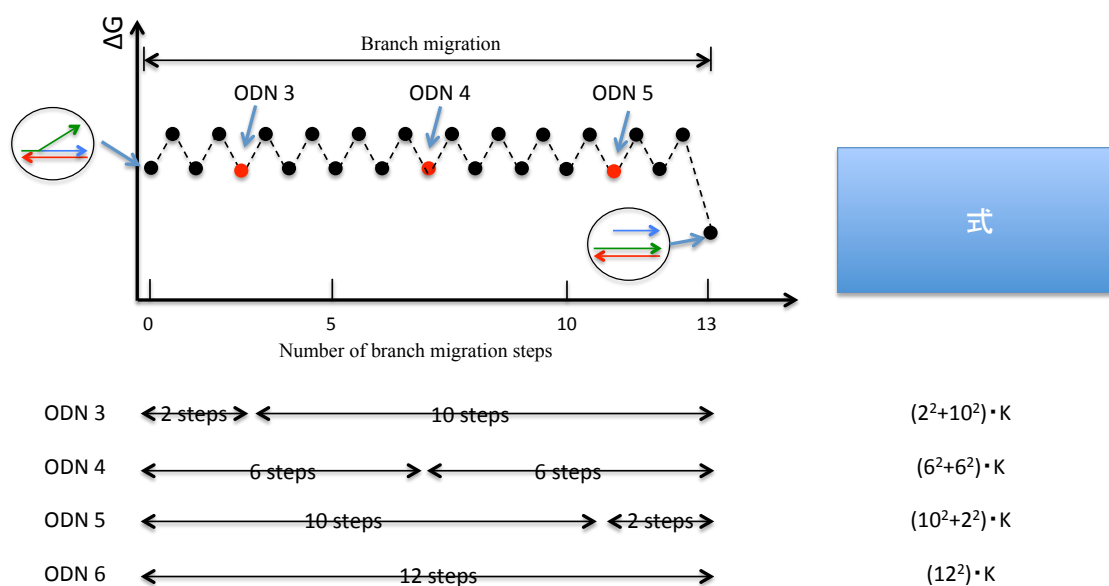ODN 6 $\overset{\text{12 steps}}{\longleftrightarrow}$ $(12^2)\cdot K$

Figure. 5.6 Mechaistic investigation for DNA strand displacement rate.

These results suggested that the inserting position of $^{\text{CNV}}$K was important factor which has an influence on acceleration effect. In previous report, the strand displacement rate was proportional to the square of the length of the branch migration step. The photocrosslinking reaction of $^{\text{CNV}}$K separated two equilibrium reactions in branch migration step. In using ODN 6 as invader strand, it is possible to regard the branch migration step as one equilibrium reaction. On the other hands, the branch migration step was composed two equilibrium reactions which is divided in photocrosslinking site when ODN 3, 4, and 5 were used as invader strand with a photoirradiation (Fig. 5.6). In ODN 3, there are two equiblirium reactions which are consisted in 2 nucleotides and 10 nucleotides in branch migration step. Similarly, in ODN 4, they are consisted in 6 nt and 6 nt, in ODN 5, they are consisted in 10 nt and 2 nt in branch migration step. So, the biggest accelerating effect was acquired when $^{\text{CNV}}$K was inserted center position in branch migration pairt. It seems that the DNA photocrosslinking plays an important role in the final extrusion of DNA strand displacement as the reason for acquiring the acceleration effect of inserting $^{\text{CNV}}$K into the 3'-position.
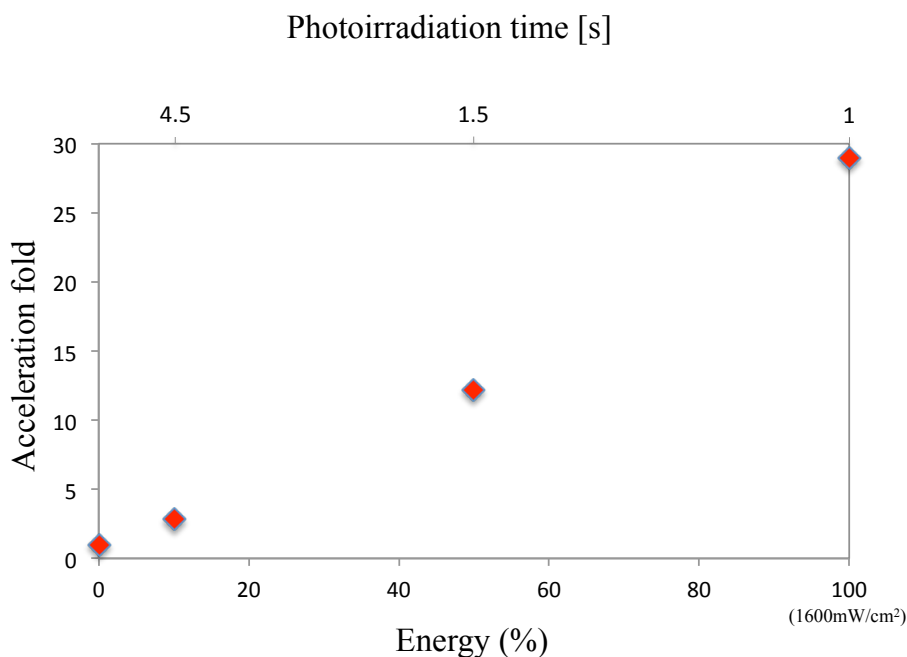
Photoirradiation time [s]

Figure 5.7 The relation between the photocrosslinking rate and acceleration effect.

One of the reasons that the acceleration of DNA strand displacemen by DNA photocrosslinking could be achieved is the high photoresponsive ability of ^{CNV}K. The ^{CNV}K was able to photocrosslink to thymidine base with a 366 nm photoirradiation in 1600 mW/cm^2 for approximately 1 second, and the acceleration effect 29-fold was acquired about DNA strand displacement. Furthermore, incase of 366 nm photoirradiation at 800 mW/cm^2, ^{CNV}K photocrosslinked for 1.5 second and the 12-fold acceleration effect was acquired. In case of 160 mW/cm^2 photoirradiation ^{CNV}K photocrosslinked for 4.5 second and 3-fold acceleration effect was acquired. It is seemed that a little acceleration effect is acquired by the other photocrosslinkers which required photoirradition for minitule-scale. The great acceleration effect is acquired by the ultrafast photocrosslinker '^{CNV}K' for the first time.

4.4. Conclusion

In conclusion, we explored the effect of DNA photocrosslinking of ^{CNV}K on DNA strand displacement. The DNA strand displacement was accelerated by DNA photocrosslinking over photoirradiation time. The insertion position of ^{CNV}K greatly affected the acceleration, which a maximum of 29-fold as acceleration effect acquired in inserting ^{CNV}K into the center-position. We expected that this knowledge will contribute to improvement the speed of DNA logic circuits based on DNA strand displacement.

4.5 Reference

1   Wu A M, Bianchi M, DasGupta C, Radding C M, Unwinding associated with synapsis of DNA molecules by recA protein. *Proc. Natl. Acad. Sci. U.S.A.,* **1983**, 80, 1256-1260.

2   Howard-Flanders P, West S C, Stasiak A, Role of RecA protein spiral filaments in genetic recombination. *Nature*, **1984**, 309, 215-219.

3   Sung P, Catalysis of ATP-dependent homologous DNA pairing and strand exchange by yeast RED51 protein. *Science*, **1994**, 265, 1241-1243.

4   Mullis K B, Faloona F A, Specific synthesis of DNA in vitro via a polymerase-catalyzed chain reaction. *Methods. Enzymol.,* **1987**, 155, 335-350.

5   Notomi T, Okayama H, Masubuchi H, Yonekawa T, Watanabe K, Amino N, Hase T, Loop-mediated isothermal amplification of DNA. *Nucleic Acids Res.,* **2000**, 28, E63.

6   Stojanovic M N, Semova S, Kolpashchikov D, Macdonald J, Morgan C, Stefanovic D, Deoxyribozyme-based ligase logic gates and their initial circuits. *J. Am. Chem. Soc.,* **2005**, 127, 6914-6915.

7   Penchovsky R. Breaker R R, Computational design and experimental validation of oligonucleotide-sensing allosteric ribozymes. *Nat. Biochnol.,* **2005**, 23, 1424-1433.

8   Seelig G, Soloveichik D, Zhang D Y, Winfree E, Enzyme-free nucleic acid logic circuits. *Science*, **2006**, 314, 1585-1588.

9   Zhang D Y, Turberfield A J, Yurke B, Winfree E, Engineering entropy-driven reaction and network catalyzed by DNA. *Science*, **2007**, 318, 1121-1125.

10 Yin P, Choi H M, Calvert C R, Pierce N R, Programming biomolecular self-assembly pathways. *Nature*, **2008**, 451, 318-323.

11 Yurke B, Turberfield A J, Mills A P, Simmel F C, Neumann J, A DNA fueled molecular machine made of DNA. *Nature*, **2000**, 406, 605-508.

12 Dirks R M, Pierce N A, Triggered amplification by hybridization chain reaction. *Proc. Natl. Acad. Sci. U.S.A.,* **2004**, 101, 15275-15278.

13 Pei R, Taylor S K, Stefanovic D, Rudchenko S, Mitchell T E, Stojanovic M N, Behavior of polycatalytic assemblies in a substrate-displaying matric. *J. Am. Chem. Soc.,* **2006**, 128, 12693-12699.

14 Green S J, Bath J, Turberfield A J, Coordinated chemomechanical cycles: a mechanism for autonomous molecular motion. *Phys. Rev. Lett.,* **2008**, 101, 238101.

15 Bath J, Turberfield A J, DNA nanomachines. *Nat. Nanotechnol.,* **2007**, 2, 275-284.

16 Zhang D Y, Seelig G, Dynamic DNA nanotechnology using strand-displacement reaction. *Nat. Chem.,* **2011**, 3, 103-113.

17 Krishnan Y, Simmel F C, Nucleic acid based molecular devices. *Angew. Chem. Int. Ed.,* **2011**, 50, 3124-3156.

18 Zhang D Y, Winfree E, Control of DNA strand displacement kinetics using toehold exchange. *J. Am. Chem. Soc.,* **2009**, 131, 17303-17314.

19 Soloveichik D, Seelig G, Winfree E, DNA as a universal substrate for chemical kinetics. *Proc. Natl. Acad. Sci. U.S.A.,* **2010**, 107, 5393-5398.

20 Qian L, Winfree E, Bruck J, Neural network computation with DNA strand displacement cascades. *Nature,* **2011**, 475, 368-372.

21 Qian L, Winfree E, Scalling up digital circuit computation with DNA strand displacement cascades. *Science,* **2011**, 332, 1196-1201.

22 Lund K, Manzo A J, Dabby N, Johnson-Buck A, Nangreave J, Taylor S, Pei R, Stojanovic M N, Walter N G, Winfree E, Yan H, Molecular robots guided by prescriptive landscape. *Nature,* **2010**, 465, 206-210.

23 Kin W J, Akaike T, Maruyama A, DNA strand exchange stimulated by spontaneous complex formation with cationic comb-type copolymer. *J. Am. Che. Soc.,* **2002**, 124, 12676-12677.

24 Choi S W, Kano A, Maruyama A, Activation of DNA strand exchange by cationic comb-type copolymers: effect of cationic moieties of the copolymers. *Nucleic. Acids. Res.,* **2008**, 36, 342-351.

25 Srinivas N, Quldridge T E, Sulc P, Schaeffer J M, Yurke B, Louis A A, Doye J P, Winfree E, On the biophysics and kinetics of thoehold-mediated DNA strand displacement. *Nucleic. Acids. Res.,* **2013**, 41, 10641-10658.

26 Yoshimura Y, Fujimoto K, Ultra-fast reversible photocrosslinking reaction: Toward in situ DNA manipulation. *Org. Lett.,* **2008**, 10, 3227-3230.

27 Fujimoto K, Yamada A, Yoshimura Y, Tsukaguchi T, Sakamoto T, Details of ultra-fast DNA photocrosslinking reaction of 3-cyanovinylcarbazole nucleotide; Cis-trans isomeric effect and the application for SNP based genotyping. *J. Am. Chem. Soc.,* **2013**, 135, 16161-1616

Chapter 5.

Reversible photocrosslinking reaction of

3-cyanovinylcarbazole nucleotide using branch migration

5.1. Introduction

A reversible DNA photocrosslinking technology is a useful tool for detecting, manipulating, and releasing of nucleic acid. Psoralen and its derivatives are well-know photocrosslinkers. Oligonucleotides containing psoralen stabilize double stranded formation by the covalent bond, and these oligonucleotides successfully regulate gene expression in a photoresponsive manner [1-4]. However, the use of a photocrosslinking reaction with psoralen limits the choice of the target DNA as an efficient crosslinking reaction requires a TpA step [5-6]. Additionally, the photocrosslinked DNA via [2+2] cycloaddition between psoralen and thymidine base, were generated to the normal DNA by 254 nm irradiation resulting in fatal damage to normal DNA.

We have already reported on ultrafast photocrosslinker 3-cyanovinylcarbazole ([CNV]K) [7,8], oligonucleotides including [CNV]K can photocrosslink to pyrimidine base in a complementary strand with a few seconds of photoirradiation. Applications using [CNV]K such as creation of a stable DNA structure [9-11], photochemical regulation of antisence effect [12,13], and C→U RNA editing [14,15] have been reported. Thus, the ultrafast photocrosslinking reaction of [CNV]K has been used for various applications. However, photoirradiation at 312 nm also results in fatal damage to normal DNA due to the formation of pyrimidine dimer. Thus, one problem associated with ultrafast reversible photocrosslinking is the fact that the efficiency of repeated DNA photoligation declines gradually due to DNA photodamage. The development of a reversible photocrosslinking system, which can be repeatedly crosslink and split, would represent a useful technique for DNA nanotechnology such as DNA computing, editing RNA, DNA nanoarchitecture.

Carbazole derivatives have strongly hydrophobic surfaces and have been used as electron donors [16]. These properties of carbazole derivatives are expected to be exploited as electron donor to study the photosplitting of a photoadduct of CNVK. When ODN containing carbazole nucleoside was photoirradiated in the presence of ODN containing thymidine dimer, the thymine dimer in DNA was catalytically repaired

through reductive photoinduced electron transfer. And the photosplitting was performed not only thymidine dimer but also photoligation product using carboxydeoxyuridine by a 366 nm irradiation using carbazole modified ODN as electron donor [17]. In similar mechanism, it is expected [2+2] cyclobutane ring can be split by using carbazole derivatives by irradiation at 366 nm. The ^{CNV}K is carbazole derivative, the photoadduct of ^{CNV}K has carbazole, which works as donor by photoirradiation by 366 nm, and it is expected the photosplitting was peformed with a 366 nm irradiation.

  In this study, we attempted photosplitting the photoadduct of ^{CNV}K using branch migration with a 366 nm photoirradiation without heating in sequence specific manner (Fig. 6.1).   As DNA strand displacement is expected to undertake dissociation of the DNA duplex in the same way as heating, we demonstrated the photosplitting using strand displacement instead of heating by irradiation at 366 nm.
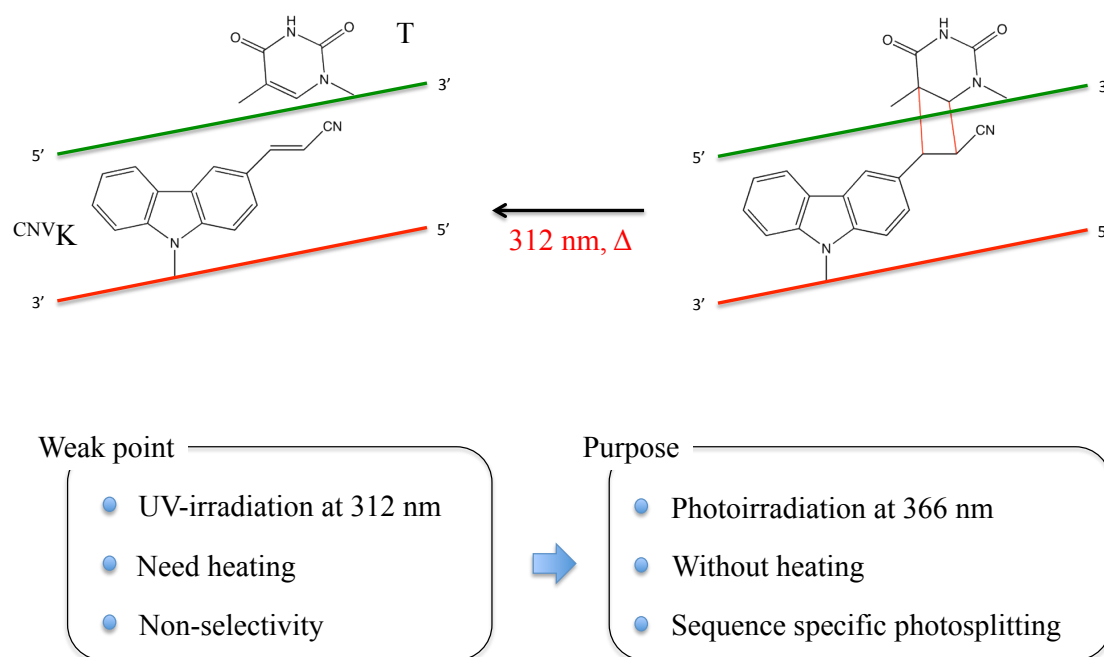

Figure. 6.1 The photosplitting of ^{CNV}K required UV-irradiation at 366 nm and heating.

5.2. Materials and Methods

General

Mass spectra were recorded on a Voyager-DE PRO-SF, Applied Biosystems. Irradiation was performed by UV-LED (OMRON, ZUV, 366 nm, 1.6 W/cm^2). HPLC was performed on a Chemcobond 5-ODS-H column (10 × 150 mm, 4.6 × 150 mm) or a Chemcosorb 5-ODS-H column (4.6 × 150 mm) with a JASCO PU-980, HG-980-31, DG-980-50 system equipped with a JASCO UV 970 detector at 260 nm. The reagents for the DNA synthesizer such as A, G, C, T-β-cyanoethyl phosphoramidite, and CPG support were purchased from Glen Research. Calf intestine alkaline phosphatase (AP) was purchased from Promega. Nuclease P1 was purchased from Yamasa.

Denaturing polyacrylamide gel electrophoresis

For analysis of the sizes of DNA nanostructures by gel electrophoresis, sample solutions were diluted by 8M Urea in formamide and heated at 70°C for 5 min. Loading samples were prepared with an appropriate amount of 6×loading buffer [36% (v/v) glycerol, 30 mM EDTA and 0.05% (w/v) each of bromophenol blue and xylene cyanol] and loaded onto gels prepared with 10% polyacrylamide (29:1, polyacrylamide: bisacrylamide) containing 8 M Urea and running buffer (1×TBE). The gels were run at 150 V on a gel electrophoresis apparatus (Bio-RAD). After electrophoresis, the gels were imaged by Cy3 fluorescence on an Imaging System LAS-3000(FUJIFILM Inc.).

FRET assay for real-time monitoring of DNA strand displacement

Cy3/dabcyl-labeled ds DNA (50 nM) was incubated at 25°C with invader strand (60 nM) in 50 mM Cacodylate buffer (pH7.4) conyaining 100 mM NaCl in the absence or presence of photoirradiation. The changein fluorescence intensity of the mixture (total volume 100 μL) in a 0.5 × 0.5 cm^2 quarz cell was recorder on a JASCO FP-6500 spectrofluprpmeter at excitation and emission wavelengths of 550 nm and 520 nm, respectively, with excitation and emission slits at 3 nm. The degree of DNA strand

displscement was calculated using the following equation.

Degree of strand displacement = ($[FI]_t - [FI]_0$) / ($[FI]_\infty - [FI]_0$) * 100

Where $[FI]_0$ is the initial fluorescence intensity and $[FI]_t$ and $[FI]_\infty$ are fluorescence intensities at time *t* and after the reaction reached equilibrium, respectively. The value of $[FI]_\infty$ was obtained by measuring fluorescence intensity after one day.

5.3. Results and Discussion

We designed a length of sticky end of 8 nt and branch migration of 21 nt, respectively, in photosplitting of ^{CNV}K using branch migration (Fig. 6.2). The sequences of ODNs are shown in Table 6.1. The Cy3-labeled passenger strand and template strand in buffer solution was photoirradiation at 366 nm for 300 s at 25°C or 37°C to create photocrosslinked ds DNA.
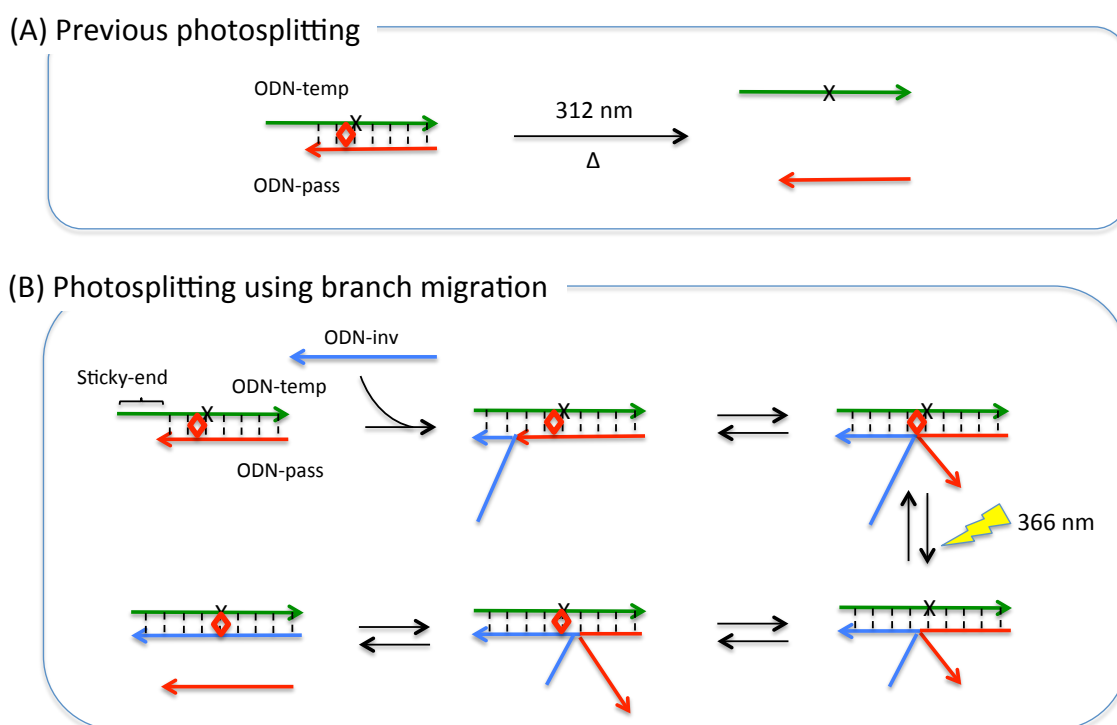

Figure. 6.2 (A) Illustrated scheme of two types photosplitting of ^{CNV}K (A) Previous photosplitting (B) Photosplitting using branch migration.

Table. 6.1 The sequence of ODNs

Entry	Role	The Sequence of ODNs (5'-3')	Length [nt]	
ODN 1	Template	CCTGGAAGGCG**X**AACTTAGCCACTGTGAA	29	
ODN 2	Passenger	Cy3-TTCACAGTGGCTAAGTTC**C**GC	21	
ODN 3	Invader	TTCACAGTGGCTAAGTTCCGCCTTCCAGG	29	(X = ^{CNV}K)

First, we evaluated the photosplitting ratio of the photoadduct of ^{CNV}K⊏C using branch migration with a 366 nm irradiation at 25°C (Fig. 6.3A). After the creation of the photocrosslinked dsDNA which was consisted of a Cy3-labeled passenger strand and a

template strand containing ^{CNV}K, invader strand was added in solution and then incubated at 25°C for 1 h. The solution was photoirradiated at 366 nm for 300 min at 25°C and then analyzed by denaturing PAGE imaged by Cy3 fluorescence. A band having high mobility compared with Cy3-photocrosslinked dsDNA appeared clearly and such band did not appear in the absence of the invader strand, suggesting that photocrosslinked ds DNA clearly photosplitted to Cy3-passenger strand by photoirradiation (Fig. 6.3B). By using branch migration, the photoadduct was splitted over 60% with a 366 nm irradiation for 300 min (Fig. 6.3C). On the other hand, without the invader strand, the photosplitting ratio did not change by photoirradiation at 366 nm, suggesting the photosplitting reaction of ^{CNV}K was not processed with a photoirradiation at 366 nm in double strand. The photoreaction of ^{CNV}K is considered to take a photostationary state of photocrosslinking and photosplitting under photoirradiation at 366 nm. In two strand hybridization, the reaction rate constant of photocrosslinking was much faster than that of photosplitting so that we can observe only the photocrosslinking reaction.
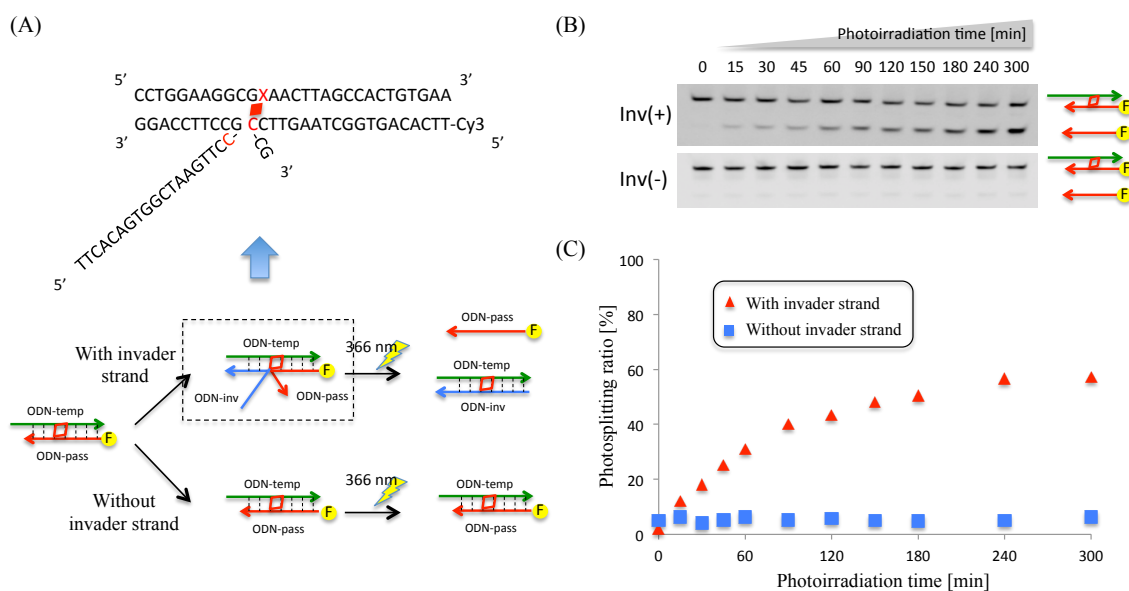

Figure. 6.3 The photosplitting using branch migration with a 366 nm photoirradiation. (A) The (B) Denaturing PAGE analysis; (C) The time course of photosplitting ration. (▲) and (■) show the photosplittinf ration with and wihout invader strand, respectively.

The photophysical and photochemical process of photosplitting with branch migration by a 366 nm photoirradiation are illustrated with a simple mechanistic scheme (Fig. 6.4). Upon illuminated with light, the carbazole moiety absorbs a photon to produce the excited state. The excited state has the foolowing relaxation pathway: electron transfer to covalently linked dimer. The charge-separated species, formed by the electron transfer, undergoes two competitive processes: splitting to produce thymine and carbazole$^{\cdot+}$-thymine$^{\cdot-}$(it then becomes carbazole-thymine by carge combination) and back electron transfer to return to the ^{CNV}K and thymine. However, under the photoirradiation with a 366 nm, photosplitted ^{CNV}K crosslinked to thymine very fast one again. So, 366 nm was used as the wavelength for photocrosslinking reaction. In this photosplitting using branch migration, photosplitted ODN is pushed out from photocrosslinking position and the passenger strand was blocked photocrosslinking to template strand. DNA strand displacement thermodynamically driven forward by the net gain in base pairs due to the toehold so that template-invader strand is stable duplex.

It is considered that the photoreaction of ^{CNV}K was consisted form photocrosslinked dsDNA, non-photocrosslinked dsDNA, and ssDNA (Fig. 6.5). The ^{CNV}K take photostationally state of photosplitting (k_{P1}) and photocrosslinking (k_{P2}) under the photoirradiation with a 366 nm and the rate constant photovrosslinking k_{P2} is great higher than one of photosplitting k_{P1}. The part of photosplitting dsDNAwill was dissociateion and take ssDNA state in thermal stationally state of dissociation (k_{T1}) and hybridization (k_{T2}). Those states could be regulated that photostationally state was irradiation wavelength and thermal equilibrium was incubated temperature. The branch migration makes the k_{P1} of template and passenger strand big so that the photosplitting using branch migration with a 366 nm irradiation without heating was achieved.
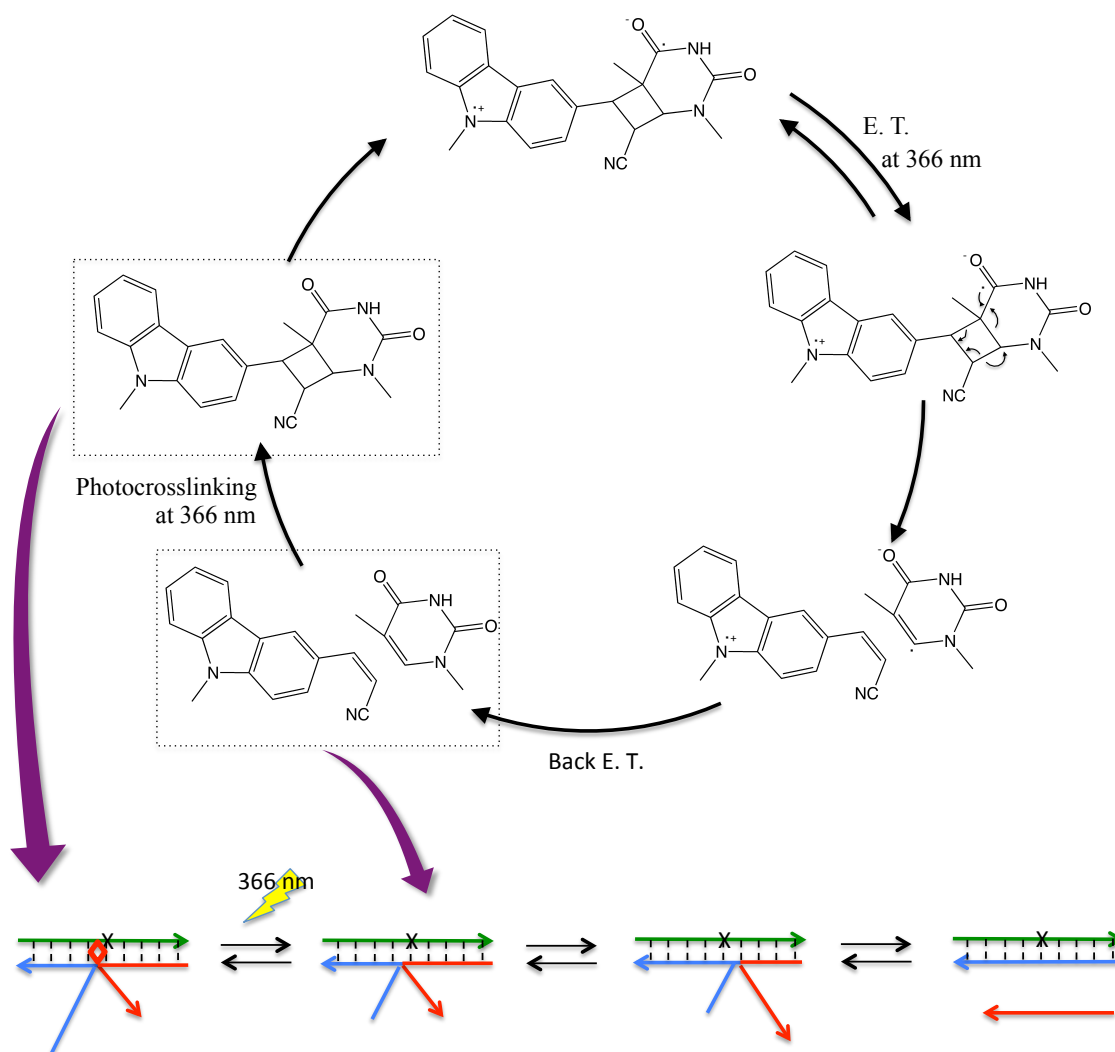
Figure. 6.4 The mechanism of photosplitting using branch migration with a 366 nm irradiation without heating.
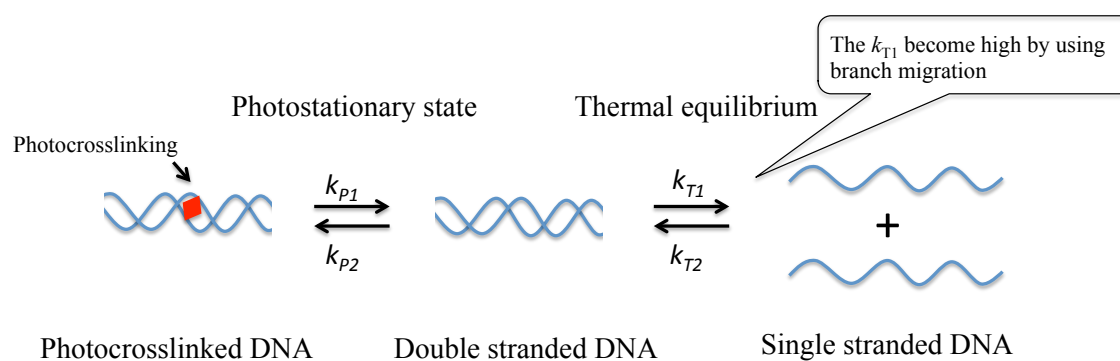

Figure. 6.5 The illustrated scheme of photoreaction of ^{CNV}K.

Table. 6.2 The sequence of ODNs.

Entry	Role	The Sequence of ODNs (5'-3')	Length [nt]	
ODN 4	Template	CCTGGAAGGCA**X**AACTTAGCCACTGTGAA	29	
ODN 5	Passenger	Cy3-TTCACAGTGGCTAAGTTC**T**GC	21	
ODN 6	Invader	TTCACAGTGGCTAAGTTCTGCCTTCCAGG	29	(X = ^{CNV}K)

The ^{CNV}K can be cross-linked by irradiation at 366 nm with an adjacent pyrimidine base in a [2+2] manner and the photocrosslinking rate constant in the target thymine base was 30-fold higher than that in the target cytosine. As shown in Fig. 6.5, the k_{P2} was difference in target thymidine or cytosine so it is expected the rate of photosplitting ration using branch migration was different in the ^{CNV}K⊡T and ^{CNV}K⊡C. We investigated the photosplitting ratio of ^{CNV}K⊡T and ^{CNV}K⊡C (Fig. 6.5A). The results of denaturing PAGE analysis and the time course of photosplitting are shown in Fig. 6.5B and 6.5C. The photosplitting rate of ^{CNV}K⊡C was faster than that of ^{CNV}K⊡T, and the photoadduct of ^{CNV}K⊡C was splitted 60% with a 366 nm irradiation for 300 min. In contrast, photoadduct ^{CNV}K⊡T was splitted 50% with a photoirradiation at 366 nm for 300 min. It is presumed that the ODN that photosplitted once was photocrosslinked to the template strand again in splitting of ^{CNV}K⊡T since the photocrosslinking reaction of target T advanced faster that of target C.

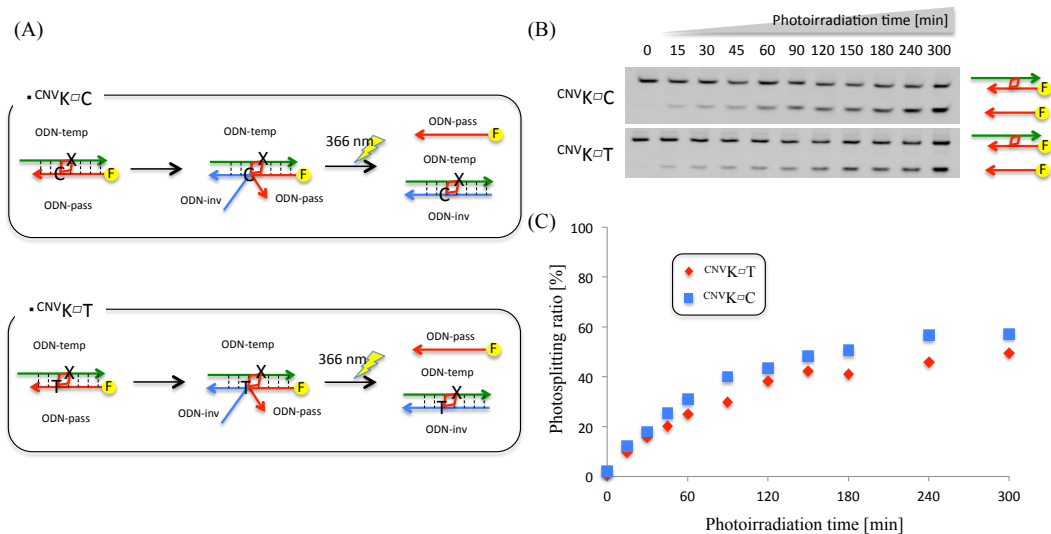**Figure. 6.5** The photosplitting of $^{CNV}K\square C$ and $^{CNV}K\square T$ (A) illustrated photosplitting using branch migration in the $^{CNV}K\square C$ and $^{CNV}K\square T$ (B) The time course of photosplitting.

Next, it is consider that the reason which the photosplitting can be performed at 25°C with a 366 nm irradiation using branch migration was the reaction rate constant k_{T1} became higher by using branch migration. The k_{T1} was changed by the factor which the hybridization to toehold and the temperature. So, to investigate the effect of temperature on the photosplitting using branch migration, I demonstrated the photosplitting using branch migration with a 366 nm irradiation performed at 25°C and 37°C and then analyzed by denaturing PAGE (Fig. 6.6A). In photosplitting performed at 25°C, the photoadduct was splitted 60% with photoirradiation at 366 nm for 300 min. On the other hand, the photoadduct was splitted 80% when the photosplitting was performed ay 37°C. The photosplitting rate at 37°C was faster than that at 25°C because of k_{T1} at 37°C was higher than that at 25°C.

To investigate the effect of hybridization to toehold, the photosplitting rate was performed with a 366 nm irradiaiton after the addition of 0, 0.6, 0.8, 1, 2, 3, and 5 mol ratio invader strands (Fig. 6.6B). As a result, the photosplitting rate increased as the molar equivalent of the invader strand increased. The photosplitting advances by the photoirradiation at 366 nm for the first time because the added invader strand takes a branch migration structure.
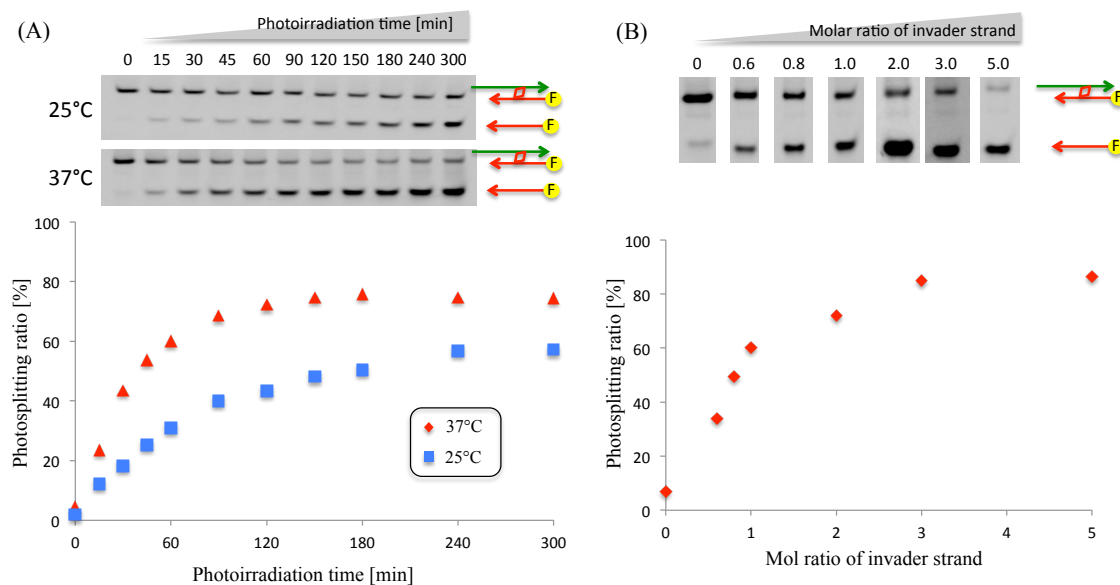
Figure. 6.6 The relation of the amount of invader strand and photosplitting rate with 366 nm irradiation of 5 h

Table. 6.3 The sequence of ODNs

Entry	Role	The Sequence of ODNs (5'-3')	Length [nt]
ODN 7	Invader	TTCACAGTGGCTAAGTTCAGCCTTCCAGG	29
ODN 8	Invader	TTCACAGTGGCTAAGTTCGGCCTTCCAGG	29

Figure. 6.7 (A) Scheme of photosplitting using branch migration; X and Y indicate ^{CNV}K and A, G, T, or C. (B)Time course of photosplitting using ODN 3(inv(C), ◆), ODN 6(inv(T), ■), ODN 7(inv(A), ×), and ODN 8 (inv(G), ▲).

In this photosplitting using branch migration, the ^{CNV}K on the template strand photocrosslinked to the pyrimidine base on the invader strand after the photosplitting reaction. I investigated the influence by which 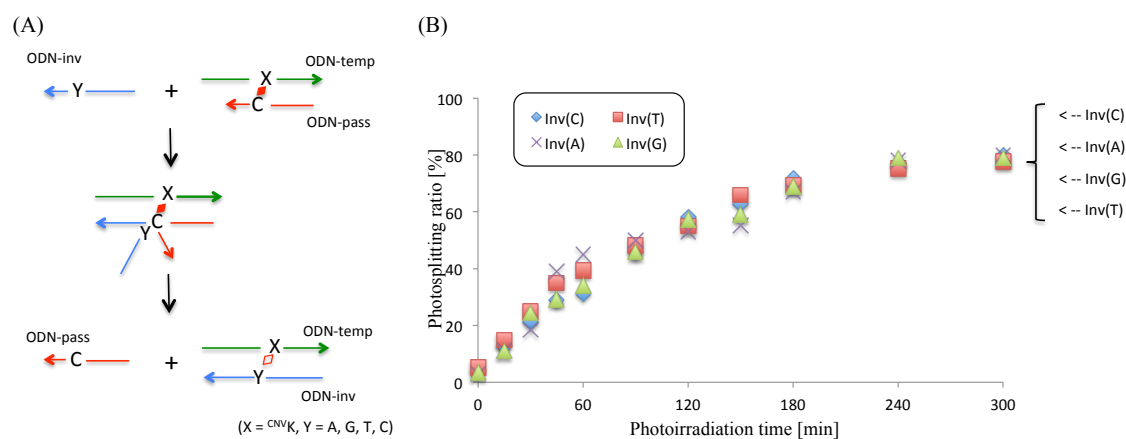the phorocrosslinking between template and invader strand gives to rate of photosplitting with branch migration. The ODN 3, ODN 6, ODN 7, and ODN 8 have C, T, A, and G in the photocrosslinking position on invader strand, respectively (Table. 6.3). The photocrosslinking rates were analyzed by denaturing PAGE when the photoadduct ODN 1 and ODN 2 was photosplitted in addition of ODN 3, ODN 6, ODN 7, or ODN 8 as invader strand (Fig 6.7). The change of photocrosslinking rate has not been confirmed with either of A, T, or G base, suggesting that the photocrosslinking between ODN-temp and ODN-inv does not play an important role in photosplitting using branch migration.

Table 6.4 The sequence of ODNs

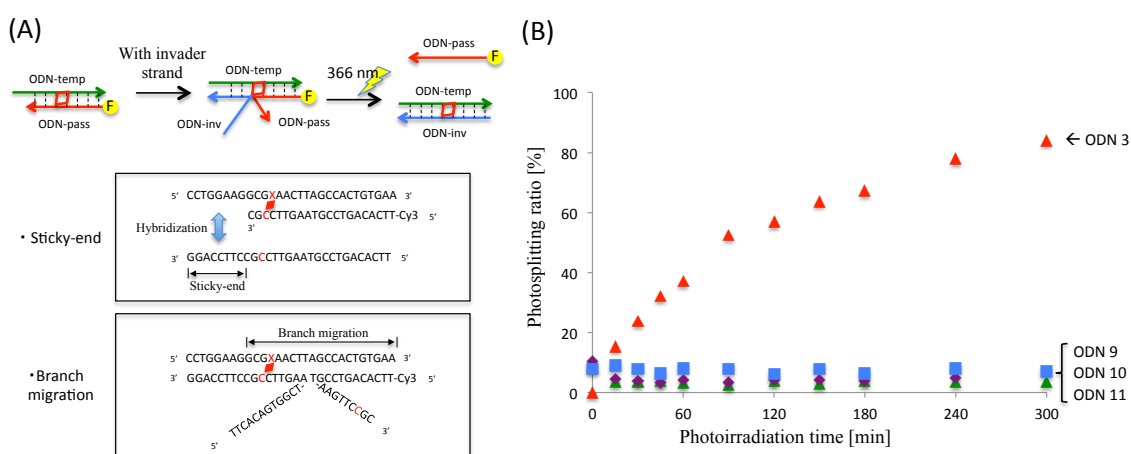| Entry	The Sequence of ODNs(5'-3')	Brach migration	Sticky-end
ODN 3	TTCACAGTGGCTAAGTTCCGC-CTTCCAGG	Match	Match
ODN 9	CGCCTTGAATCGGTGACACTT-CTTCCAGG	Mismatch	Match
ODN 10	TTCACAGTGGCTAAGTTCCGC-GGACCTTC	Match	Mismatch
ODN 11	CGCCTTGA-ATCGGTGACACTT-GGACCTTC	Mismatch	Mismatch

Figure. 6.8 The

(A) Illustrated sheme of

(B) The time course of photosplitting using match or mismatcg invader strand.

Next, to confirm the sequence specific photosplitting reaction, I demonstrated the photosplitting reaction that ODN 3, ODN 9, ODN 10, and ODN 11were used as invader strand (Table. 6.4). The sequence of ODN 3 is complementary sequence of template but the ODN 9 to 11 had mistamch pairts in sticky-end or branch migration to template strand. The photosplitting ratioss analyzed denaturing PAGE were shown in Fig. 6.8. The photosplitting reaction was processed with a 366 nm irradiation only in the presence of the full match invader strand, which suggests that this photosplitting reaction was processed by mediated branch migration. It is expected that this photosplitting using branch migration had been performed in a sequence specific manner dependent on the sequence of the invader strand. So, to confirm the sequence specific photosplitting reaction, we demonstrated the photosplitting ration that added the invader strand into three photocrosslinked adducts, respectively. The photocrosslinked adduct were labeled with fluorescence Cy2, Cy3, and Cy5, and the photosplitting rate was calculated by the gel shift assay imaged by each fluorescence. With the addition of ODN 3 as the invader strand, photoadduct 1 was splitted about 20% with 366 nm irradiation for 1.5 h, but photoadduct 2 and 3 were hardly splitted. With the addiation of ODN 6 as the invader strand, only photoadduct 2 had splitted 40%. Photoadduct 3 was splitted 40% with 366 nm irradiation after the addition of ODN 9 as the invader strand. The results suggest that this photspllitting reaction using branch migration was processed in a sequence specific manner, and that only target photoadduct was photosplitted in three photoadducts on sequence selectivity. Conventional photosplitting of ^{CNV}K does not have sequence selectivity, and all photoadducts in a single tube were photosplitted with 312 nm irradiation under the heating condition. On the other hand, photosplitting using branch migration has sequence selectivity, and only the target photoadduct can be splitted with 366 nm irradiation at room temperature.
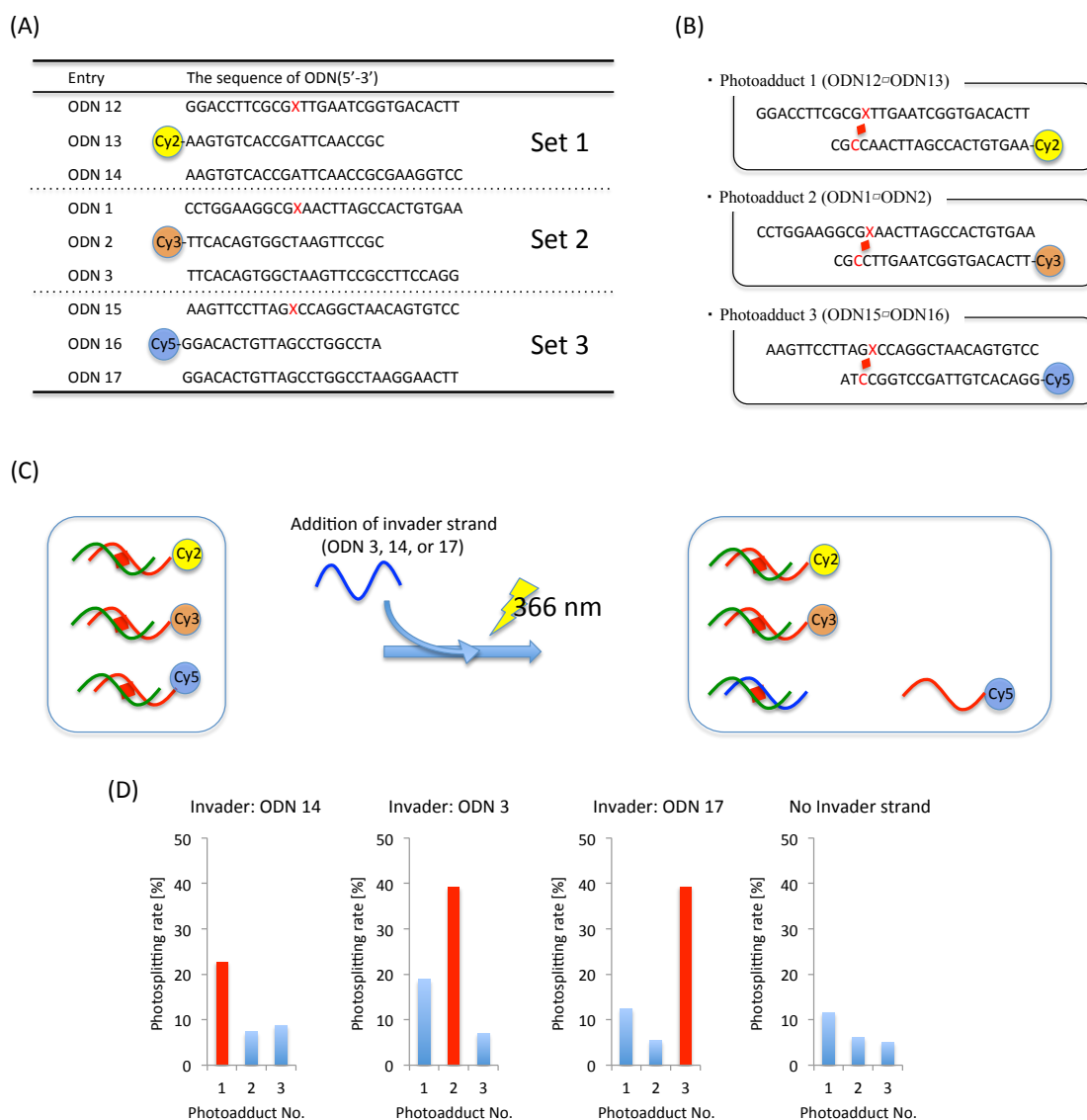
(A)

Entry	The sequence of ODN(5'-3')	
ODN 12	GGACCTTCGCGXTTGAATCGGTGACACTT	
ODN 13	Cy2-AAGTGTCACCGATTCAACCGC	Set 1
ODN 14	AAGTGTCACCGATTCAACCGCGAAGGTCC	
ODN 1	CCTGGAAGGCGXAACTTAGCCACTGTGAA	
ODN 2	Cy3-TTCACAGTGGCTAAGTTCCGC	Set 2
ODN 3	TTCACAGTGGCTAAGTTCCGCCTTCCAGG	
ODN 15	AAGTTCCTTAGXCCAGGCTAACAGTGTCC	
ODN 16	Cy5-GGACACTGTTAGCCTGGCCTA	Set 3
ODN 17	GGACACTGTTAGCCTGGCCTAAGGAACTT	

(B)

・Photoadduct 1 (ODN12▫ODN13)

GGACCTTCGCGXTTGAATCGGTGACACTT
CGCCAACTTAGCCACTGTGAA-Cy2

・Photoadduct 2 (ODN1▫ODN2)

CCTGGAAGGCGXAACTTAGCCACTGTGAA
CGCCTTGAATCGGTGACACTT-Cy3

・Photoadduct 3 (ODN15▫ODN16)

AAGTTCCTTAGXCCAGGCTAACAGTGTCC
ATCCGGTCCGATTGTCACAGG-Cy5

(C)

(D)

Figure. 6.5 Sequence specific photosplitting using branch migration. (A) The schematic illustration of sequence specific photosplitting. (B) The sequence of photocrosslinked dsDNA and invader strand. The photosplitting rate of each photocrosslinked dsDNA when addition of (C)ODN 3, (D) ODN 6, or (E) ODN 9 as invader strand. The photosplitting was calculated gel shift assay, the gel was imaged by Cy2, Cy3, or Cy3 fluorescence.

To examine the affect of the photosplitting rate on the position of the photosplitting site, we designed the three photoadducts having different photocrosslinking positions. Each photoadduct was photosplitted at 366 nm after the addition of an invader strand, and then the photosplitting rates at different photocrosslinking points were compared. The photosplitting rate in which the photocrosslinking site was inserted in the center position was faster than the other photosplitting rates; the photosplitting reaction was hardly processed when the photocrosslinking site was in the 3'-position. When photocrosslinking exists in a position distant form the sticky end, photosplitting using branch migration was hardly processed. According to the results of accelerating of DNA strand displacement using DNA photocrosslinking in Chapter 4, the DNA strand displacement of the last half was advanced slowly compared with that of the first half. So the photosplitting reaction using branch migration is difficult to advance in a photocrosslinking site located far from the sticky-end.

Finally, we confirmed that the photosplitted ODN was pushed out by DNA strand displacement, it was monitored by FRET system using Cy3-labeled passenger strand as fluorescence and Dabcyl-labeled template strand as Quencher. The Cy3 fluorescence was rose by the photoirradiation after addition of the invader strand, suggesting the distance between Cy3 and Dabcyl is long since the photosplitted passenger strand was pushed out.

Table. 6.5 The sequence of ODN

Entry	Role	The sequence of ODN(5'-3')	Length [nt]	
ODN 18	Template	TGACCGTA-GGA**X**CGATAA**T**GAAGCA**T**CTT	29	
ODN 19	Template	TGACCGTA-GGA**T**CGATAA**X**GAAGCA**T**CTT	29	
ODN 20	Template	TGACCGTA-GGA**T**CGATAA**T**GAAGCA**X**CTT	29	
ODN 21	Passenger	Cy3-AAGATGCTTCATTATCGATCC	21	
ODN 22	Invader	AAGATGCTTCATTATCGATCC-TACGGTCA	29	(X = ^{CNV}K)

(A)

5'-position

ODN 18

5' ————————►X———————► 3'

3' ◄———————————————
ODN 22

ODN 21

5'

3'

5'

Center-position

ODN 19

5' ————————◊———————► 3'

3' ◄———————————————
ODN 22

ODN 21

5'

3'

3'-position

ODN 20

5' ————————◊———————► 3'

3' ◄———————————————
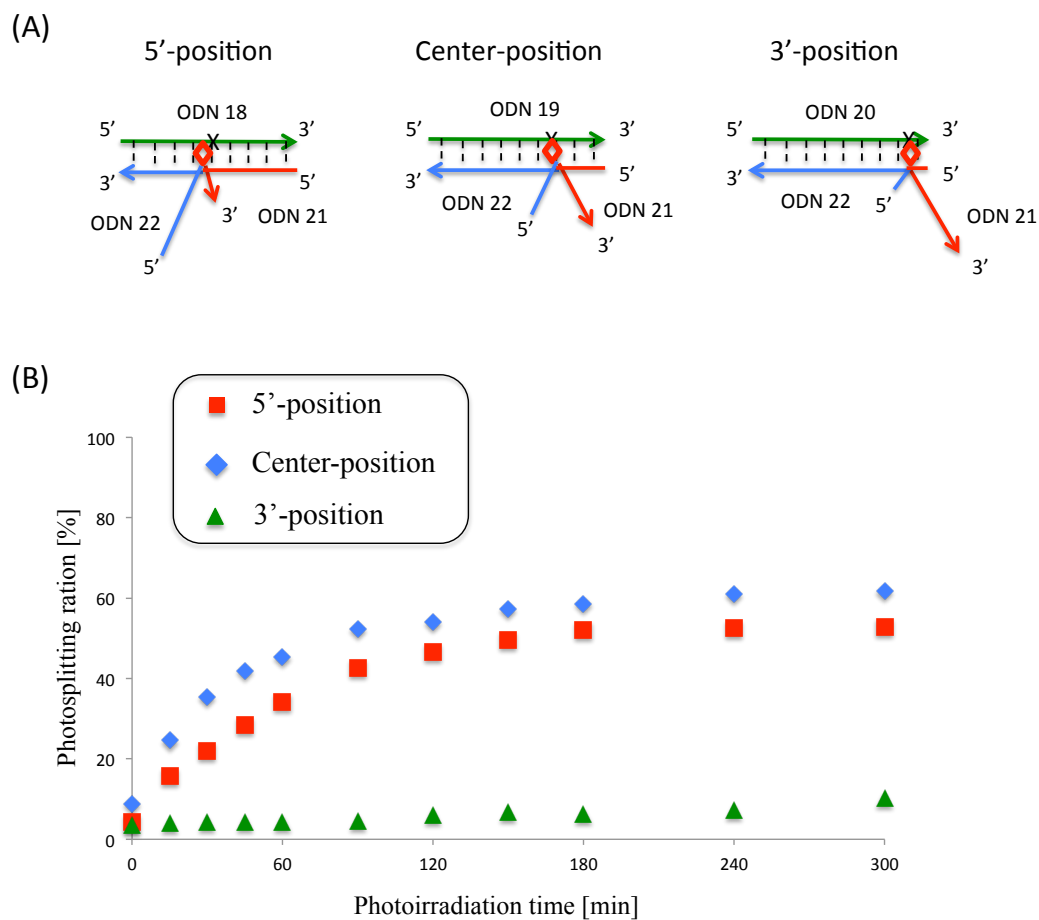ODN 22

ODN 21

5'

3'

(B)

Figure. 6.7 (A) Illustrated branch migration state of photocrosslinked ds DNA inserted ^{CNV}K into the 5'-, center-, or 3'-position. (B) Time course of photosplitting rate of photoadduct crosslinked 5'(■), center (◆), and 3'-position (▲).

5.4. Conclusion

In conclusion, sequence specific photosplitting using branch migration was processed at room temperature without heating. The photoadduct of $^{CNV}K{⊏}C$ was splitted faster than the photoadduct of $^{CNV}K{⊏}T$, and photosplitting using branch migration processed in the photocrosslinking site was located at the 5'-position(near the sticky-end) or center position of photocrosslinked dsDNA. With this technique, photocrosslinking can be regulated with the same wavelength photoirradiation and temperature.

5.5 Reference

1 Higuchi M, Kobori A, Yamayoshi A, Murakami A, Synthesis of antisense of oligonucleotides containin 2'-O-psoralenymethoxyadenosine for photodynamic regulation of point mutation in RNA. *Bioorg. Med. Chem.,* **2009**, 17, 475-483.

2 Higuchi M, Yamayoshi A, Yamaguchi T, Iwase R, Yamaoka T, Kobori A, Murakami A, Slective photo-cross-linking of 2'-O-psoralen conjugated oligonucleotide with RNAs having point mutations. *Nucleoside Nucleotides. Nucleic Acids.,* **2007**, 26, 277-290.

3 Murakami A, Yamayoshi A, Iwase R, Nishida J, Yamaoka T, Wake N, Photodynamic Antisense Regulation of Human Cervical Carcinoma Cell Growth using Psoralen-conjugated Oligo(nucleoside phosphorothioate). *Eur. J. Pharmac. Sci.,* **2001**, 13, 25-34.

4 Giovannanegeli C, Diviacco S, Labrousse V, Gryaznov S, Charneau P, Helene C, Padlock oligonucleotides for duplex DNA based on sequence-specific triplex helix formation. *Proc. Natl. Acad. Sci. U.S.A.,* **1997**, 94, 79-84.

5 Zhen W-P, Buchardt O, Nielsen H, Nielsen P, Site specificity of psoralen-DNA interstrand cross-linking determined by nuclease Bal31 digestion. *Biochemistry*, **1986**, 25, 6598-6603.

6 Weidner M H, Millard J T, Hopkins P B, Determination at single nucleotide resolution of the sequence specificity of DNA interstrand crosslinking agent in DNA fragments. *J. Am. Chem. Soc.,* **1989**, 111, 9270-9272.

7 Yoshimura Y, Fujimoto K, Ultrafast reversible photocrosslinking reaction: Toward in situ DNA manipulation. *Org. Lett.,* **2008**, 10, 3227-3230.

8 Fujimoto K, Yamada A, Yoshimura Y, Tsukaguchi T, Sakamoto T, Details of ultra-fast DNA photocrosslinking reaction of 3-cyanovinylcarbazole nucleotide; Cis-trans isomeric effect and the application for SNP based genotyping. *J. Am. Chem. Soc.,* **2013**, 135, 16161-1616.

9 Tagawa M, Shohda K, Fujimoto K, Suyama A, Stabilization of DNA nanostructures by photo-cross-linking. *Soft. Matter.,* **2011**, 7, 10931-10934.

10 Gerrard R S, Hardiman C, Shelbourne M, Nandhakumar I, Noedén B, Brown T, A new modular approach to nanoassembly: stable and addressable DNA nanoconstructs via orthogonal click chemistries. *ACS. Nano.,* **2012**, 6, 9221-9228.

11 Nakamura S, Fujimoto K, Creation of DNA array structure equipped with heat resistance by ultrafast photocrosslinking. *Journal of chemical Technology and Biotechnoogy*, **2014**, 89, 1086-1090.

12 Shigeno A, Sakamoto T, Yoshimura Y, Fujimoto K, Quick regulation of mRNA functions by a few seconds of photoirradiation, *Organic & Biomolecular Chemistry*, **2012**, 10, 7820-7825.

13 Sakamoto T, Shigeno A, Ohtaki Y, Fujimoto K, Photo-regulation of constitutive gene expression in living cells by using ultrafast photo-crosslinking oligonucleotides. *Biomaterials Science,* **2014**, 2, 1154-1157.

14 Fujimoto K, Konishi-Hiratsuka K, Sakamoto T, Yoshimura Y, Site-Specific photochemical RNA editing. *Chem. Comm.,* **2010**, 46, 7545-7547.

15 Fujimoto K, Futamura D, Sakamoto T, Diamine derivatives accelerate photochemical C→U transition in DNA double Strand. *Chem. Lett.,* **2013**,42, 289-291.

16 Yoshimura Y, Fujimoto K, Repair of a thymine dimer in DNA via Carbazole Nucleoside. *Chem. Lett.,* **2006**, 35, 386-388.

17 Ogasawara S, Kyoi Y, Fujimoto K, Non-enzymatic Parallel DNA Logic Circuits. *ChemBioChem*, **2007**, 8, 1520-1525

Chapter 6.

Template directed reversible photochemical ligation of

Oligodeoxynucleotides

6.1. Introduction

There are many methods of template-directed chemical ligation of oligonucleotides (ODNs) via a native phosphodiester bond [1] or non-native linking [2]. Template-directed chemical ligation can ligate not only DNA but also other biomolecules such as protein-like molecules [3]. Template directed synthesis has been used for DNA nanotechnology [4], the selection of amplifiable small-molecule libraries [5], the release of drugs [6], and as a diagnostic means of detecting the presence of the nucleic acid template [7]. One method of template-directed chemical ligation is non-enzymatic chemical ligation [8, 9]. This method was researched for new gene manipulation and as a design method for nanostructures, because it does not have restrictions of a substrate and reaction conditions are suitable for an enzyme reaction. In particular, photochemical ligation has many useful characteristics. For example, there is no need to add other reagents and the ligate reaction is easily regulated by irradiation wavelength and intensity. However, there are only a few methods of performing photochemical reactions [10-12]. Previously reported methods for DNA photochemical ligation are thymine dimer formation [10], photoreactions of DNA containing appended stilbenes [11] and ligate DNA using the anthracene [12]. However, these methods have a serious problem toward utilization, such as the low yields of photochemical ligation products and the use of short wavelengths that injure other biological components. We reported that 5-Vinyldeoxyuridine (^{V}U) can be used to photolink a longer ODN from five smaller identical ODNs on a template with high efficiency without any side reactions by photoirradiation at 366 nm [13]. This reaction ligated T and ^{V}U via [2+2] photocyclization [14]. Moreover, we have reported artificial nucleotide 5-Carboxyvinyldeoxyuridine (^{CV}U) [15], which is more responsive than ^{V}U. The photochemical reaction of ^{CV}U is shown in Fig. 7.1A. We demonstrated the template-directed photochemical ligation with ^{CV}U, short four ODNs were ligated dependent on sequence of template. And, we create photoligated self-assembly long dsDNA using ^{CV}U.

6.2. Materials and Method

General

^{1}H NMR spectra were measured with AVANCE III NMR 400 (Bruker, 400 MHz) spectrometer. Mass spectra were recorded on a Voyager-DE PRO-SF, Applied Biosystems. Irradiation was performed by UV-LED (OMRON, ZUV, 366 nm, 1.6 W/cm^2) or 2 W transilluminator (FUNAKOSHI, TR-312R/J, 312 nm). HPLC was performed on a Chemcobond 5-ODS-H column (10 × 150 mm, 4.6 × 150 mm) or a Chemcosorb 5-ODS-H column (4.6 × 150 mm) with a JASCO PU-980, HG-980-31, DG-980-50 system equipped with a JASCO UV 970 detector at 260 nm. The reagents for the DNA synthesizer such as A, G, C, T-β-cyanoethyl phosphoramidite, and CPG support were purchased from Glen Research. Calf intestine alkaline phosphatase (AP) was purchased from Promega. Nuclease P1 was purchased from Yamasa.

5-(2-Carboxymethoxyvinyl)-2'-deoxyuridine

A mixture of palladium (II) acetate (0.15 g, 0.90 mmol), triphenylphosphine (0.37 g, 1.90 mmol) and triethylamine (2.5 mL, 18 mmol) in dry dioxane (25 mL) was stirred at 70 °C until an intense red color had developed. To this there was then added 2′-deoxy-5-iodouridine (5.0 g, 14 mmol) and methyl acrylate (2.35 g, 27.0 mmol) and the mixture was refluxed for 1 h. It was then filtered while still hot and evaporated *in vacuo*. The crude product was purified by column chromatography (4% MeOH/EtOAc) to give 5-(2-carboxymethoxyvinyl)-2′-deoxyuridine

(3.1 g, 70%) as a white powder. ^{1}H-NMR (400 MHz, DMSO-*d6*) δ 2.14-2.18 (m, 2H, H-2′), 3.54-3.64 (m, 2H, H-5′), 3.67 (s, 3H, OCH$_3$), 3.77-3.80 (m, 1H, 4′-OH), 4.23-4.27 (m, 1H, H-3′), 5.16 (bs, 1H, 3′-OH), 5.25 (bs, 1H, 5′-OH), 6.84 (d, J = 16 Hz, 1H, alpha vinyl), 7.36 (d, J = 16 Hz, 1H, beta vinyl), 8.41 (s, 1H, H-6), 11.63 (bs, 1H, NH). HRMS (positive ion FAB) calcd for C$_{13}$H$_{17}$O$_7$N$_2$ [(M+H)$^+$] 313.1036, found 313.1034.

5′-O-(4,4′-Dimethoxytriryl)-5-(2-Carboxymethoxyvinyl)-2′-deoxyuridine

5-(2-Carboxymethoxyvinyl)-2′-deoxyuridine (1.210 g, 3.87 mmol) was dissolved in dry pyridine and coevaporated three times. 4,4′-Dimethoxytrityl chloride (1.575 g, 4.64 mmol), *N,N*-dimethylaminopyridine (30.2 mg, 0.248 mmol) was added to a solution of 5-vinyl-2′-deoxyuridine in dry pyridine (30 mL). The solution was stirred at ambient temperature under nitrogen atmosphere 18 h. The TLC analysis ($CHCl_3$/MeOH 9:1) showed the presence of starting material, but the reaction mixture was evaporated to dryness in vacuo. The crude product was purified by silica gel column chromatography with $CHCl_3$/MeOH (8:1), and 5′-*O*-(4,4′-dimethoxytrityl)-5-vinyl-2′-deoxyuridine (1.67 g) was isolated in 70.0% yield as a yellow solid. ^{1}H-NMR (400 MHz,$CDCl_3$) δ 2.25–2.35 (m, 2H, H-2′α, H-2′β), 2.52–2.57 (m, 1H, H-3′), 3.38–3.48 (m, 2H, H-1′, H-4′), 3.65 (s, 3H, OCH_3), 3.77 (d, 6H, J = 1.2 Hz, OCH_3 ×2), 4.52 (s, 1H, 3′-OH), 6.28 (dd, J = 6.4 Hz, 2.4 Hz, 1H, H-1′), 6.95–6.68 (m, 4H, H-ortho to OCH_3 ×4), 6.92–6.96 (m, 2H, alpha and beta vinyl), 7.20–7.30 (m, 9H, phenyl), 7.86 (s, 1H, NH), 8.86 (s, 1H, H-6). HRMS (positive ion FAB) calcd for $C_{34}H_{34}N_2O_9$ [(M+H)$^+$] 615.2342, found 615.2345.

5′-O-(4,4′-Dimethoxytriryl)-3′-O-[2-cyanoethoxy-(N,N-diisopropylamino)-phosphino]-5-(2-carboxy-methoxyvinyl)-2′-deoxyuridine

5′-*O*-(4,4′-Dimethoxytriryl)-5-(2-carboxymethoxyvinyl)-2′-deoxyuridine (183 mg, 0.298 mmol) in a sealed bottle with septum was dissolved in dry acetonitrile and coevaporated three times *in vacuo*. After substitution with argon, 2-cyanoethyl-*N,N,N′,N′*-tetraisopropylphosphoroamidite (99.0 μL, 0.309 mmol) in dry acetonitrile (2.0 mL), 0.5 M tetrazole in dry acetonitrile were stirred for 1.0 h. After the completion of the reaction as evidence by TLC, the reaction mixture was extracted with ethyl acetate (20 mL × 2), which was washed with saturated sodium bicarbonate aqueous solution and water (15 mL). The organic layer was collected, dried over anhydrous sodium sulfate, filtered, and evaporated to dryness under reduced pressure.

Then, the crude product 5′-*O*-(4,4′-dimethoxytrityl)-3′-*O*-[2-cyanoethoxy-(*N,N*-diisopropylamino)-phosphino]-5-vinyl-2′-deoxyuridine (228 mg) in a sealed bottle with sepum was dissolved in dry acetonitrile and coevaporated three times and was used for automated DNA synthesizer without further purification.

Synthesis of Oligonucleotides

Oligonucleotides were prepared by β-(cyanoethyl) phosphoramidite method on controlled pore glass supports (1 mmol) by using ABI3400 DNA synthesizer. Cyanoethylphosphoramidite of elaborated compounds was prepared as described above. After automated synthesis, the oligomer was detached from the support by soaking in conc. aqueous ammonia for 1 h at room temperature. Deprotection was conducted by heating the conc. aqueous for 10 h at 55 °C conc. aqueous ammonia was then removed by speedvac, and the crude oligomer was purified by reverse phase HPLC and lyophilized. The Purity and concentration of all oligonucleotides were determined by complete digestion with s.v. PDE, P-1 nuclease, and AP to 2′-deoxymononucleosides. DNA base sequence was shown in table 1.

Annealing and Photoirradiation

A reaction mixture (total volume 20 μL) containing initial ODN (10 μM), 2nd ODN (11 μM), 3rd ODN (12 μM), 4th ODN (13 μM) and template (10 μM) in 50 mM Sodium cacodylate buffer (pH 7.0) in an Eppendorf tube was cooled from 90 °C to 4 °C over 72 h by thermal cycler. Next, an annealed mixture was irradiated at 366 nm at 4 °C with LED (Omron, 1.6 W/cm^2) and 312 nm at room temperature with transilluminator (Funakoshi, 2 mW/cm^2).

Photoirradiation of DNA Oligomer as Monitored by PAGE

The reaction mixture was diluted with 8M Urea in formamide 10 times. To this diluted solution (3 μL) containing initial ODN (200 nM), 2nd ODN (220 nM), 3rd ODN (240 nM), 4th ODN (260 nM) and template (200 nM) 3 μL of loading buffer (36% glycerol

and 30 mM EDTA) were added. The solution was loaded onto 15% (19:1) polyacrylamide, 8M Urea and 25% formamide denatured gel and electrophoresed at 150 V for 120 min. The gel was exposed to Cy3 or Cy5 fluorescence.

Time Course of the Self-Assembled Structure by PAGE

A reaction mixture (total volume 20 μL) containing ODN 11 (25 μM) and 5 mM Magnesium chloride in 50 mM sodium cacodylate buffer (pH 7.0) in an Eppendorf tube was cooled 90 °C for 5 min and from 70 °C to 4 °C over 72 h by thermal cycler. This annealed mixture was irradiated at 366 nm at 4 °C with LED (Omron, 1.6 W/cm^2) for 0 s, 1 s, 5 s, 10 s, 30 s, 60 s, 120 s, 300 s, 600 s, 900 s and 1800 s. This reaction mixture was diluted with 8M urea in formamide 10 times. To this diluted solution (3 μL) containing ODN 11 (500 nM) 3 μL of loading buffer (36% glycerol, 30 mM EDTA, 0.05% xylene cyanol and 0.05% bromophenol blue) was added. The solution was loaded onto 15% (19:1) polyacrylamide, 8M Urea and 25% formamide denatured gel and electrophoresed at 150 V for 120 min. The gel was stained by SYBRgold

6.3. Results and Discussions

We designed template directed synthetic DNA having branched DNA. The branched structure was illustrated in Fig. 7.1A. branched DNA has various uses in signal amplification technology and in several types of nanotechnology, such as DNA computing, DNA nanostructures from self-assembled branched units, DNA sensors [17], and nano-electronic devices [18]. We previously reported Multiple-Branched DNA [15] and DNA computing [19] using branched DNA. We demonstrated the feasibility of reversible photoligation with ^{CV}U. The wavelengths used were 366 nm and 312 nm, the same wavelengths as when using ^{V}U. After elaborating the ^{CV}U, we synthesized ODNs containing ^{CV}U by automated DNA synthesizer (Table. 7.1). We synthesized ODNs containing ^{CV}U inside so we made branched DNA toward developing DNA nanotechnology. ODN 1 containing Cy3 fluorescence at the 5′ end, ODN 2, ODN 3, ODN 4 and template 1 was annealed and irradiated at 366 nm for 900 s. The result of denaturing PAGE analysis is shown in Fig. 7.1B, it imaged by Cy3 fluorescence.

Table. 7.1. The Seuqence of ODNs

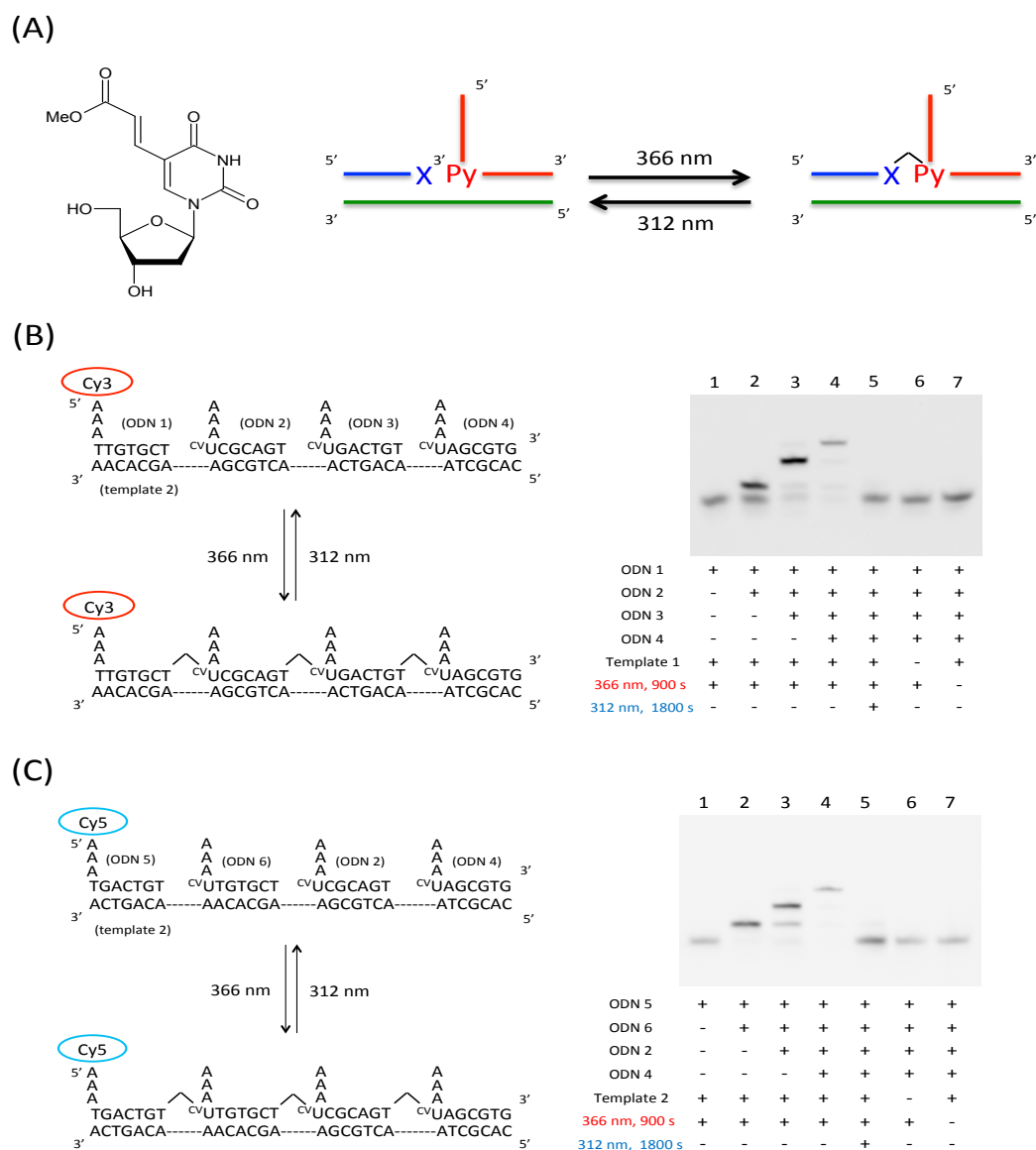| Entry	Sequence(5′ to 3′)	Entry	Sequence(5′ to 3′)
ODN 1	Cy3-AAATTGTGCT	ODN 4	AAA^{CV}UAGCGTG
ODN 2	AAA^{CV}UCGCAGT	ODN 5	Cy5-AAATGACTGT
ODN 3	AAA^{CV}UGACTGT	ODN 6	AAA^{CV}UTGTGCT
Template 1	CACGCTAACAGTCAACTGCGAAGCACAA		
Template 2	CACGCTAACTGCGAAGCACAAACAGTCA		
Template 3	CACGCTAACTGCAACAGTCAAAGCACAA		

134

(A)

(B)

(C)

Figure. 7.1 (A) Schematic illustration of chemical structure and reaction of ^{CV}U. (B) (C) Schematic illustration for reversible photoligation and result of denaturing PAGE analysis. Denaturing polyacrylamide gel electrophoresis of photoligation for first part (10 μM), second part(12 μM), third part(14 μM) fourth part(16 μM) and template (10 μM) after irradiation at 366 nm in sodium cacodylate buffer (50 mM) containing NaCl (100 mM). Lane 1, first part + template, irradiation at 366 nm for 1800 s; lane 2, first part + second part + template, irradiation at 366 nm for 1800 s; lane 3, first part + second part + third part + template, irradiation at 366 nm for 1800 s; lane 4, first part + second part + third part + fourth part + template, irradiation at 366 nm for 1800 s; lane 5, irradiation at 302 nm for lane 4; lane 6, without template for lane 4; lane 7, not irradiation at 366 nm for lane 4.

135

Lane 1, which is ODN 1, was irradiated at 366 nm for 900 s in the presence of a template. We obtained the 10 mer band, which is only ODN 1. Lane 2 is ODN 2 added to Lane 1. We obtained the 20 mer band ligated ODN 1 and 2. Lane 3 is ODN 3 added to Lane 2. We obtained the 30 mer band ligated ODN 1, 2 and 3. Lane 4 is ODN 4 added to Lane 3. We obtained the 40 mer band ligated ODN 1, 2, 3 and 4. Lane 5 is lane 4 irradiated at 312 nm for 1800 s. Lane 6, which is ODN 1, 2, 3 and 4, was irradiated at 366 nm for 900 s in the absence template. Lane 7, which is ODN 1, 2, 3 and 4, was nonirradiated at 366 nm. We obtained the 10 mer band, which is only ODN 1 in Lane 5, 6 and 7. The DNA becomes longer by adding DNA sequentially from the initial domain, which shows that ^{CV}U and T are connected by photochemical ligation. This reaction was completely finished for irradiation at 366 nm for 900 s as shown by the results of lane 4. Thus, 900 s is considered sufficient for utilization. And, this reaction did not advance in the absence of a template and nonirradiation at 366 nm. The photoligated ODNs were quantitatively reverted to the original ODNs by irradiation at 312 nm.

Next, we demonstrated photochemical ligation in other sequences (Fig. 7.1C). ODN 5 is ODN 3 linked Cy5 fluorescence at the 5′ end. The result of denaturing PAGE analysis is shown in Fig. 7.1C. We obtained Cy5 fluorescence.

Lane 1, which is ODN 5, was irradiated at 366 nm for 900 s in the presence of a template. We obtained the 10 mer band, which is only ODN 5. Lane 2 is ODN 6 added to Lane 1. We obtained the 20 mer band ligated with ODN 5 and 6. Lane 3 is ODN 2 added to Lane 2. We obtained the 30 mer band ligated with ODN 5, 6 and 4. Lane 4 is ODN 4 added to Lane 3. We obtained the 40 mer band ligated with ODN 5, 6, 2 and 4. Lane 5 is irradiated at 312 nm to Lane 4 for 1,800 s. Lane 6, which is ODN 5, 6, 2 and 4, was irradiated at 366 nm for 900 s in the absence of a template. Lane 7, which is ODN 5, 6, 2 and 4, was nonirradiated at 366 nm. We obtained the 10 mer band, which is only ODN 5 in Lane 5, 6 and 7. The same as the result above, we confirmed that the ligated product was produced by photochemical ligation, so we can use photochemical ligation regardless of the sequence. As photochemical ligation did not advance without a

template, we can use this reaction for sensing the template. Additionally, these results show the difference of reactivity of ^{V}U and ^{CV}U on photochemical ligation so we can make the system only ^{CV}U ligated if photoirradiation was short and ^{V}U and ^{CV}U was ligated if the photoirradiation time was long by using these compounds respectively.

Next, we demonstrated the template dependence for changing the template in the same three domains (Fig. 7.2A). By using template 1, 2 or 3, we confirmed the size of the ligated product. In the presence of template 1, we should be able to confirm ligated ODN 1 and 2. In the presence of template 3, we should be able to confirm only ODN 1. In the presence of template 2, we should be able to confirm ligated ODN 1, 2 and 4.

ODN 1, 2 and 4 and template 1, 2 or 3 were annealed and photoirradiated at 366 nm. The result of PAGE analysis is shown in Figure 7.2B. We observed Cy3 fluorescence and it showed the size of the ligation product of ODN 1. We confirmed that ODN 1 and ODN 2 were ligated in the presence of template 1 and only ODN 1 was ligated in the presence of template 3. In the presence of template 2, ODN 1, 2 and 4 were ligated. This result reflects the template dependence of photochemical ligation. Generally, template-directed DNA ligation can generate a related to the template DNA in a sequence-specific manner. However, this photochemical ligation method is a reversible ligation method, so we can rearrange ODNs using templates. Furthermore, this photochemical ligation is reversible so we can rearrange another sequence after ligated ODN is reverted to original ODNs by irradiation at 312 nm. *In vivo*, DNA works as an information carrier so it is suggested that we can re-edit the information of DNA.

Finally, we researched the activities of photochemical ligation with a self-assembled DNA structure (Fig. 7.2B). A self-assembled DNA structure is made by the characteristic of complementarity of DNA such as a holiday junction [20] and DNA origami [21]. Our construction of a self-assembled structure contributes toward developing DNA nanotechnology. We synthesized ODN containing ^{CV}U.
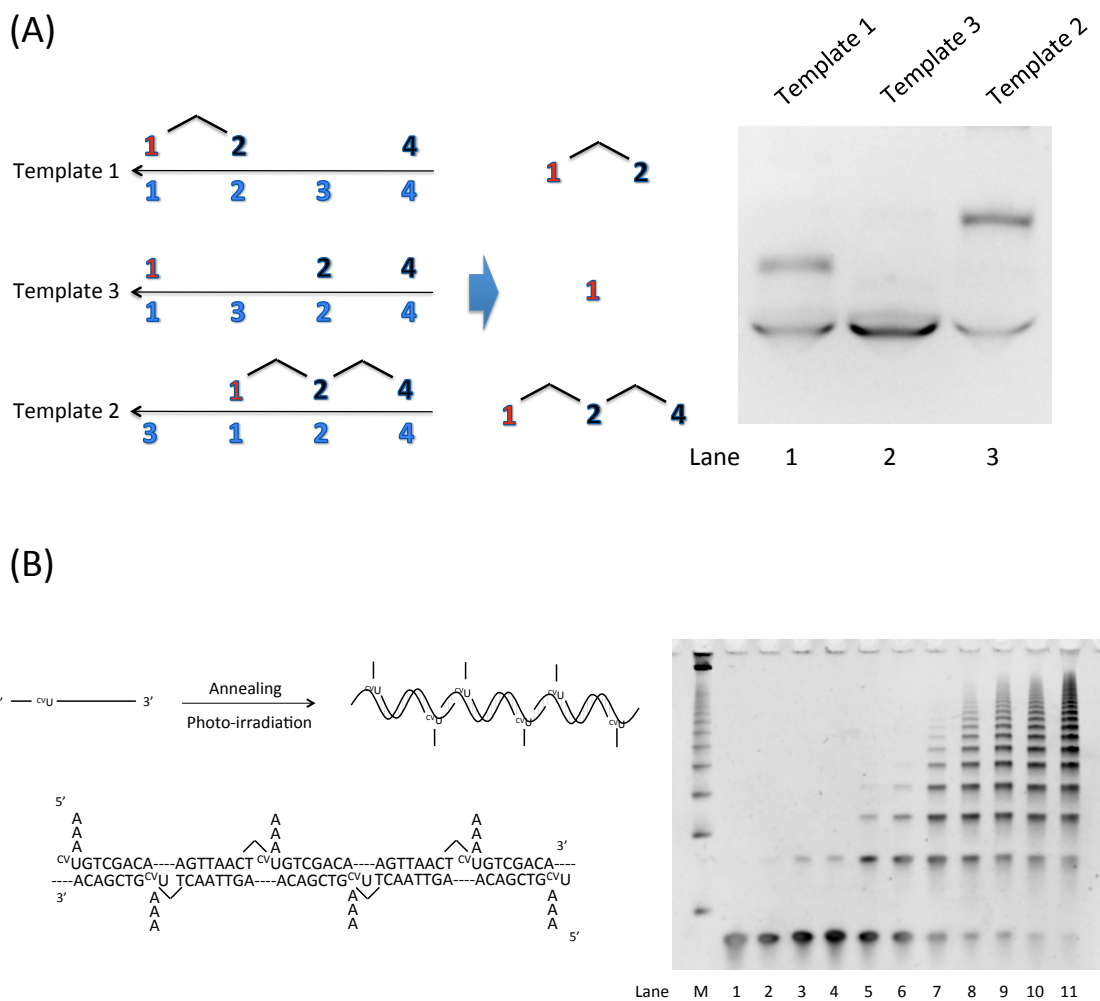
Figure. 7.2 Scheme and denaturing polyacrylamide gel electrophoresis of template directed DNA photoligation. (A) ODN-1(10 µM), ODN-2(10 µM), ODN-4(10 µM) and template1, 2 or 3(10 µM) irradiation at 366 nm for 1800 s and then Cy3 fluorescent of denaturing polyacrylamide gel electrophoresis. Lane 1, template 1; lane 2, template 2; lane 3, template 3. (B) Self-assemble photoligated long dsDNA. (A) Schematic illustrate of self-assemble structure and denaturing polyacrylamide gel electrophoresis analysis of the photoreaction. Lane 1, control 25 bp Lader Maker; lane 2, non-photoirradiation at 366 nm; lane 3, photoirradiation at 1 s; lane 4, 5 s; lane 5, 10 s; lane 6, 30 s; lane 7, 60 s; lane 8, 120 s; lane 9, 300 s; lane 10, 600 s; lane 11, 900 s; lane 12, 1800 s.

ODN 11 was annealed and irradiated at 366 nm from 1 s to 1,800 s at 4 °C. Ligation products should become bigger according to photoirradiation time. The PAGE analysis result is shown in Fig. 7.2B. We confirmed that ligation products become bigger according to photoirradiation time. Samples of 900 s and 1,800 s showed no change so this reaction was completely irradiated at 366 nm for 1,800 s. The size of the final structure became longer by optimization of the sequence. The average of nucleotide photoirradiation time was plotted, it shows that the nucleotide average increases very fast at first and does not change over 900 s. This photochemical ligation is not a bimolecular reaction such as enzyme-substrate [22] but all reactions advance in parallel simultaneously by photoirradiation over the whole reaction field. Moreover, this structure is not a normal double strand but a double strand containing branched DNA. This branched DNA is not made by a ligation enzyme. So, we can modify branched DNA such as biotin and nucleotide aptamer. In a previous study, a molecule was spotted onto DNA origami [23]. We can spot various molecules using this linear structure too.

6.4 Conclusion

In conclusion, the reactivity of ^{CV}U is very high so the reaction of ^{CV}U advances quickly with high efficiency. This photochemical ligation did not advance without a template and a change of alignment sequence by the sequence of the template and therefore we can confirm the existence and sequence of the template. Finally, we made a self-assembled structure for researching photochemical ligation. We confirmed that all reactions advanced simultaneously by photoirradiation in parallel across the whole of the reaction field. In addtion, it is possible to spot various molecules periodically by using this structure containing branched DNA.

6.5 Reference

1. Lohman G J, Chen L, Evans T C, Kinetic characterization of single strand break ligation in duplex DNA by T4 DNA Ligase. *J. Biol. Chem.,* **2011**, 286, 44187-44196.

2. Liu J, Taylor J S, Template-directed photoligation of oligodeoxyribonucleotides via 4-thiothymidine. *.,* **1998**, *26*, 3300-3304.

3. He Y, Liu D R, A sequential strand-displacement strategy enables efficient six-step DNA-templated synthesis. *J. Am. Chem. Soc*., **2011**, 133, 9972-9975.

4. Gothelf K V, Thomsen A, Nielsen M, Cló E, Brown R S, Modular DNA programmed assembly of linear and branched conjugated nanostructures. *J. Am. Chem. Soc*., **2004**, 126*,* 1044-1046.

5. Kleiner R E, Dumelin C E, Tiu G C, Sakurai K, Liu D R, *In vitro* selection of a DNA-templated small-molecule library reveals a class of macrocyclic kinase inhibitors. *J. Am. Chem. Soc*., **2010**, *132*, 11779-11791.

6. Zhou Q, Rokita S E, A general strategy for target-promoted alkylation in biological systems. *Proc. Natl. Acad. Sci. USA.,* **2003**, 100, 15452-15457.

7. Yoshinaga Y, Daisuke O, Masayuki O, Kenzo F, Highly selective and sensitive template-directed photoligation of DNA via 5-carbamoylvinyl-2-deoxyuridine. *Org. Lett*., **2006**, 8, 5049.

8. Leubke K J, Dervan P B, Nonenzymatic ligation of oligodeoxyribonucleotides on a duplex DNA template by triple-helix formation. *J. Am. Chem. Soc.,* **1987**, 111, 8733-8735.

9. El-Sagheer A H, Cheong V V, Brown T, Rapid chemical ligation of oligonucleotides by the Diels-Alder reaction. *Org. Biomol. Chem*., **2011**, 9, 232-235.

10. Lewis R J, Hanawalt P S, Nick Sealing T4 DNA Ligase on a modified DNA template: Tethering a functional molecules on $_D$-threoninol. *Nature,* **1982**, 298, 393.

11. Ligang Z, Hai L, George C S, Frederick D L, Synthesis and properties of nicked dumbbell and bumbbell DNA conjugates having stilbenedicarboxamide linkers. *Org. Biomol. Chem.,* **2007**, 5, 450-456.

12. Ihara T, Fuji T, Mukae M, Kitamura Y, Jyo A, Photochemical ligation of DNA conjugates through anthracene cyclodimer formation and its fidelity to the template sequences. *J. Am. Chem. Soc*., **2004**, 126, 8880-8881.

13. Fujimoto K, Matuda S, Takahashi N, Saito Isao, Template-directed photoreversible ligation of deoxyoligonucleotides via 5-vinydeoxyuridine. *J. Am. Chem. Soc*., **2000**, 122, 5646-5647.

14. You Y H, Lee D H, Yoon J H, Nakajima S, Yasui A, Pfeifer G P, Cyclobutane pyrimidine dimers are responsible for the vast majority of mutations induced by UVB irradiation in mammalian cells. *J. Biol. Chem.,* **2001**, 276, 44688-44694.

15. Ogasawara S, Fujimoto K, A novel method to synthesize versatile multiple-branched DNA (MB-DNA) by reversible photochemical ligation. *Chem. Bio. Chem*., **2005**, 10, 1756.

16. Fujimoto K, Matuda S, Ogawa N, Hayashi M, Saito I, Template-directed reversible photocircularization of DNA via 5-vinyldeoxycytidine. *Tetrahedron. Lett*., **2000**, 41, 6451-6454.

17. Nakamura F, Ito E, Sakao Y, Ueno N, Gatuna I N, Ohuchi F S, Hara M, Preparation of a branched DNA self-assembled monolayer toward sensitive dna biosensors. *Nano. Lett.,* **2003**, 3, 1083-1086

18. Becerril H A, Stoltenberg R M, Wheeler D R, Davis R C, Harb J N, Woolley A T, DNA-templated three-branched nanostructures for nanoelectronic devices. *J. Am. Chem. Soc*., **2005**, 127, 2828-2829.

19. Ogasawara S, Ami T, Fujimoto K, Autonomous DNA computing machine based on photochemical gate transition. *J. Am. Chem. Soc.,* **2008**, 130, 10050-10051.

20. Seeman N C, Nucleic acid junction and lattices. *J. Theor. Biol*., **1982**, 99, 237-247.

21. Pothemund P W, Folding DNA to create nanoscale shaped and patterns. *Nature,* **2006**, 16, 297-302.

22. Lehman I R, DNA ligase: Structure, mechanism, and function. *Science,* **1974**, 29, 790-797.

23. Rinker S, Ke Y, Liu Y, Chhabra R, Yan H, Self -assembled DNA nanostructures for distance dependent multivalent ligand-protein binding. *Nat. Nanotechnol.,* **2008**, 3, 418-422.

24. Maniatis T, Fritsch E F, Sambrool J, Molecular Cloning; Cold Spring Harbor Laboratory Press: Plainview, New York, NY, USA, **1982**.

25. Sambrook J, Fritsch E F, Maniatis T, Molecular Cloning: A Laboratory Manual, 2nd ed.; Cold Spring Harbor Laboratory Press: New York, NY, USA, **1989**.

General Conclusion

In Chapter 1, I reported the ultrafast photopolymerization of ODNs using ^{CNV}K with 366 nm irradiation and photodegradation with 312 nm irradiation. The photopolymerized long DNA mediated [2+2] cyclobutance ring formed stable B-formed DNA with a covalent bond. And, this photopolymerization can create a DNA/RNA hetero polymer incorporating miRNA in a sequence specific manner. By using a pyrene modified probe including ^{CNV}K, target miRNA by pyrene excimer emission was achieved.

In Chapter 2, I created DNA array structures equipped with heat resistance by ultrafast photocrosslinking with ^{CNV}K. The photocrosslinked structure was maintained, when heating at 80°C, and it acquired heat resistance at least over 40°C compared to the non-photocrosslinked DNA structure. Moreover, the inserting position and number of ^{CNV}K allowed regulation of the size and conformation of the DNA structure.

In Chapter 3, I reported the 19F MR signal of trifluorothymidine in duplex DNA was shifted -63.2 ppm to -71.2 ppm by photocrosslinking, which reflects the change of spatial proximity and electronic state in the trifluoromethyl group. I designed the miRNA-detection system based on the chemical shift, and10 mM miRNA could be detected in a sequence specific manner.

In Chapter 4, I explored the effect of ultrafast DNA photocrosslinking of ^{CNV}K on a DNA strand displacement. The DNA strand displacement was accelerated by DNA photocrosslinking in a photoirradiation time manner. The insertion position of ^{CNV}K had a great influence on the acceleration rate. A maximum of 29 folds as the acceleration rate was acquired when inserting ^{CNV}K into the center-position.

In Chapter 5, I presented the concept of the photosplitting of ^{CNV}K using branch migration without heating with a 366 nm photoirradiation. By using the branch migration, the photoadduct was splitted over 80% with a 366 nm irradiation for 5h. The photoreaction of ^{CNV}K is considered to take the photostationary state of photocrosslinking and photosplitting under the photoirradiation at 366 nm. In two-strand hybridization, the reaction rate constant of photocrosslinking was much faster than that of photosplitting so that photosplitting can be observed with 366 nm photoirradiation using branch migration.

In Chapter 6, I demonstrated template directed photochemical ligation of ODNs using 5-carboxyvinyldeoxyuridine (^{CV}U). The short four ODNs were ligated to long branched ODN with a 366 nm photoirradiation on the template strand, and this reaction has reversibility with 312 nm photoirradiation. A photoirradiated self-assembled long DNA, was constructed, which grew by photoirradiation.

In this thesis, I focus on changes in the creation of covalent bonds, the rapidity of reactions, and the conformation and electronic state following the reaction [2+2] cyclobutan formation by which the ^{CNV}K photocrosslinks to the pyrimidine base in a complementary strand. DNA nanotechnology utilizing chemical reactions related to photoresponsive artificial nucleosides may realize novel functions that could not be realized only by the complementarity according to the Watson-Crick base pair of DNA, will be realized. In the future, I will create a photo-driven DNA nanomachine based on the engineering reported this time.

Achievements

Publication

Chapter 1

Shigetaka Nakamura and Kenzo Fujimoto, "Rapid photopolymerization of oligonucleotides by 3-cyanovinylcarbazole mediated DNA photocrosslinking" *Journal of photopolymer Science and Technology*, **2014**, 27, 485-490.

Chapter 2

Shigetaka Nakamura and Kenzo Fujimoto, "Creation of DNA Array Structure Equipped with heat resistance by Ultrafast Photocrosslinking" *Journal of chemical Technology & biotechnology,* **2014**, 89, 1086-1090.

Chapter 3

Shigetaka Nakamura and kenzo Fujimoto. "19F NMR chemical shift imaging of nucleic acids by DNA photocrosslinking" submitted to *Chemical Comminication*.

Chapter 4

Shigetaka Nakamura, Hirokazu Hashimoto, Satoshi Kobayashi, and Kenzo Fujimoto "Photochemical regulation of DNA strand exchange by DNA photocrosslinking reaction" in prepared.

Chapter 5

Shigetaka nakamura, Hayato Kawabata, and Kenzo Fyjimoto
"Reversible photocrosslinking reaction of 3-cyanovinylcarbazole using branch migration" in prepared.

Chapter 6

Shigetaka Nakamura, Shinzi Ogasawara, Shigeo Matsuda, Isao Saito, and Kenzo Fujimoto, "Template Directed Reversible Photochamical Ligation of Oligodeoxynucleotides" *Molecules*, **2012**, 17, 163-178.

Presentation

International Conference

1. <u>Shigetaka Nakamura</u>, Takehiro Ami, Shinzi Ogasawara, Takashi Sakamoto, and Kenzo Fujimoto. "DNA computing based on photochemical DNA manipulation." The 2010 International Chemical Congress of Pacific basin Societies. December, 2010, in Hawaii.

2. <u>Shigetaka Nakamura</u>, Yoshinaga Yoshimura, and Kenzo Fujimoto. "Catalytic Repair of a Thymine Dimer in DNA via Carbazole Nucleoside and its Application for DNA Nanotechnology" XXV International Conference on Photochemistry, August, 2011, in Beijing.

3. <u>Shigetaka Nakamura</u>, Shinzi Ogasawara, Kenzo Fujimoto. "Photochemical DNA manipulation toward for DNA computing "17th International Conference on DNA computing and Molecular Programming, September, 2011, in Los Angeles.

4. <u>Shigetaka Nakamura</u>, Kenzo Fujimoto. "Template directed reversible photochemical ligation for DNA nanotechnology" ACS national Meeting 2012 spring, March, 2012, in San Diego.

5. <u>Shigetaka Nakamura</u>, Kenzo Fujimoto. "Template directed reversible photochemical ligation toward for construction of DNA architecture" 13th Tetrahedron Symposium, June, 2012, in Amsterdam.

6. <u>Shigetaka Nakamura</u>, Kenzo Fujimoto. "Template directed photochemical organization of oligonucleotides" The 39th International Symposium on Nucleic Acids Chemistry, November, 2012, in Nagoya.

7. <u>Shigetaka Nakamura</u>, Kenzo Fujimoto. "Creation of DNA array structure equipped with heat resistance by ultrafast photocrosslinking using 3-cyanovinylcarbazole" The XXVth IUPAC Symposium on Photochemistry, July, 2014, in Bordeaux.

8. <u>Shigetaka Nakamura</u>, Kenzo Fujimoto. "Improvement of thermal stability of DNA structure by photocrosslinking reaction using 3-cynaovinylcarbazole" ISACS15 Challenge in Nanoscience, August, 2014, in San Diego.

9. <u>Shigetaka Nakamura</u>, Hirokazu Hashimoto, Kenzo Fujimoto. "Photochemical regulation of DNA strand exchange using DNA photocrosslinking" 20th International Conference on DNA computing and Molecular Programming, September, 2014, in Kyoto.

10. <u>Shigetaka Nakamura</u>, Hayato Kawabata, Kenzo Fujimoto " The reversible photochemical reaction using branch migration" The 41st International Symposiumu on Nucleic Acids Chemistry. November, 2014, in Kokura

National Conference

1. <u>中村重孝</u>・坂本隆・藤本健造"光クロスリンクオリゴ DNA によるナノ構造の安定化" 平成 21 年度日本化学会北陸地区講演会と発表会、2010 年 11 月

2. <u>中村重孝</u>・坂本隆・藤本健造"可逆的 DNA 光クロスリンクオリゴによる DNA ナノ構造の安定性制御"日本ケミカルバイオロジー学会年会、2011 年 5 月

3. <u>中村重孝</u>・坂本隆・藤本健造"光クロスリンクオリゴ DNA による DNA ナノ構造の安定化"平成 23 年度日本化学会北陸地区講演会と研究発表会、2011 年 11 月

4. <u>中村重孝</u>・藤本健造"光応答性人工核酸を用いた DNA の組織化"平成 24 年度日本化学会北陸地区講演会と研究発表会、2012 年 11 月

5. <u>中村重孝</u>・藤本健造"耐熱性を獲得したプログラマブルな DNA タイル創製"第 1 回バイオマテリアル北陸若手研究会、2012 年 12 月

6. <u>中村重孝</u>・藤本健造"光架橋反応による耐熱性を獲得した DNA タイル創製"日本化学会第９３回春期年会、2013 年 3 月

7. <u>中村重孝</u>・藤本健造"3-シアノビニルカルバゾールを用いた光架橋による DNA ナノワイヤーの安定化と miRNA のセンシング"日本化学会第９４回春期年会、2014 年 3 月

8. <u>中村重孝</u>・藤本健造・亀山武志・高岡晃教"シグナル制御のツールとしての人工核酸を用いた DNA-motif の構築"第 79 回日本インターフェロン・サイトカイン学会学術集会、2014 年 7 月

9. <u>中村重孝</u>・坂本隆・藤本健造"光架橋反応を用いた核酸類の 19F ケミカルシフトイメージング法の開発"第 8 回バイオ関連化学シンポジウム、2014 年 9 月

10. <u>中村重孝</u>・藤本健造"生体内 19F-NMR ケミカルシフトイメージングを指向した光化学的超高速核酸類光架橋反応の開発"第 37 回日本分子生物学会年会、2014 年 11 月

Patent

1. 藤本健造、<u>中村重孝</u>、”核酸ナノワイヤーの製造方法、該方法に使用される核酸”2012-15889、**2012**

2. 藤本健造、<u>中村重孝</u>、橋本浩寿、小林聡、”鎖交換された二重鎖オリゴヌクレオチドの製造方法”、2013-133163、**2013**

3. 藤本健造、<u>中村重孝</u>、”光架橋形成抑制方法、及び自己架橋形成抑制型光応答性核酸”、特願 2013-225799、**2013**

4. 藤本健造、<u>中村重孝</u>、”光架橋形成によって 19F ケミカルシフトの変化を生じさせる方法” 特願 2013-259334、**2013**

5. 藤本健造、<u>中村重孝</u>、“ブランチマイグレーションを用いた可逆的光開裂反応” 特願 2014-224574、**2014**

Acknowledgement